

DEUTSCHES ELEKTRONEN-SYNCHROTRON **DESY**

DESY 67/40
November 1967

DESY-Bibliothek
- 8. JAN. 1968 ✓

RESONANCES (BUBBLE CHAMBER)

by

E. Lohrmann

DESY, Hamburg

2 HAMBURG 52 · NOTKESTIEG 1

RESONANCES (BUBBLE CHAMBER)*

by

E. Lohrmann

DESY, Hamburg

*Rapporteur talk given at the International Symposium on Electron and Photon Interactions at High Energies, Stanford, California, 1967.

I. SURVEY OF EXPERIMENTAL MATERIAL

This is an account of photoproduction of mesonic and baryonic resonances on protons and neutrons observed in bubble chambers.

The range of photon energies covered is from threshold up to about 6 GeV. The following new data came from two experiments.

1. A bubble chamber experiment carried out at CEA by the Cambridge Bubble Chamber Group.¹
2. A bubble chamber experiment carried out with the bubble chamber at DESY by the Aachen-Berlin-Bonn-Hamburg-Heidelberg-München-(ABBHM) Collaboration.²

Table I gives a survey of the total material available.

TABLE I

| Reaction | Number of Pictures | Number of Events | Reference |
|--------------|--------------------|------------------|-----------|
| | Taken | Evaluated | |
| $\gamma + p$ | 865,000 | ~ 9,300 | 1 |
| $\gamma + p$ | 1,700,000 | ~ 31,000 | 2 |
| $\gamma + d$ | 1,300,000 | ~ 3,900 | 2 |

The data from the Cambridge Bubble Chamber Group have already been partly published,⁴⁻⁷ and this published material will not be presented in detail. The data given here by the ABBHM - Collaboration represent an increase of statistics by roughly a factor of two compared with previous publications by that group.⁸

We shall also mention data on rho production presented from a spark chamber experiment done at DESY.³ The experimental details of that experiment are described in the talk of Professor Pipkin.

The experimental procedure used in the bubble chamber experiments has been published^{6,8} and will not be described here.

II. CROSS SECTIONS

Figure 1 shows the total cross section for the reaction

$$\gamma p \rightarrow p \pi^+ \pi^- \quad (1)$$

as a function of the photon energy E_γ (Ref. 2). A similar measurement was made by the Cambridge Bubble Chamber group and published in Ref. 6. The cross sections given here by the ABBHHM-Collaboration are in the average about 10% smaller than those of Ref. 6. About half of this difference (5%) comes from the different values of the electron-positron pair production cross section in hydrogen used by the two groups to normalize their nuclear cross sections (at 5 GeV, the authors of Ref. 2 use 19.8 mb for the e^+e^- pair cross section on hydrogen, whereas the Cambridge Bubble Chamber Group⁶ uses 20.62 mb).

Figure 2 shows the cross section for the reaction (from Ref. 2)



This cross section agrees, within statistics, with the one published in Ref.6. The points labelled "prediction from π -N data" in Fig.2 are theoretical predictions by Satz.⁹ He used the vector dominance model to connect the cross section $\sigma(\gamma p \rightarrow p \pi^+ \pi^+ \pi^- \pi^-)$ with the cross section to produce the same final state by an incident vector meson, $\sigma(\text{vector meson} + p \rightarrow p \pi^+ \pi^+ \pi^- \pi^-)$ and finally the quark model and the statistical model to connect the vector meson cross section with experimental cross sections $\pi^+ p \rightarrow \text{nucleon} + \text{four pions}$ published in the literature. Up to 6 GeV there is good agreement of these models with the experimental cross section for reaction (2). It will be interesting to see, whether this agreement will also hold at the higher energies now available at SLAC.

III. PHOTOPRODUCTION OF RHO MESONS

III.1 The Reaction $\gamma p \rightarrow p \rho^0$ (1a)

In order to obtain the cross sections and experimental distributions for reaction (1a) from events of the type $\gamma p \rightarrow p \pi^+ \pi^-$, the following fitting procedure was used by the ABBHHM-Collaboration. The probability distributions of the two-particle invariant masses were fitted to a combination of phase space background plus a Breit-Wigner distribution for Δ^{++} production in the $p \pi^+$ mass combination plus an appropriate resonance shape in the $\pi^+ \pi^-$ mass distribution to describe ρ^0 production. The effect of the ρ^0 -decay angular distribution was taken into account more carefully than in the previous work of that group.⁸ Three choices for the form of the $\pi^+ \pi^-$ mass distribution resulting from ρ^0 decay were tried in the fits:

- (i) A Breit-Wigner distribution with energy-dependent width according to Jackson.¹⁰
- (ii) A Breit-Wigner distribution as in (i), multiplied by a term $(m_\rho / m_{\pi^+ \pi^-})^4$, as suggested by Ross and Stodolsky,¹¹ to account for the diffractive character of ρ^0 -production.
- (iii) A Breit-Wigner distribution as in (i) plus an OPE background term interfering with the Breit-Wigner amplitude, as suggested by Söding.¹²

Below 1.4 GeV the distribution (i) gave acceptable fits to the data. Above 1.4 GeV choice (i) gave a poor fit to the data and too low a value for the ρ^0 -mass.

Above 1.4 GeV method (ii) gave acceptable fits and values for the ρ^0 -mass, which varied slightly with photon energy. This slight variation comes probably from fitting the total rho cross section, whereas the prescription of Ross and Stodolsky was meant to cover only rho production in the forward direction.

Method (iii) gave acceptable fits and a value of the ρ^0 -mass compatible with 770 MeV.¹³






The width of the rho meson was kept fixed at 143 MeV for all three fits.

Figure 3 shows the $\pi^+ \pi^-$ mass distribution² for various intervals of the photon energy E_γ . It can be seen, that both methods (ii) and (iii) give acceptable fits to the data. Therefore the results with both fitting methods were given by Ref.2.

Figure 4 shows the total rho production cross section as a function of E_γ . For $E_\gamma < 1.4$ GeV the values obtained by fit (i) are displayed, since fits (ii) and (iii) should only be applied at high energies. For $E_\gamma > 1.4$ GeV both the results according to method (ii) and (iii) are shown.

The difference between them allows an estimate of systematic errors for the rho cross section due to our lack of knowledge of the background and of the precise form of the $\pi^+ \pi^-$ mass distribution from rho decay.

The Cambridge Bubble Chamber group has used a Breit-Wigner shape with energy dependent width¹⁰ to fit the $\pi^+ \pi^-$ mass distribution from ρ decay. I have multiplied the fraction of ρ -production, as reported in Ref.1, by the total cross section for reaction (1), as reported in Ref.6, to obtain the cross section for rho production reaction (1a) for the Cambridge Bubble

Chamber group. This cross section, labelled "CEA" , is also included in Fig.4. It is consistent with the cross section obtained by the ABBHMH-Collaboration² (points labelled , , , ).

The following figures show details about the ρ -production in reaction (1a), as obtained by the ABBHMH-Collaboration.

Figure 5 shows the differential cross section for ρ^0 -production for various intervals of E_γ . The quantity $d\sigma/d\Delta^2$ is given, where Δ^2 is the square of the four momentum transfer. The arrows shown in the first interval of Δ^2 signify a possible scanning loss of very short proton tracks.

More evidence that the differential cross section $d\sigma/d\Delta^2$ is most likely underestimated by the first data point with the smallest Δ^2 (kinematical limit $< \Delta^2 < 0.05 \text{ GeV}^2$) in Fig.5 comes from a spark chamber experiment carried out at DESY³. In this experiment, the reaction $\gamma p \rightarrow p\rho^0$ was studied for photon energies $3.2 \text{ GeV} < E_\gamma < 4.4 \text{ GeV}$, in addition to rho production on carbon and aluminum. These data are shown in Fig.6. It is seen that for all three elements the differential cross section $d\sigma/d\Delta^2 = A \exp(-B\Delta^2)$ down to the smallest values of Δ^2 , which are kinematically allowed.

Except for the first point in the differential angular distribution, which has just been discussed, the spark chamber and the bubble chamber experiments agree within statistics.

The differential cross section $d\sigma/d\Delta^2$ of Fig.5 was fitted by the ABBHMH group to a relation

$$d\sigma/d\Delta^2 = A \exp(-B\Delta^2) \quad (2)$$

for $0.05 \text{ GeV}^2 < \Delta^2 < 0.5 \text{ GeV}^2$.

Values for A and B resulting from this fit are given in Table II for various E_γ intervals.

TABLE II

Reaction $\gamma p \rightarrow p\rho^0$. Fit of the differential cross sections $d\sigma/d\Delta^2$ to $A \exp(-B\Delta^2)$ for $0.05 < \Delta^2 < 0.5 \text{ GeV}^2$.

| E_γ (GeV) | A ($\mu\text{b}/\text{GeV}^2$) | B (GeV^{-2}) |
|---------------------|-------------------------------------|----------------------------|
| 1.4 - 1.8 | 140.7 ± 13.5 | 5.75 ± 0.46 |
| 1.8 - 2.5 | 128.8 ± 8.1 | 5.43 ± 0.28 |
| 2.5 - 3.5 | 146.8 ± 9.2 | 6.92 ± 0.31 |
| 3.5 - 4.5 | 149.3 ± 13.2 | 8.10 ± 0.49 |
| 4.5 - 5.8 | 129.7 ± 11.6 | 7.90 ± 0.47 |

However, it must be noted that these results were obtained by averaging over the whole rho peak in the $\pi^+\pi^-$ -mass distribution. Actually a strong variation of the slope B with the mass of the $\pi^+\pi^-$ system was observed by the ABBHHM-Collaboration. This is shown in Fig.7, which shows $d\sigma/d\Delta^2$ for four intervals of the $\pi^+\pi^-$ invariant mass. A fit of Equ. 2 was made for $E_\gamma > 3.5$ GeV and various intervals of the invariant $\pi^+\pi^-$ -mass. The dependence of B on the $\pi^+\pi^-$ -mass is shown in Table III.

TABLE III

Reaction $\gamma p \rightarrow p\pi^+\pi^-$ at photon energies
 $3.5 \text{ GeV} < E_\gamma < 5.8 \text{ GeV}$. Fit of the double
differential cross sections $d\sigma/d\Delta^2 dM_{\pi\pi}$
to $A \exp(-B\Delta^2)$ for $0.05 < \Delta^2 < 0.5 \text{ GeV}^2$.

| $M_{\pi\pi}$ (GeV) | B (GeV^{-2}) |
|-----------------------|----------------------------|
| 0.56 - 0.70 | 9.30 ± 0.65 |
| 0.70 - 0.76 | 8.00 ± 0.56 |
| 0.76 - 0.82 | 6.08 ± 0.59 |
| 0.82 - 0.96 | 5.04 ± 0.65 |

Figure 8 shows a sample of rho decay distributions. They are given in the "helicity system," in which the decay angle θ_H is measured in the rho CM system between the outgoing proton and the π^+ meson. The azimuth angle ϕ_H is taken to be zero for decay in the production plane. It is seen that for small production angles the decay distribution is compatible with $\sin^2 \theta_H$ which is expected for complete spin alignment of the rho meson in its direction of flight. However, for large production angles of the rho meson, this is seen to be no longer true.

The complete information on the decay distribution $W(\cos \theta_H, \phi_H)$ of the ρ^0 -meson is contained in the spin space density matrix elements ρ_{ik} of the ρ^0 -meson.¹⁴

$$W(\cos \theta_H, \phi_H) = \frac{3}{4\pi} \left\{ \frac{1}{2} (1 - \rho_{00}) + \frac{1}{2} (3\rho_{00} - 1) \cos^2 \theta_H \right. \\ \left. - \rho_{1-1} \sin^2 \theta_H \cos 2\phi_H - \sqrt{2} \text{Re } \rho_{10} \sin 2\theta_H \cos \phi_H \right\} \quad (3)$$

The results for the ρ_{ik} as a function of the overall CMS production angle θ_{CM} of the rho meson are shown in Figs.9 through 11.

For comparison, curves are included in Figs.9 through 11 giving the prediction of the "strong absorption model" (SAM) proposed by Eisenberg et al.¹⁵ The predictions follow essentially from the assumption $m_\gamma = m_\rho$, $m_p = m_p$, where m_γ , m_ρ , m_p , and m_p are the spin components of the photon, the ρ meson and the incoming and outgoing protons relative to a fixed direction, e.g. the photon direction in the CMS.

In the helicity frame used in Figs.9 through 11, the density matrix elements are according to Kramer¹⁶:

$$\rho_{00} = \frac{1}{2} \sin^2 \theta_{CM}$$

$$\rho_{1-1} = \frac{1}{4} \sin^2 \theta_{CM}$$

$$\rho_{10} = -\frac{1}{4\sqrt{2}} \sin 2\theta_{CM}$$

These predictions are in reasonable agreement with the data in Fig.9. There are deviations indicated in Figs. 10 and 11, but more work should be done to make sure of this.

Comparison between the data of the Cambridge Bubble Chamber and the ABBHHM-Collaboration: It has already been shown that the total cross sections for the reaction $\gamma p \rightarrow p\rho^0$ as obtained by the two bubble chamber experiments agree within statistics (see Fig.4, and remember the 5% difference in normalization mentioned in Section II). For the differential cross sections it is easiest to compare the slopes B resulting from a fit to $d\sigma/d\Delta^2$ according to an exponential law $\exp(-B\Delta^2)$ (see Equ.2). The Cambridge Bubble Chamber Group finds⁴ $B = (8.8 \pm 1.5) \text{ GeV}^{-2}$ for $E_\gamma > 1.8 \text{ GeV}$. This value is, within statistics, compatible with the results of the ABBHHM-Collaboration (Table II). The procedure to obtain $d\sigma/d\Delta^2$ as used by two groups differs in the treatment of the background. No background subtraction was made by the Cambridge Bubble Chamber Group, whereas the ABBHHM group used a fitting procedure to the $\pi\pi$ mass distribution similar to the one described for the determination of the total cross section.

The decay angular distribution of the rho meson, as obtained by the two groups, can most easily be compared by reference to the decay matrix elements ρ_{ik} in the Gottfried-Jackson system, which can be found in Ref.15 for the Cambridge Bubble Chamber Group and in Ref.8 (Nuovo Cim. 48, 262) for the ABBHMM group. The results of the two groups are in good agreement.

III.2 Upper Limit for the Rho Decay into Four Pions

A total of 1550 ρ^0 mesons in the mass region $M_{\pi\pi} < 900$ MeV was observed in reaction (1) for $E_\gamma > 2.5$ GeV by the ABBHMM-Collaboration. They have looked for the decay $\rho^0 \rightarrow \pi^+ \pi^+ \pi^- \pi^-$ in the reaction $\gamma p \rightarrow p \pi^+ \pi^+ \pi^- \pi^-$. No event was found in the four pion mass region specified above. From these numbers they obtain on a 90% confidence level the following upper limit for the branching ratio:

$$\Gamma (\rho^0 \rightarrow \pi^+ \pi^+ \pi^- \pi^-) / \Gamma (\rho^0 \rightarrow \pi^+ \pi^-) < 0.0015.$$

IV. OMEGA PRODUCTION IN THE REACTION $\gamma p \rightarrow p\omega$

Omega production was studied in the reaction $\gamma p \rightarrow p \pi^+ \pi^- \pi^0$ by the Cambridge Bubble Chamber Group⁵ and by the ABBHMM-Collaboration.² Figure 12 shows the cross section for ω production as a function of the photon energy E_γ , as obtained by the two bubble chamber groups. The observed cross sections have been multiplied by a factor¹³ $1/0.90$ to account for the unobserved decay modes. The results of the two experiments are in satisfactory agreement with each other. The cross section decreases significantly with increasing photon energy, which suggests that a diffraction model alone cannot give a good description of the experimental cross sections between threshold and 6 GeV.

The following figures show more details of the ω production, as observed by the ABBHMM-Collaboration. Figures 13 and 14 show the differential cross sections $d\sigma/d\Delta^2$ for various photon energy intervals. The distribution $d\sigma/d\Delta^2$ has been fitted to an exponential law of the form Equ.(2) in the four momentum transfer range $\Delta^2 < 0.5$ GeV². The results are given in Table IV for various values of E_γ .

TABLE IV

Reactions $\gamma p \rightarrow p\omega^0$ and $\gamma p \rightarrow p\phi^0$. Fit of the differential cross sections $d\sigma/d\Delta^2$ to $A \exp(-B\Delta^2)$

| Reaction | E_γ (GeV) | A ($\mu\text{b}/\text{GeV}^2$) | B (GeV^{-2}) | Range of Δ^2 used (GeV^2) |
|---------------------------|---------------------|-------------------------------------|----------------------------|--|
| $p \rightarrow p\omega^0$ | 1.4 - 1.8 | 42.2 ± 9.4 | 6.2 ± 1.2 | 0.06 - 0.5 |
| | 1.8 - 2.5 | 35.0 ± 6.2 | 5.1 ± 0.8 | 0.04 - 0.5 |
| | 2.5 - 5.8 | 27.2 ± 3.8 | 7.5 ± 0.9 | 0.02 - 0.5 |
| $p \rightarrow p\phi^0$ | 1.58 - 2.5 | 0.45 ± 0.17 | 1.85 ± 0.75 | 0.065 - 1.0 |
| | 2.5 - 5.8 | 0.73 ± 0.21 | 3.35 ± 0.70 | 0.015 - 1.0 |

Figures 15 and 16 show the experimental values for the spin density matrix elements of the ω as a function of the CMS production angle θ_{CM} . They were obtained from the distributions in $\cos \theta$ and ϕ , where θ is the angle between the photon and the normal to the ω decay plane in the ω rest system, ϕ is the corresponding azimuth angle (Jackson system). The form of the angular distribution as a function of the spin density matrix elements ρ_{ik} is given by Equ.(3). Figures 15 and 16 show also values for ρ_{ik} in the helicity system, in which the decay polar angle θ_{H} is measured between the ω decay normal and the outgoing proton in the ω CMS, and ϕ_{H} is the azimuth angle in this system.

V. PHI MESON PRODUCTION IN THE REACTION $\gamma p \rightarrow p\phi$

The following results were communicated by the ABBHMM-collaboration:² For all three-prong events they tried a kinematical fit to the hypothesis

$$\gamma p \rightarrow pK^+K^-.$$

Figure 17 shows the K^+K^- mass distribution of all events, which gave a good fit for this hypothesis and could not be excluded on the basis of ionization. The figure shows evidence for ϕ production in the charged K mass distribution. Figure 17 shows furthermore ϕ production in the $K^0\bar{K}^0$ mass distribution from events which are compatible with the hypothesis

$$\gamma p \rightarrow pK^0\bar{K}^0$$

with one visible K^0 decay in the chamber. After correction for the neutral decay mode of the K_S^0 and for decays outside the chamber, the number of events in the ϕ region of the $K^0\bar{K}^0$ and K^+K^- mass distributions agrees well

with the known decay branching ratio of the ϕ .¹³ The cross section for ϕ production as a function of the photon energy E_γ is shown in Fig.18. The experimental values have been corrected by a factor 1/0.88 for the unobserved decay modes of the ϕ .¹³

The somewhat lower value of this cross section compared to their previous publications⁸ can be attributed to statistical effects (somewhat smaller number of events in the ϕ peak and more events in the background, resulting in a larger background subtraction, for the second half of the experiment).

The cross section shows no marked dependence on E_γ and is consistent with the assumption of a diffractive production of the ϕ meson.

The differential cross section $d\sigma/d\Delta^2$ and $d\sigma/d\Omega$ in the CMS for ϕ production is also shown in Fig.18. The ϕ decay distribution in the helicity system is shown in Fig.17.

The differential cross section $d\sigma/d\Delta^2$ was fitted to an exponential law of the form Equ. (2) in the range $\Delta^2 < 1.0 \text{ GeV}^2$. The resulting values for the slope B and the absolute height A are included in the table given in Section IV.

VI. PHOTOPRODUCTION OF OTHER MESONIC RESONANCES

VI. 1 Production of η , X^0 , and f mesons

Figure 19 shows the cross section for the reaction

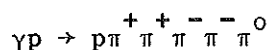


as a function of the photon energy from Ref.2. The experimental values are corrected for the unobserved decay modes using a branching ratio¹³ of

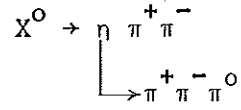
$$\Gamma(\eta \rightarrow \pi^+ \pi^- \pi^0) / \Gamma(\eta \rightarrow \text{all}) = 0.224.$$

The cross section shows a characteristic peaking at about 0.8 GeV. This is generally attributed to the production and decay of an intermediate S_{11} isobar state at 1570 MeV.¹⁷ The production angular distribution of the η for two E_γ intervals is also shown in Fig.19. These results are in agreement with a number of counter measurements and with results of the Cambridge Bubble Chamber Collaboration.¹

The $\pi^+ \pi^- \pi^+ \pi^- \pi^0$ effective mass distribution of the reaction

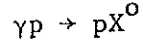


is shown in Fig. 20 according to results of the ABBHHM-Collaboration. There is evidence for X^0 (960) production, whose decay via



is observed.

The cross section for X^0 production in the reaction

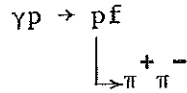


is also shown in Fig.20. The experimental values have been corrected for the unobserved decay modes of the X^0 using the branching ratio¹³

$$\Gamma(X^0 \rightarrow \pi^+ \pi^+ \pi^- \pi^- \pi^0) / \Gamma(X^0 \rightarrow \text{all}) = 0.112.$$

The production angular distribution in the CMS is also shown in Fig.20.

There is very little evidence for the production of the f -meson in the reaction



Using various fitting methods, which gave consistent results, the ABBHHM-Collaboration obtains the cross sections contained in Table V.

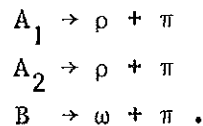
TABLE V

Cross sections for reaction $\gamma p \rightarrow p f^0$. The values are corrected for the decay $f^0 \rightarrow \pi^0 \pi^0$ by a factor 3/2

| E_γ (GeV) | σ (μb) |
|---------------------|-------------------------------|
| 2.5 - 3.5 | 0.90 ± 0.45 |
| 3.5 - 4.5 | 0.40 ± 0.30 |
| 4.5 - 5.8 | 0.06 ± 0.30 |

VI.2 Upper Limits for the Cross Section of A_1 , A_2 , and B Meson Production

The ABBHHM-Collaboration has looked for the production of the A_1 , and A_2 mesons and of the B meson, by searching for the decay modes



No significant production of these resonances was found in the reaction channels studied. Table VI gives upper limits to the production cross section for some of the reactions studied.

TABLE VI

Reactions $\gamma p \rightarrow p \pi^+ \pi^- \pi^0$ ($\pi^0 \dots$) and $\gamma p \rightarrow p \pi^+ \pi^+ \pi^- \pi^-$.
Upper limits for the production cross sections of A_1, A_2 and B mesons.

| Reaction | E_γ (GeV) | σ (μb) | Confidence Level (%) |
|---|---------------------|-------------------------------|-------------------------|
| $\gamma p \rightarrow p A_1^0$ | 1.7 - 5.8 | < 0.35 | 90 |
| $\gamma p \rightarrow p A_2^0$ | 2.2 - 5.8 | < 0.34 | 90 |
| $\gamma p \rightarrow N_{1236}^{*++} A_1^-$ | 2.5 - 5.8 | < 0.15 | 90 |
| $\gamma p \rightarrow N_{1236}^{*++} A_2^-$ | 2.9 - 5.8 | < 0.2 | 90 |
| $\gamma p \rightarrow N_{1236}^{*++} B^-$ | 2.7 - 5.8 | < 0.15 | 90 |

VI.3 The Reaction $\gamma p \rightarrow \Delta^{++} \rho^-$

This reaction was observed by both bubble chamber groups.^{1,2} Figure 21 shows evidence for this reaction in the $\pi^- \pi^0$ and $p \pi^+$ mass distributions from the reaction $\gamma p \rightarrow p \pi^+ \pi^- \pi^0$, as observed by the Cambridge Bubble Chamber Group. Table VII shows a summary of the cross sections.

TABLE VII

Cross section for reaction $\gamma p \rightarrow \Delta^{++} \rho^-$

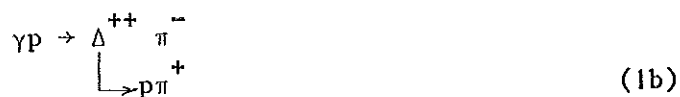
| Photon Energy (GeV) | Cross Section From Ref. 2 μb | Cross Section From Ref. 1 μb |
|------------------------|---|---|
| 1.8 - 2.5 | 2.8 ± 0.7 | 6.4 ± 2.4 |
| 2.5 - 3.5 | 1.8 ± 0.8 | } 3.1 ± 0.8 |
| 3.5 - 5.8 | 1.0 ± 0.4 | |

The cross sections from Ref.1 are larger than those of Ref.2, but because of the large errors it cannot be excluded that the discrepancy may be largely due to a statistical fluctuation.

If the OPE model could be applied to describe this reaction, it could be used in principle to determine the $\rho\pi\gamma$ -coupling constant. More work on the details of this reaction must be done, before one might be able to get this number.

VII. PHOTOPRODUCTION OF THE N_{33}^* (1236)

Production of the $N^*(1236)$, hereafter denoted by Δ , is observed in the reactions



The cross section for reaction (1b) is reasonably large even at high energies and dominates the channel $\gamma p \rightarrow p \pi^+ \pi^-$ at energies below 1 GeV. Reaction (1b) has been observed by a number of experiments. Figure 22 shows a survey of cross sections from a number of recent experiments. The results of the two bubble chamber experiments,^{1,2} and of two counter experiments^{18,19} are all compatible within the limits of error.

Attempts to compare the experimental data with model calculations were made by the Cambridge Bubble Chamber Group¹ and by Stichel, Scholz, Scheunert and Lüke.^{20,21} Figure 23 gives a survey of the models considered in terms of Feynman diagrams.

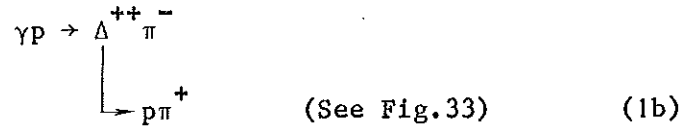
The Cambridge Bubble Chamber Group assumed the reaction $\gamma p \rightarrow \Delta^{++} \pi^-$ to proceed via intermediate higher isobar states whose decay into $\Delta^{++} \pi^-$ is observed (diagram a). In particular, they considered as intermediate states: $N^*(1420)$, $N^*(1512)$, $N^*(1688)$, and $N^*(1924)$. The type of fit to their data, which can be obtained by their model, is shown in Fig.24 (total cross section for reaction (1b)), Fig.27 (decay angular distribution for the Δ^{++} in its CMS), and Fig. 25 (differential CMS cross section). The theoretical curves are in qualitative agreement with the data; however, they disagree in the details of Figs. 25 and 27. This is further exemplified in Fig.26 which shows the differential cross section for reaction (1b) as obtained by the ABBHBM-Collaboration. The curves are taken over from

the work of Ref.1 with arbitrary normalization. One sees that both experiments show the same systematic deviations from the model. This shows two things: (1) The experimental results of the two bubble chamber groups are in good agreement. (2) The deviations between experiment and the intermediate isobar model are not statistical fluctuations, but are of a systematic nature.

A different starting point for model interpretation of reaction (1b) is provided by the OPE diagram (b) in Fig.23. More terms must be added to make the model gauge invariant. There is no unique way to do this; one suggestion was made by Stichel and Scholz²⁰ who added certain parts of diagrams (c,d,e). This model agreed qualitatively with the data on reaction (1b), but disagreed in certain details.⁸ Subsequently, Stichel et al.²¹ included the effects of the first two higher isobar states P_{11} (1400) and D_{13} (1512). This combination of the two models yielded better agreement with the data, at least for small energies and small momentum transfers. The following figures will show this on data contributed by the ABBHM-Collaboration. Figure 29 shows the same cross section for small momentum transfers. The magnitude of the contributions of the N^* (1400) and N^* (1512) intermediate states was chosen by Stichel et al. so as to give a best fit to the cross section in Fig.29. From this fit they get unique predictions for the production and decay angular distributions. Figure 30 show the differential cross section $d\sigma/d\Delta^2$ for reaction (1b) for a number of different photon energies, and Fig.31 shows the decay angular distribution of the Δ^{++} for a number of different photon energies. There is reasonable agreement for the differential cross section for small angles, but the agreement is much worse at larger momentum transfers. The decay angular distribution agrees quite well with the model for the lower energies. For the three highest energies investigated there seems to be a systematic discrepancy, however. It is interesting to note that the decay angular distribution at high energies is in much better accord with a quark model prediction,²² $5 - 3 \cos^2\theta$ for Δ^{++} produced in the forward direction.

Figure 32 shows the azimuth angular distribution for the Δ^{++} decay for a number of different photon energies. There is reasonable agreement with the model.

Let us now compare the production of $\Delta(1236)$ in the two reactions



Whereas the cross section for reaction (1b) is reasonably large up to the highest energies studied, the cross section for reaction (1c) is very small. Inspection of the Dalitz plots $M^2(p\pi^+)$ vs. $M^2(p\pi^-)$ (see Fig.33), and $M^2(\pi^+\pi^-)$ vs. $M^2(p\pi^-)$ shows that below 1 GeV the Δ^0 and Δ^{++} bands overlap strongly. Above 1 GeV there is an appreciable overlapping of the Δ and ρ^0 bands.

Because the cross sections for Δ^{++} and ρ^0 production are much larger than for Δ^0 production, it is very important to take possible interference effects between the Δ^{++} and Δ^0 production amplitudes and between Δ^0 and ρ production amplitudes into account.

Below 1.1 GeV the authors of Ref.2 made a maximum-likelihood fit to the two-dimensional probability distribution $f [M^2(p\pi^+), M^2(p\pi^-)]$.

This Dalitz plot distribution was fitted to the following expression:

$$f = |A^{++} \cdot B(\Delta^{++}) + A^0 \cdot B(\Delta^0)|^2 + a_{PS} f_{PS}$$

Here A^{++} and A^0 are the absolute values of the Δ^{++} and Δ^0 amplitudes to be fitted. B is a Breit-Wigner amplitude whose modulus is normalized to unity:

$$B(\Delta^{++}) = (R + iI) \cdot e^{i\phi} \Delta^{++}$$

$$R = \left(\frac{M(\pi^+ p) \Gamma}{q} \cdot W \right)^{1/2} \cdot \frac{M_\Delta^2 - M(\pi^+ p)^2}{(M_\Delta^2 - M(\pi^+ p)^2)^2 + (M_\Delta \Gamma)^2}$$

$$I = \left(\frac{M(\pi^+ p) \cdot W}{q} \right)^{1/2} \cdot \frac{M_\Delta \Gamma}{(M_\Delta^2 - M(\pi^+ p)^2)^2 + (M_\Delta \Gamma)^2}$$

q = modulus of three-momentum of p or π^+ in the $\pi^+ p$ CMS

Γ = energy-dependent width according to Jackson¹⁴ with $\Gamma_0 = 120$ MeV

M_Δ = mass of Δ -isobar = 1.236 GeV

$M(\pi^+ p)$ = mass of $p\pi^+$ -system

W = factor which takes into account the decay angular distribution. It was made proportional to the decay angular distribution in the helicity frame. (W = constant for an isotropic decay distribution.)

$\phi_{\Delta^{++}}$ = phase angle. The quantity fitted is the difference

$$\phi = \phi_{\Delta^{++}} - \phi_{\Delta^0}$$

The phase-space background f_{PS} is added incoherently to the Breit-Wigner amplitudes, with a weight a_{PS} which is also fitted.

They have checked the stability of the fits by repeating the calculations with a number of small modifications of the form of the function f to be fitted. For the decay distribution W a number of assumptions was tried: (i) isotropic decay, (ii) decay according to the prediction of the Stichel-Scholz Model,²⁰ (iii) decay according to a best fit to the experimental decay distribution.

For the background distribution f_{PS} , Lorentz-invariant phase space and a phase space modified by an assumed S-wave $\pi\pi$ interaction was tried. Furthermore, the phase angle ϕ was not assumed a free parameter, but was kept fixed at 180° for some fits.

All these modifications produced no changes outside of the statistical errors in the values of the fitted parameters.

As a further check, they repeated the fits without interference between Δ^{++} and Δ^0 and compared the results with those obtained by a different fitting method. In addition, inspection of the Dalitz plot at photon energies, where the interference between Δ^{++} and Δ^0 is very strong, showed direct evidence for the existence of interference effects.

This fitting method was used below a photon energy of 1.1 GeV to find the total cross section for reactions (1b) and (1c). Differential cross sections for the reaction (1b) and decay angular distributions for the Δ^{++} and the total cross section for reaction (1b) above 1.1 GeV were obtained without taking interference into account.

Figure 34 shows the total cross section for reaction (1b) together with the phase angle ϕ as a function of the photon energy below 1.1 GeV.

Furthermore, the ratio of the squares of the amplitudes for

$$\gamma p \rightarrow \begin{array}{c} \Delta^0 \pi^+ \\ \searrow \\ p \pi^- \end{array} (A^0), \text{ and for } \gamma p \rightarrow \begin{array}{c} \Delta^{++} \pi^- \\ \searrow \\ p \pi^+ \end{array} (A^{++})$$

is given in Fig.34.

The ratio of the cross sections

$$R = \sigma(\gamma p \rightarrow \begin{array}{c} \Delta^0 \pi^+ \\ \searrow \\ p \pi^- \end{array}) / \sigma(\gamma p \rightarrow \begin{array}{c} \Delta^{++} \pi^- \\ \searrow \\ p \pi^+ \end{array}) = |A^0|^2 / |A^{++}|^2$$

in Fig.34 is rather small in the energy region $E_\gamma < 1.1$ GeV. OPE models, quark models,²² or a model with an intermediate $I = 1/2$ isobar, all predict $R = 1/9$ (a factor of $1/3$ comes from the decay branching ratio of $\Delta^0 \rightarrow p \pi^-$). The experimental result for R is smaller than these predictions.

VIII. PHOTOPRODUCTION ON DEUTERIUM

VIII. 1 Introduction

The ABBHHM-Collaboration has contributed some first results on photoproduction from a run in the deuterium bubble chamber at DESY. The object of this experiment is to study the photoproduction of mesons and of meson and baryon resonances on the neutron. Apart from the fact that very few such studies have up to now been made at high energies, the results allow in many instances an interesting comparison with corresponding reactions on the proton. As an example, consider a reaction such as $\gamma p \rightarrow \Delta^{++} \pi^-$. By changing the sign of the third component of I-spin for all hadrons, we get $\gamma n \rightarrow \Delta^- \pi^+$. Both reactions can be measured. If the photon would have a defined I-spin (e.g., either zero or one), the cross sections of the two processes would be equal. Deviations from equality come from interference between the isovector and isoscalar parts of the photon. We shall call pairs of such reactions "charge symmetric" in what follows.

In addition (coherent) photoproduction on the deuteron can be studied. This is interesting in view of recent developments in the coherent diffraction production of vector mesons.

In the experiment a scan was made for all 3,5,7 prong events with at least one slow track (spectator proton or deuterium recoil) with a momentum (projected) < 0.4 GeV/c. In addition all events were taken which had an invisible recoil (events with an even number of tracks).

In terms of the spectator model of the deuteron, this scanning procedure picks up practically all events which represent interactions on the neutron, and which have therefore a spectator proton. The events were measured, and reconstructed with standard geometry programs. For the kinematical analysis they used the program GRIND with a special routine which is able to fit an invisible recoil track.²³

To deduce photoproduction cross sections on the (free) neutron from observations in deuterium, the authors followed the customary procedure to use the spectator model of the deuteron. In this picture one assumes that a collision of the photon with the neutron does not affect the proton, which has the same momentum before and after the collision. If this assumption is true, the laboratory momentum distribution of the spectator proton should follow the Hulthén distribution.

Figure 35 shows the laboratory momentum distribution of the spectator protons from the reaction $\gamma d \rightarrow pp\pi^-$. Of the two protons, the proton with the smaller momentum was taken to be the spectator. The result is compared with the Hulthén distribution

$$dN/dp = \frac{4\alpha(\alpha + \mu)(2\alpha + \mu)}{\pi\mu^2} \cdot \left[\frac{1}{p^2 + \alpha^2} - \frac{1}{p^2 + (\alpha + \mu)^2} \right]^2 \cdot p^2$$

with $\alpha = 45.7$ MeV and $\mu = 214$ MeV as obtained from an experiment by White et al.²⁴

The agreement is satisfactory, especially since for $p < 0.1$ GeV/c the spectator tracks are invisible and their momentum was determined with the fitting program. The laboratory angular distribution of the spectator protons for various intervals of their laboratory momentum is shown in Fig.36.

VIII. 2 The Reaction $\gamma n \rightarrow p\pi^-$

For the reaction $\gamma d \rightarrow pp\pi^-$ the photon energy can be determined uniquely from the kinematics (3C-fit). Assuming the spectator model for the deuteron, one can deduce the cross section for the reaction

$$\gamma n \rightarrow p\pi^- \tag{3a}$$

as a function of the photon energy, using a procedure, as described, e.g., by White et al.²⁴ The total cross section as a function of the photon energy is given for reaction (3a) in Fig.37. The results have been corrected for scanning loss, the loss of events due to the cut-off

in the Hulthén-function at 0.3 GeV/c plus a 5% correction due to final state interactions, taken from measurements of Neugebauer et al.²⁵ on $\gamma d \rightarrow nn\pi^+$ and $\gamma p \rightarrow n\pi^+$.

For comparison results from counter measurements are also shown. For the total $\gamma n \rightarrow p\pi^-$ cross section, counter measurements had extended up to now to an energy of about 1 GeV.²⁶ For the reaction $\gamma p \rightarrow n\pi^+$ the total cross section is known up to 16 GeV. It is in reasonable agreement with the new measurements of the symmetric reaction $\gamma n \rightarrow p\pi^-$ up to about 3 GeV.

VIII. 3 Reaction $\gamma n \rightarrow n\pi^+\pi^-$

For the study of this reaction one uses events of the type $\gamma d \rightarrow pn\pi^+\pi^- (\pi^0 \dots)$. To exclude as much as possible events representing collisions with a quasi free proton, one chooses only events having very small proton recoils (momentum < 0.1 GeV/c). Almost all of these tracks should be spectator protons.



Figure 38 shows the $n\pi^-$ mass distribution for two intervals of the photon energy E_γ . There is evidence for the production of the $\Delta(1236)$ isobar state.

Estimates for the cross section were made after subtraction of a phase space background. The resulting cross section for reaction (5a) is shown in Table VIII as a function of the photon energy. For comparison, the results for the symmetric reaction $\gamma p \rightarrow \Delta^{++}\pi^-$ are also included.

TABLE VIII

| E_γ (GeV) | $\sigma(\gamma n \rightarrow \Delta^- \pi^+)$ | $\sigma(\gamma p \rightarrow \Delta^{++} \pi^-)$ |
|------------------|---|--|
| 0.4 - 0.8 | $(29 \pm 6) \mu\text{b}$ | 42 μb |
| 0.8 - 1.1 | $(44 \pm 8) \mu\text{b}$ | 52 μb |

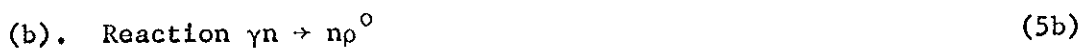


Figure 39 shows the $\pi^+\pi^-$ mass distribution for $1.4 \text{ GeV} < E_\gamma < 2.5 \text{ GeV}$. There is evidence for rho production. In contrast to the situation for

reaction (5a), reaction (5b) cannot be unambiguously separated from reactions with additional π^0 production, e.g., $\gamma n \rightarrow n\rho^0(\pi^0\dots)$.

From the experience with the symmetric reactions $\gamma p \rightarrow p\rho^0$, $p\rho^0(\pi^0\dots)$, one believes that the contribution of rho events with one or more π^0 mesons is very small. Otherwise the results are upper limits for the cross section of reaction (5b).

Between 1.4 GeV and 2.5 GeV one gets

$$\sigma(\gamma n \rightarrow n\rho^0) = 21 \pm 6 \mu\text{b.}$$

For comparison, the cross section for the symmetric reaction $\gamma p \rightarrow p\rho^0$, in the same energy interval, is $\sim 18 \mu\text{b.}$

IX. FUTURE EXPERIMENTS WITH BUBBLE CHAMBERS

I believe that the bubble chamber will also in the future be a very important instrument to study photoproduction, particularly if use can be made of a new powerful accelerator like SLAC. A very good example is the almost monochromatic photon beam built at SLAC for the bubble chamber. This beam is produced by the annihilation of positrons in a hydrogen target. If one looks at the annihilation photons under a fixed lab. angle, their energy is determined uniquely by kinematics. This beam offers a decisive advantage over a bremsstrahlung beam, since it contains by an order of magnitude less low energy photons, which form an uninteresting background. Figure 40 shows one of the first events obtained by the new 1-meter SLAC hydrogen bubble chamber taken in that beam.

Further opportunities for very interesting bubble chamber work lie in the possible use of highly polarized, almost monochromatic photon beams. Two methods are available to produce such beams. The first method uses bremsstrahlung from a single crystal. Linear polarization of up to 80% is obtainable with this method for energies up to about one-third of the primary electron beam energy. The second method uses reflection of laser light from an electron beam. This method, in order to yield an interesting beam for the bubble chamber, needs a very high energy electron beam. This is connected with the relation between maximum reflected photon energy k , the frequency V of the laser light, and the electron beam energy E :

$$k = 4(hV) \cdot E^2 / (m_e^2 + 4 \cdot hV \cdot E).$$

In addition, the beam must have an extremely small angular aperture. It appears that such experiments may be feasible at SLAC. Very interesting

physics should become accessible with the help of these beams. For example, one can study reactions like $\gamma p \rightarrow \Delta\pi$, $p\rho$, $p\omega$, $p\phi$. One has experimental information on spin orientations both in the initial state (from the beam), and in the final state (from analyzing the decay of the resonances). This will provide an important handle for the evaluation of the different models for photoproduction.

Acknowledgement

I want to express my appreciation to Dr. G. Wolf for help with the manuscript, and to Drs. Eisenberg, Schmitz, Söding, Wolf, and to the other members of the ABBHHM-Collaboration for their cooperation and for useful discussions.

References

1. Cambridge Bubble Chamber Group (Brown University, Cambridge Electron Accelerator, Harvard University, MIT, University of Padova, The Weizmann Institute of Science, Rehovoth), contribution to this conference.*
2. Aachen-Berlin-Bonn-Hamburg-Heidelberg-München-Collaboration, contribution to this conference.**
3. H. Blechschmidt, J.P. Dowd, B. Elsner, K. Heinloth, K.H. Hohne, S. Raither, J. Rathje, D. Schmidt, J.H. Smith, F.H. Weber, contribution to this conference.
4. Cambridge Bubble Chamber Group, Phys. Rev. 146, 994 (1966): ρ production.
5. Cambridge Bubble Chamber Group. Phys. Rev. 155, 1468 (1967): ω production.
6. Cambridge Bubble Chamber Group, Phys. Rev. 155, 1477 (1967): Cross sections.
7. Cambridge Bubble Chamber Group, Phys. Rev. 156, 1426 (1967): Strange particles.
8. Aachen-Berlin-Bonn-Hamburg-Heidelberg-München-Collaboration, DESY Report 66/32 (1966). Phys. Letters 23, 707 (1966). Nuovo Cim. 46, 795 (1966); 48, 262 (1967); 49, 504 (1967). Nucl. Phys. B1, 668 (1967).
9. H. Satz, DESY Report 67/17 (1967) and Phys. Letters to be published.
10. J.D. Jackson, Nuovo Cimento 34, 1644 (1964).
11. M. Ross and L. Stodolsky, Phys. Rev. 149, 1172 (1966).
12. P. Söding, Phys. Letters 19, 702 (1965).

*) Authors of this contribution: H.R. Crouch, Jr., R. Hargraves, B. Kendall, R.E. Lanou, A.M. Shapiro, M. Widgoff, G.E. Fischer, C. Bordner, Jr., A.E. Brenner, M.E. Law, U. Maor, T.A. O'Halloran, Jr., F.D. Rudnick, K. Strauch, J.C. Street, J.J. Szymanski, P. Bastien, B.T. Feld, V.K. Fischer, I.A. Pless, A. Rogers, L. Rosenson, T.L. Watts, R.K. Yamamoto, G. Calvelli, F. Gasparini, L. Guerriero, J. Massimo, G.A. Salandin, L. Ventura, C. Voci, F. Waldner, A. Brandstetter, Y. Eisenberg, A. Levy, and E.E. Ronat.

***) Authors: H.G. Hilpert, K.L. Kappler, G. Reimann, H. Schnackers, E. Schüttler, W. Struczinski, K. Lanius, A. Meyer, A. Pose, J. Schreiber, K. Böckmann, J. Moebes, H.H. Nagel, B. Nellen, E. Paul, W. Tejessy, H. Alvensleben, D. Lüke, H. Seebeck, P. Söding, H. Spitzer, F. Storim, H. Woidtke, H. Butenschön, G. Horlitz, E. Lohrmann, H. Meyer, S. Rieker, W.P. Swanson, G. Wolf, S. Wolff, H. Beisel, S. Brandt, O. Braun, H. Filt-huth, H. Kolar, V. Lüth, P. Steffen, J. Stiewe, H. Wenninger, P. Freund, P. Schlamp, N. Schmitz, P. Seyboth, J. Seyerlein, and J. Weigl.

13. A.H. Rosenfeld et al., Rev. Mod. Phys. 39, 1 (1967)
14. K. Gottfried and J.D. Jackson, Nuovo Cimento 33, 309 (1964)
15. Y. Eisenberg, E.E. Ronat, A. Brandstetter, A. Levy and E. Gotsman, Phys. Letters 22, 217 and 223 (1966).
16. G. Kramer, private communication. I thank Prof. Kramer for having pointed out to me this property of the SAM.
17. R.K. Logan and F. Uchiyama-Campbell, Phys. Rev. 153, 1634 (1967).
18. J.V. Allaby, H.L. Lynch, and D.M. Ritson, Phys. Rev. 142, 887 (1965).
19. M.G. Hauser, CALT-68-123.
20. P. Stichel and M. Scholz, Nuovo Cimento 34, 1381 (1964).
Absorption Corrections by: M.P. Locher and W. Sandhas, Zeitschrift für Physik 195, 461 (1966).
21. D. Lüke, M. Scheunert, and P. Stichel, contribution to this conference.
22. K. Kajantie and J.S. Trefil, Nucl. Phys. B1, 648 (1967).
23. CERN-TC-Program-Library. Here especially Section Grind A 005 by H. Schneider.
24. D.H. White, R.M. Schectman, and B.M. Chasan, Phys. Rev. 120, 614 (1960).
25. G. Neugebauer, W. Wales and R.L. Walker, Phys. Rev. 119, 1726 (1960).
26. Data Compilation Below 1.5 GeV, by J.T. Beale, S.D. Ecklund and R.L. Walker, Report CTSL-42, CALT-68-108.
27. V.B. Elings et al., Phys. Rev. 156, 1433 (1967);
G. Buschhorn et al., quoted by P. Schmüser, Thesis, Hamburg, 1967.

DISCUSSION

S. Barshay, University of California, Riverside

It seems to me that your statement that in the process $\gamma p \rightarrow p \rho^0$, the decay density matrix elements of the ρ^0 as a function of the production angle support the Strong Absorption Model (SAM) of Eisenberg and coworkers is a very imaginative reading of those graphs you showed in the helicity system. I think it neither supports nor does not support SAM.

Secondly, it is a pity that although you put the more scanty data on ω production in the Jackson system, you did not put the very large amount of data for ρ^0 production in that system. The Jackson system is a natural

system for studying the effects of particles exchanged in the t channel. In the process $\gamma p \rightarrow p \rho^0$ we know that the π plays little role because of the smallness of the $\rho^0 \pi^0 \gamma$ vertex, and one might ask whether, for example, the exchange of a neutral vector meson interacting with the $\gamma \rho^0$ system through a charge conjugate noninvariant vertex could play a role in this process. In the Jackson system, this leads to density matrix elements which give a polar decay distribution that varies from $\sin^2\theta$ through to $\cos^2\theta$ by going from small to large c.m. production angles. This has not been looked at. It also gives backward differential cross sections which tend to be flat. The backward differential cross section, as I see it, is an order of magnitude too big for the extrapolated exponential.

E. Lohrmann, DESY, Hamburg, Germany

I agree with you that it is very important to give these decay density matrix elements also in the so-called Jackson system. In the moment for $\gamma p \rightarrow p \rho^0$ this has not been done for technical reasons but, of course, it will eventually be done. It is technically simpler to give them for the ω meson; that is why they have been shown for the ω meson only. As far as the comparison with the Eisenberg model goes, you have to remember that the limits of error are only statistical and there are some unknown systematic errors which must be added because the behavior of the background is not well understood. That was the reason why I did not say that the data do not agree with the SAM. I think there are more ways to look at the data. We certainly can look at the decay matrix elements in more frames of reference, for example, in the so-called Adair frame where the SAM makes a very simple prediction for the decay correlations. These comparisons will be done.

Y. Eisenberg, Weizmann Institute of Science, Rehovoth, Israel

I first want to answer on the question of Barshay. We (CEA Bubble Chamber Group) have studied the ρ^0 density matrix elements in the Jackson frame. OPE does not agree with the experimental data; SAM does agree very well at all production angles. Indeed, it also changes sign: The polar angular distribution starts with $\sin^2\theta$ and changes to $\cos^2\theta$ by going from small to large production angles. I want to emphasize that the Adair angle is the natural angle for both SAM and the diffraction models. As a matter of fact, for all models which have a central type and spin independent potential, the helicity of the ρ^0 must have the helicity of the incoming γ .

Therefore, ρ_{00} must be zero in the Adair frame for all energies and all production angles. It will be nice to compare the DESY data with this prediction. Two more comments: One is related to the process $\gamma p \rightarrow p\phi$. With the limited data that we (CEA Bubble Chamber Groups) have, we have tried the following: Instead of comparing at the same photon energy, we have compared the ϕ production angular distribution with that for ω production at the same Q value in the c.m. system. As a result, both distributions seem to be the same. A last comment: The $N^* \pi^-$ production cross section in our (CEA Bubble Chamber Groups) case is compatible with being zero, but it is also compatible with being 1/9.

Barshay

I want to ask Prof. Eisenberg: Does his model (SAM) explain both the shape of the diffraction peak and the size of the large angle differential cross section - the flattening out of the differential cross section at large angles?

Eisenberg

Yes.

J. Ballam, Stanford Linear Accelerator Center

I would like to ask Dr. Lohrmann whether he could summarize the cross sections for ρ^0 , ω and ϕ production.

Lohrmann

At the high energies studied (4 - 5.5 GeV), these cross sections have approximately the following values:

$$\sigma_{\gamma p \rightarrow p\rho^0} \approx 16 \mu\text{b}$$

$$\sigma_{\gamma p \rightarrow p\omega} \approx 3 \mu\text{b}$$

$$\sigma_{\gamma p \rightarrow p\phi} \approx 0.2\mu\text{b}$$

In case of ω production, one may want to extract that contribution which is due to diffraction production. One can try to fit $\sigma_{\gamma p \rightarrow p\omega}$ by a sum of a part which varies slowly with energy and another part which decreases with energy like

$$\sim E_{\gamma}^{-1.6}$$

as was found for the ρ production cross section in πp collisions ($\pi p \rightarrow N\rho$). It turns out that the almost constant part of the cross section (which is

thought of being due to a diffraction mechanism) is of the order of 2 μb .

G. Kramer, Institut für Experimental Physik, Hamburg, Germany .

I would like to make a comment concerning the ρ^0 production. One should consider the t dependence of the cross section and the behavior of the decay density matrix elements separately. One always can find parameters for SAM which fit the experimental data on the t dependence - that is just a matter of fitting and does not explain too much. On the other hand, the density matrix is determined by the assumption on the spin dependence of the T matrix and is independent of the assumption made for the t dependence.

Figure Captions.

- Fig. 1 Total cross section for the reaction $\gamma p \rightarrow p\pi^+\pi^-$ as a function of the photon energy E_γ , data from Ref. 2.
- Fig. 2 Total cross section for the reaction $\gamma p \rightarrow p\pi^+\pi^+\pi^-\pi^-$ as a function of the photon energy E_γ (points labelled $\vdash\text{---}\dashv$, data Ref. 2). Points labelled $\circ\Delta\square$: Theoretical prediction by Satz⁹, using Vector dominance Model + Quark Model + Statistical Model.
- Fig. 3 Reaction $\gamma p \rightarrow p\pi^+\pi^-$. Effective mass distributions of the $\pi^+\pi^-$ combination for four photon energy intervals (Ref.2). The full curves are superpositions of ρ^0 resonance distribution, Lorentz-invariant phase space and $N^{*++}(1236)$ reflection as obtained by method (iii) (Söding). The broken curves give the analogue for method (ii) (Ross-Stodolsky).
- Fig. 4 Total cross section for the reaction $\gamma p \rightarrow p\rho^0$ as a function of the photon energy E_γ . Points labelled $\diamond, \uparrow, \blacklozenge$: Ref.2, points obtained by different fitting methods (see text), cross sections above 2.4 GeV corrected for scanning losses of events with a very short proton track. Points labelled $\vdash\text{---}\dashv$: Cambridge Bubble Chamber Group, points calculated from Ref. 1 + Ref. 6.
- Fig. 5 Reaction $\gamma p \rightarrow p\rho^0$. Differential cross sections $d\sigma/d\Delta^2$ for five photon energy intervals (Ref.2). The cross sections were obtained by fitting method (ii). The arrows near the forward direction indicate possible scanning losses.
- Fig. 6 Reaction $\gamma p \rightarrow p\rho^0$, $\gamma + C \rightarrow C + \rho^0$, $\gamma + Al \rightarrow Al + \rho^0$. Differential cross sections $d\sigma/d\Delta^2$ for a photon energy between 3.2 GeV and 4.4 GeV, data from the spark chamber experiment Ref.3.
- Fig. 7 Reaction $\gamma p \rightarrow p\pi^+\pi^-$ at photon energies $3.5 \text{ GeV} < E_\gamma < 5.8 \text{ GeV}$. Double differential cross section for production of dipion pairs $d\sigma/d\Delta^2 dM_{\pi\pi}$ for four intervals of $M_{\pi\pi}$ in the region $0.05 < \Delta^2 < 0.5 \text{ GeV}^2$. The points represent ρ^0 and background production. N^{*++} events are subtracted. The curves are fits by an exponential law $A \exp(-B\Delta^2)$ (Ref.2).
- Fig. 8 Reaction $\gamma p \rightarrow p\rho^0$ at two photon energy intervals above 2.5 GeV. Rho decay distributions $W(\cos\theta_H)$ in the helicity system for four intervals of the cm production angle $\cos\theta_{CM}$. The distributions

were taken from the mass region $0.68 \text{ GeV} < M_{\pi\pi} < 0.84 \text{ GeV}$ without background subtraction (Ref.2).

Fig. 9 Reaction $\gamma p \rightarrow p\rho^0$ at four photon energy intervals (Ref.2). Density matrix elements of the ρ^0 decay in the helicity system (see text) as a function of the cm production angle $\cos\theta_{\text{CM}}$: shown is ρ_{00}^{H} . The density matrix elements were obtained by simultaneously fitting the ρ^0 and background decay distributions. The curves follow from the strong absorption model.^{15,16)}

Fig. 10 Same as Fig. 9, this figure shows $\rho_{1,-1}^{\text{H}}$

Fig. 11 Same as Fig. 9, this figure shows $\text{Re } \rho_{10}^{\text{H}}$.

Fig. 12 Cross section for $\gamma p \rightarrow p\omega$ as a function of the photon energy,

(a) for all events: \downarrow : Ref.2, \uparrow : Ref.5.

(b) for $\Delta^2 < 0.5 \text{ GeV}^2$ } Ref.2.

(c) for $\Delta^2 < 0.3 \text{ GeV}^2$ }

The cross sections are not corrected for possible scanning losses of events with a very short proton track.

Fig. 13 Reaction $\gamma p \rightarrow p\omega$. Differential cross sections $d\sigma/d\Delta^2$ for two photon energy intervals (Ref.2). The first Δ^2 bin of each distribution starts above the kinematical limit and above the region where scanning losses occur. Therefore a small number of events at still lower values of Δ^2 is not included in the graphs.

Fig. 14 Same as Fig. 13, this figure shows two more photon energy intervals.

Fig. 15* Reaction $\gamma p \rightarrow p\omega$. Density matrix elements of the ω decay in the Jackson system and in the helicity system (see text) as a function of the CM production angle $\cos\theta_{\text{CM}}$. The density matrix elements are given for $1.4 \text{ GeV} < E_{\gamma} < 2.5 \text{ GeV}$. The matrix elements were obtained by simultaneously fitting the ω and the background decay distributions in a mass region near the ω (Ref.2).

Fig. 16* Same as Fig. 15, the figure shows the photon energy interval $2.5 \text{ GeV} < E_{\gamma} < 5.8 \text{ GeV}$.

*The sign of the values for $\text{Re } \rho_{10}$ in the helicity system shown in these figures should be inversed, in order that the definition of the angles in that system agrees with the customary definition, which was used for the Jackson system.

Fig. 17

Reactions $\gamma p \rightarrow pK^+K^-$ and $\gamma p \rightarrow K^0K^0p$. Effective mass distributions of (a) the K^+K^- combination and (b) the $K^0\bar{K}^0$ combination. (c) to (f) Decay distributions in the helicity system for events in the ϕ region $M_{KK} < 1.06$ GeV at photon energies $1.58 \text{ GeV} < E_\gamma < 5.8 \text{ GeV}$. Possible background is not subtracted.

(c) Distribution $W(\theta_H)$ and (d) distribution $W(\phi_H)$ for CM production angles $0.8 < \cos\theta_{CM} < 1.0$.

(e) Distribution $W(\theta_H)$ and (f) distribution $W(\phi_H)$ for CM production angles $-1.0 < \cos\theta_{CM} < 0.8$.

The angles θ_H and ϕ_H are defined as for the ρ^0 . The distributions (b) and (d) to (f) are not corrected for invisible decays (Ref.2).

Fig. 18

Reaction $\gamma p \rightarrow p\phi^0$.

(a) Total cross section as a function of the photon energy.

(b) and (c) Differential cross sections $d\sigma/d\Delta^2$ for two photon energy intervals.

(d) and (e) Differential cross sections $d\sigma/d\Omega$ in the center of mass system for two photon energy intervals (Ref.2).

Fig. 19

Reaction $\gamma p \rightarrow p\eta$.

(a) Total cross section as a function of the photon energy below $E_\gamma = 1.5$ GeV.

(b) Total cross section above $E_\gamma = 1.5$ GeV.

Production angular distribution in the center of mass system for two photon energy intervals.

(c) $0.71 < E_\gamma < 0.90$ GeV
and

(d) $0.9 < E_\gamma < 1.2$ GeV.

All events in the mass region $0.52 < M_{3\pi} < 0.565$ GeV are included without background subtraction (Ref.2).

Fig. 20

Reaction $\gamma p \rightarrow pX^0$ (Ref. 2).

(a) Effective mass distribution of the $\pi^+\pi^+\pi^-\pi^-\pi^0$ combination from all events compatible with the hypothesis $\gamma p \rightarrow p\pi^+\pi^+\pi^-\pi^-\pi^0$ ($\pi^0\dots$).

(b) Total cross section for $\gamma p \rightarrow pX^0$ as a function of the photon energy.

(c) Production angular distribution in the CM system for

twelve events in the X^0 mass region. The events with photon energies above 2.5 GeV are hatched.

- Fig. 21 Reaction $\gamma p \rightarrow \Delta^{++} \rho^-$ (Ref.1).
The figure shows the $p\pi^+$ and $\pi^-\pi^0$ mass distributions from the reaction $\gamma p \rightarrow p\pi^+\pi^-\pi^0$ for two intervals of the photon energy P_γ . The curves are the results of joint mass fits of the mass distributions with the fractions indicated in the figure.
- Fig. 22 Cross sections for the reaction $\gamma p \rightarrow \Delta^{++}(1236)\pi^-$ as a function of the photon energy E_γ , as measured by different authors for $E_\gamma < 1.4$ GeV:
◇ Ref. 1, ○ Ref. 19, ■ Ref. 2, ▲ Ref. 18
- Fig. 23 Feynman diagrams which have been used to obtain a model description of the reaction $\gamma p \rightarrow \Delta(1236)\pi$ (see text).
- Fig. 24 Total cross section for the reaction $\gamma p \rightarrow \Delta^{++}\pi^-$, as a function of the photon energy. The curve represents a best fit to an isobar model represented in Fig. 23 a (see text). (Ref. 1).
- Fig. 25 Production angular distribution for the Δ^{++} ($M(p\pi^+) = 1.15 - 1.30$ GeV) in the reaction $\gamma p \rightarrow \Delta^{++}\pi^-$. The curves are calculated on the basis of a best fit to the isobar model (see text). For $P_\gamma > 1.1$ GeV/c, the broken histograms represent the data before the background subtraction. (Ref.1).
- Fig. 26 Same as Fig. 26, but with the experimental data of Ref. 2, curves taken over from Ref. 1.
- Fig. 27 Adair angular distributions for the decay correlation between the incident photon and decay pion π^+ in the reaction sequence $\gamma p \rightarrow \Delta^{++}\pi^-$, $\Delta^{++} \rightarrow p\pi^+$. The curves are calculated from a best fit to the isobar model (see text). For $P_\gamma > 1.1$ GeV/c the broken histograms represent the data before background subtraction (Ref.1).
- Fig. 28 Reaction $\gamma p \rightarrow \Delta^{++}\pi^-$.
Cross section $\gamma p \rightarrow \Delta^{++}\pi^-$ as a function of the photon energy up to 5.8 GeV (Ref.2).
- Fig. 29 Reaction $\gamma p \rightarrow \Delta^{++}\pi^-$.
Cross section for events with $\Delta^2 < 0.3$ GeV², where Δ^2 is

the four momentum transfer squared between incoming proton and Δ^{++} . The curves have the same meaning as in Fig. 30 (Ref. 2).

Fig. 30 Reaction $\gamma p \rightarrow \Delta^{++} \pi^-$.
 Differential cross section $d\sigma/d\Delta^2$ for various intervals of the photon energy E_γ . The full curves are predictions from a model by Stichel et al.²¹ including OPE plus gauge invariance additions plus two intermediate isobar states. The dashed curve is an OPE model plus gauge invariance additions plus absorptive corrections (see text) (data from Ref.2).

Fig. 31 Reaction $\gamma p \rightarrow \Delta^{++} \pi^-$ $\Delta^2 < 0.3 \text{ GeV}^2$.
 Decay angular distribution of the Δ^{++} for various intervals of the photon energy E_γ . The curves have the same meaning as for Fig. 30. The figure shows distributions of θ_J , the angle between incoming and outgoing proton in the Δ^{++} CMS (Ref.2).

Fig. 32 Same as Fig. 31, the figure shows the distribution of ϕ_J , the azimuth angle of the outgoing proton in the $p\pi^+$ CMS. (Ref.2).

Fig. 33 Dalitz plot, showing the mass distributions $M^2(p\pi^-)$ vs. $M^2(p\pi^+)$ from the reaction $\gamma p \rightarrow p\pi^+\pi^-$ between 0.6 GeV and 0.8 GeV photon energy. The figure shows the overlap between the Δ^0 and the Δ^{++} mass bands (Ref.2).

Fig. 34 Reaction $\gamma p \rightarrow p\pi^+\pi^-$.
 Cross section for the production of Δ (1236) as a function of the photon energy E_γ below 1.1 GeV (Ref. 2).

Top: \downarrow cross section for $\gamma p \rightarrow \Delta^{++} \pi^-$

\downarrow cross section for background

Middle: A^0 : Amplitude for $\gamma p \rightarrow \Delta^0 \pi^+$

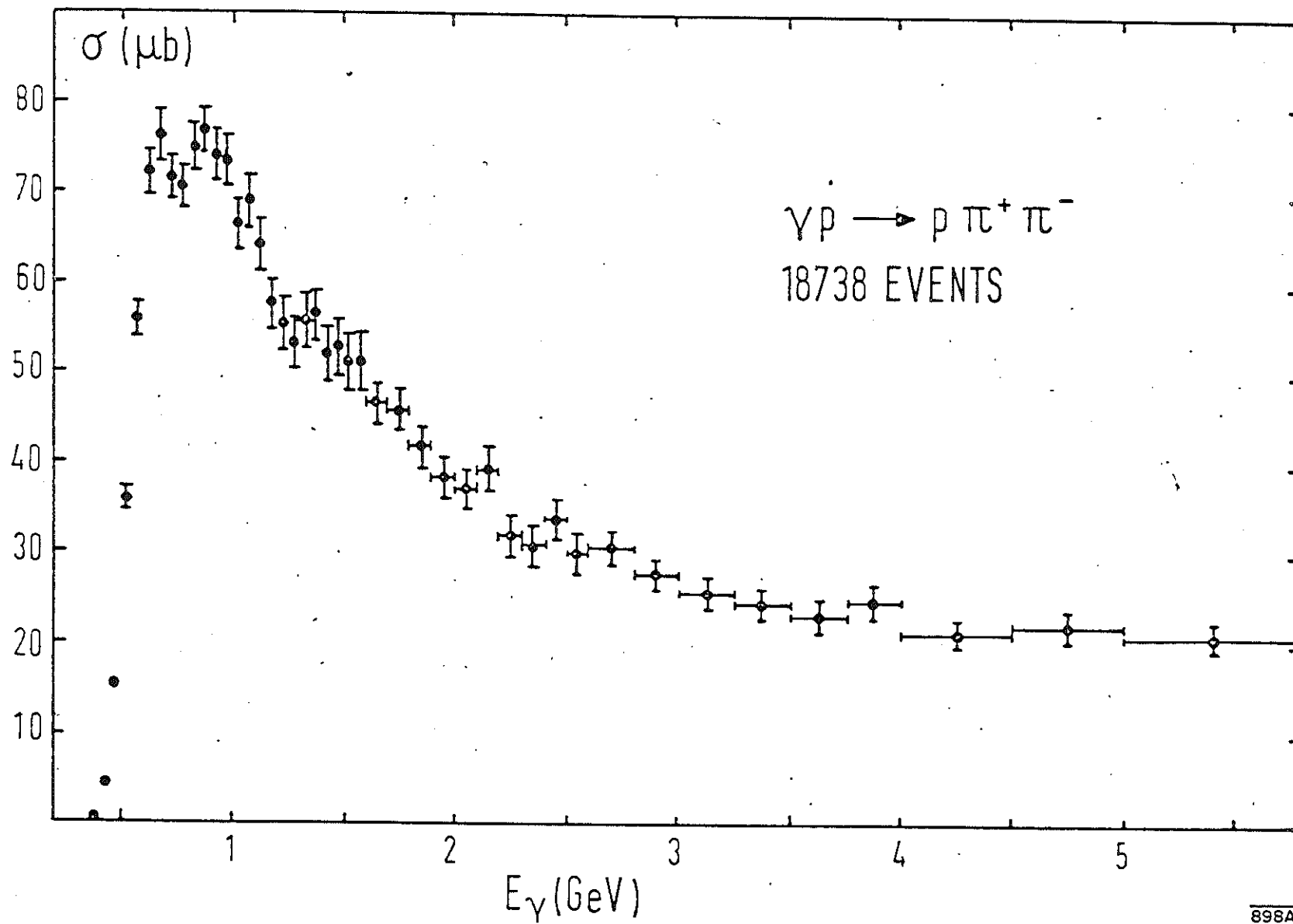
A^{++} : Amplitude for $\gamma p \rightarrow \Delta^{++} \pi^-$

$\sigma(\gamma p \rightarrow \Delta^0 \pi^+) = |A^0|^2 / |A^{++}|^2 \cdot \sigma(\gamma p \rightarrow \Delta^{++} \pi^-)$

Below: Phase angle ϕ between the Δ^0 and the Δ^{++} amplitude at resonance (see text) as a function of the photon energy E_γ .

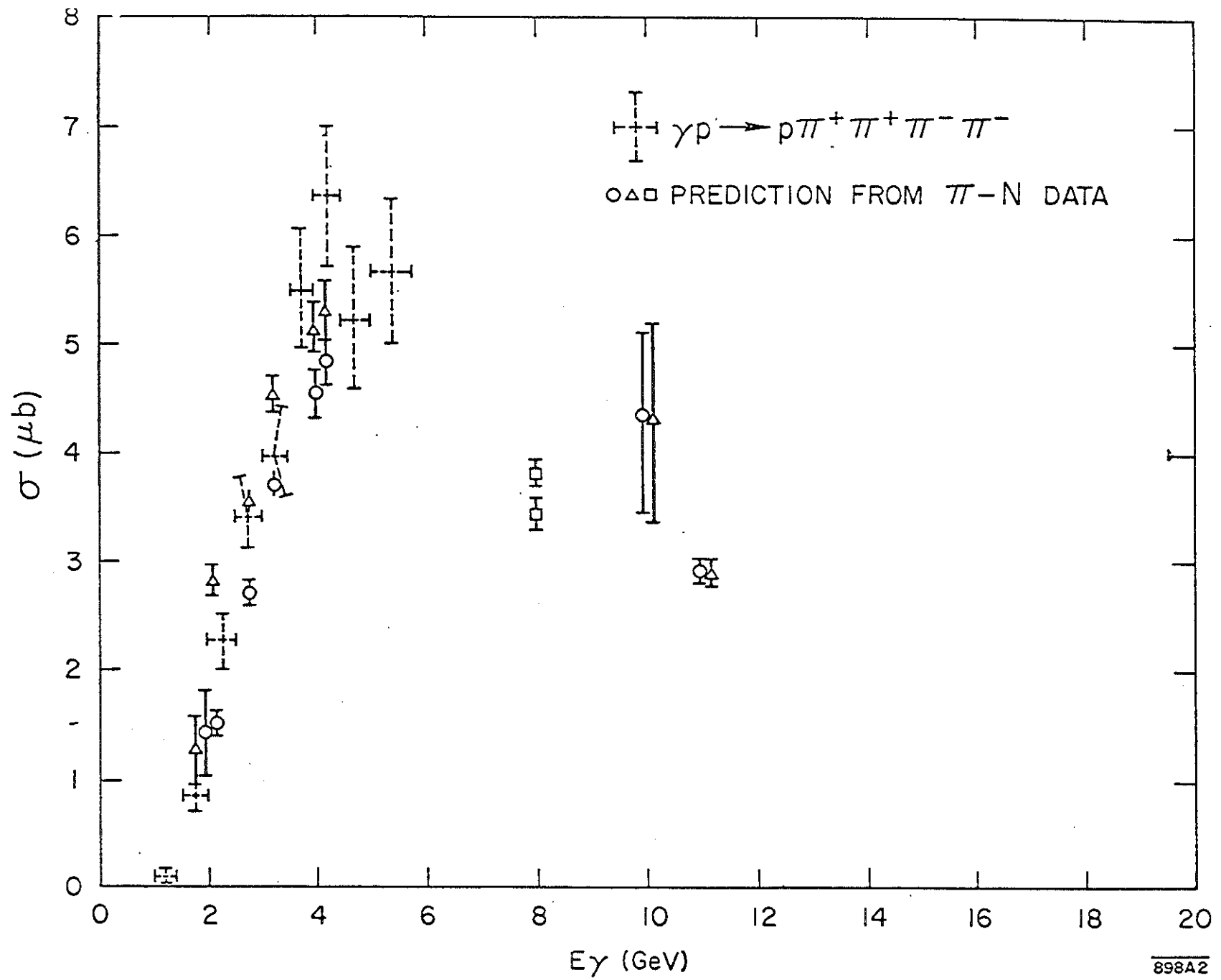
Fig. 35 Laboratory momentum distribution of spectator protons from the reaction $\gamma d \rightarrow p_s p\pi^-$. The full line is the Hulthén distribution with parameters given in the text. (Ref.2).

- Fig. 36 Laboratory angular distribution of spectator protons from the reaction $\gamma d \rightarrow p_s p \pi^-$ for different intervals of spectator momentum (Ref.2).
- Fig. 37 Total cross section of the reaction $\gamma n \rightarrow p \pi^-$ as a function of photon energy. The full line gives the results of counter measurements²⁶, the broken line is taken from measurements of the symmetric reaction $\gamma p \rightarrow n \pi^+$.²⁷ (Ref.2).
- Fig. 38 Distribution of the $(n \pi^-)$ invariant mass from the reaction $\gamma n \rightarrow n \pi^+ \pi^-$ for two intervals of photon energy. The distribution was fitted by a combination of Lorentz-invariant phase space and a Breit-Wigner resonance for the Δ^- . The dashed curve shows the phase space, the full curve gives the sum of both contributions (Ref.2).
- Fig. 39 Distribution of the $(\pi^+ \pi^-)$ invariant mass from the reaction $\gamma n \rightarrow n \pi^+ \pi^-$ for photon energies between 1.4 and 2.5 GeV. The distribution was fitted by a combination of Lorentz-invariant phase space and a Breit-Wigner resonance for the ρ^0 . The dashed curve shows the phase space, the full curve gives the sum of both contributions (Ref. 2).
- Fig. 40 One of the first photoproduction events observed in the new 1 m Hydrogen Bubble Chamber at SLAC in an annihilation beam.



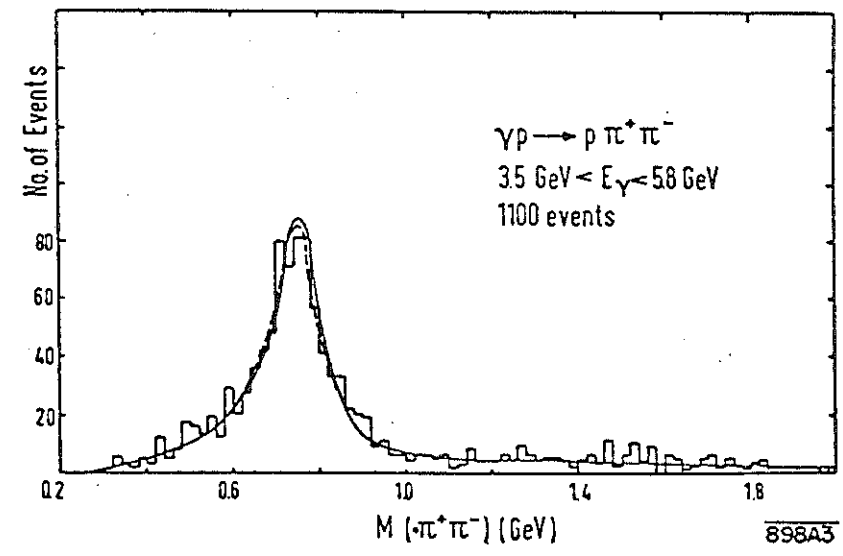
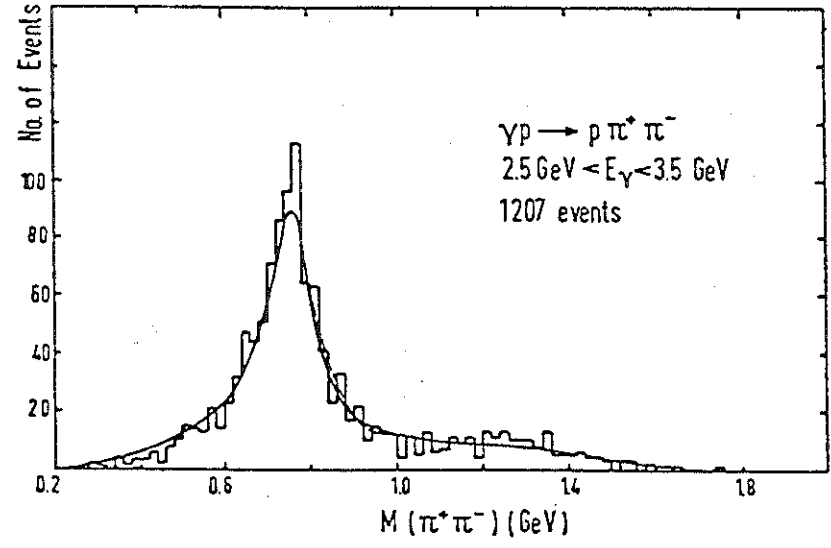
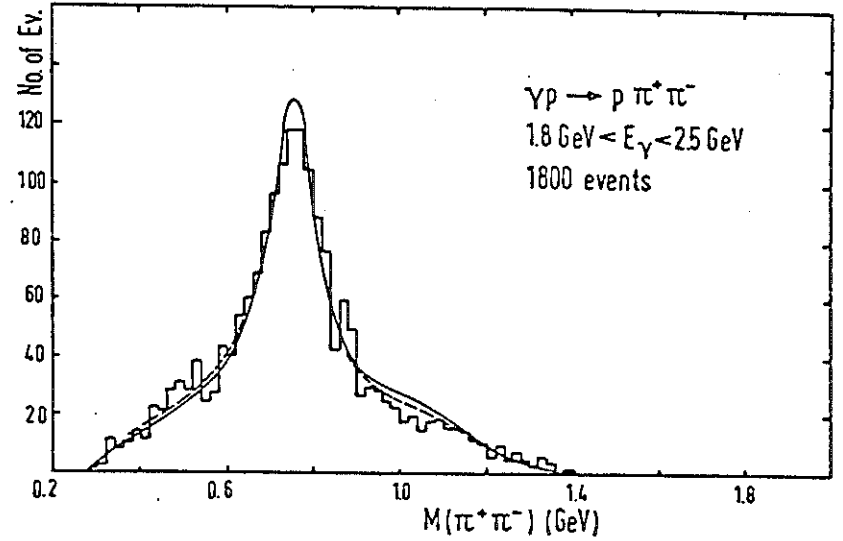
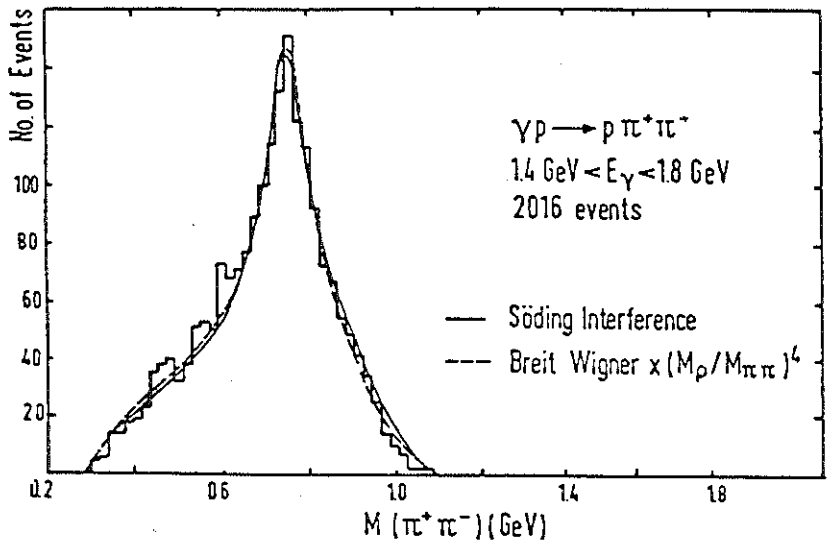
898A1

FIG. 1



898A2

FIG. 2



898A3

FIG. 3

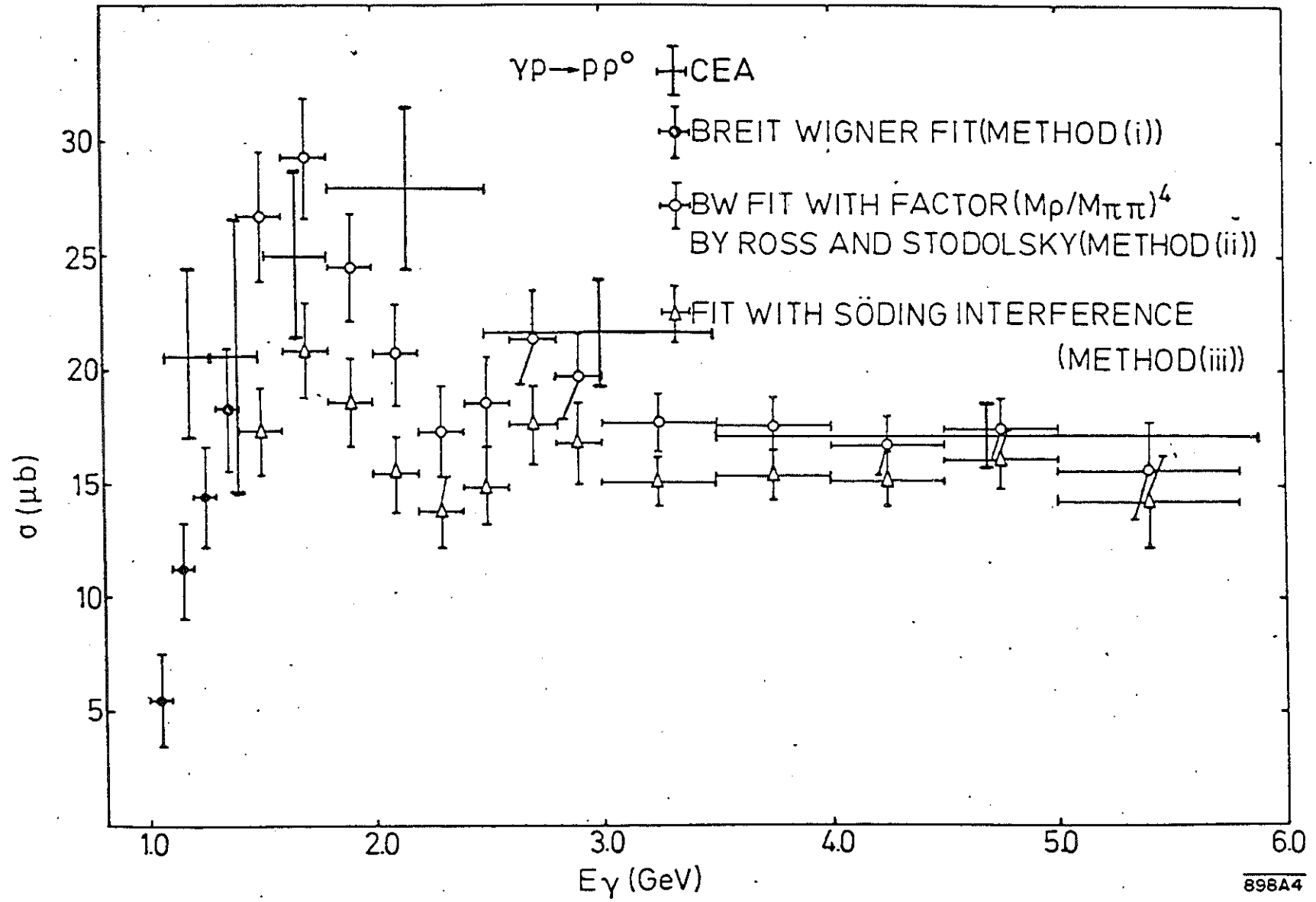
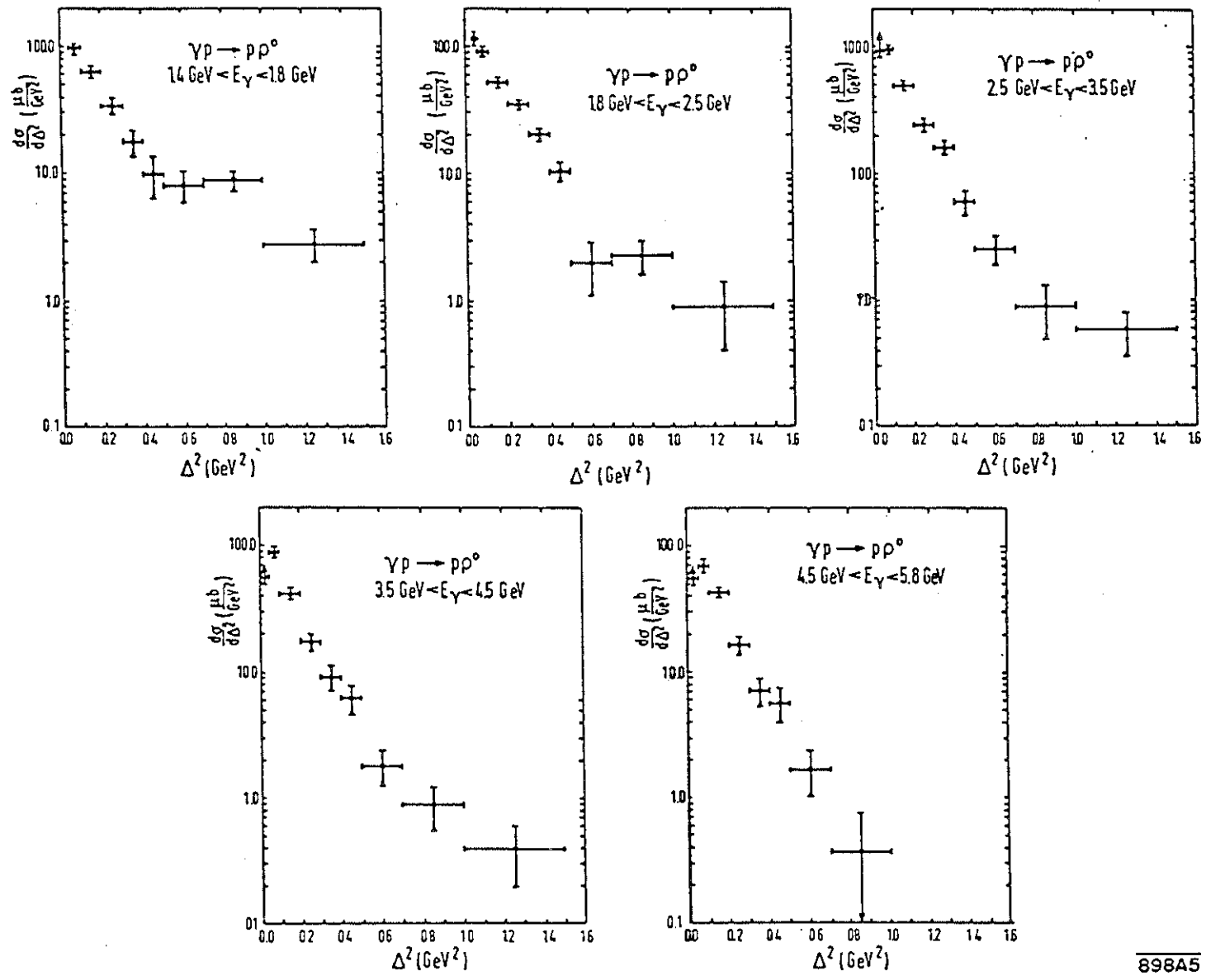


FIG. 4



898A5

FIG. 5

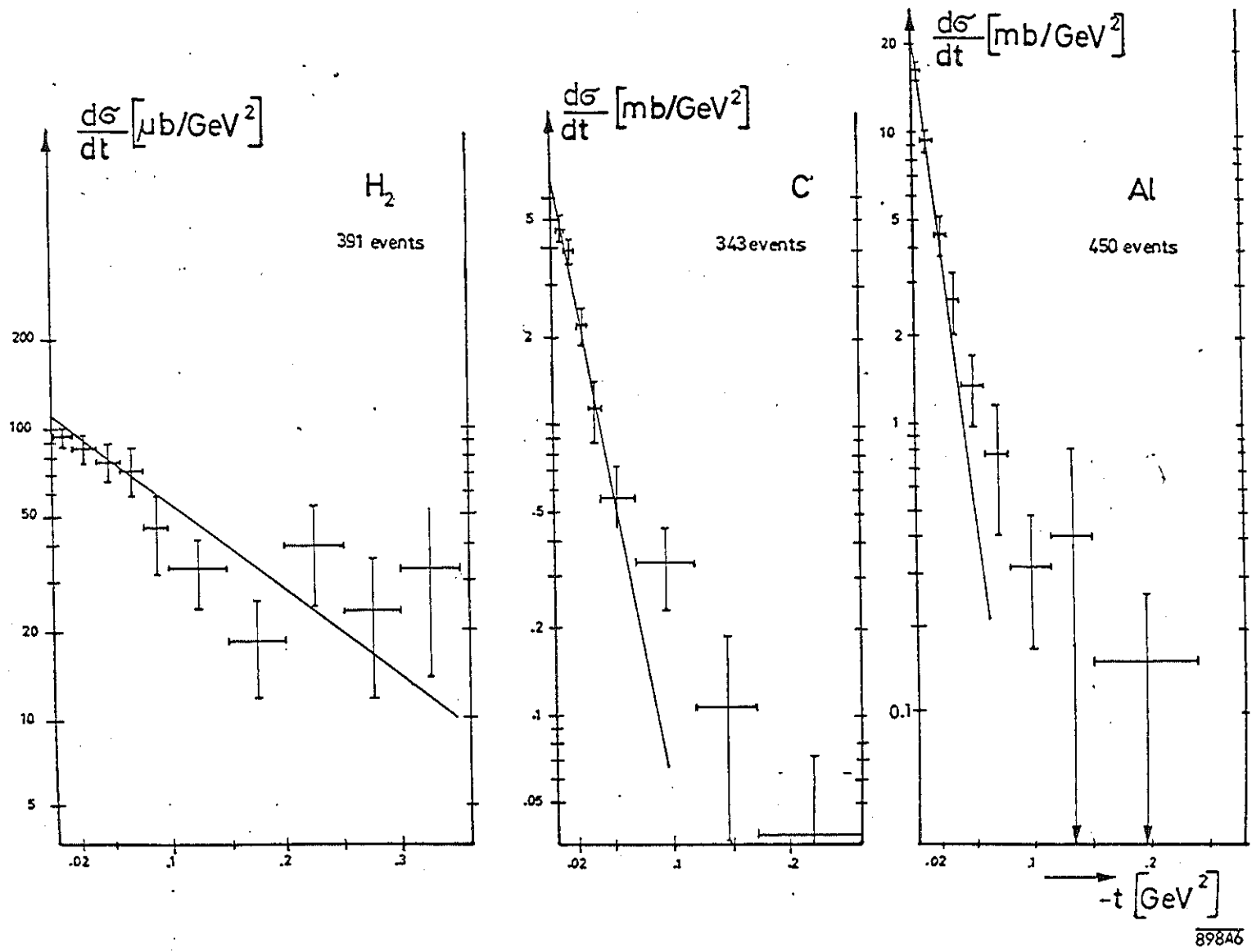
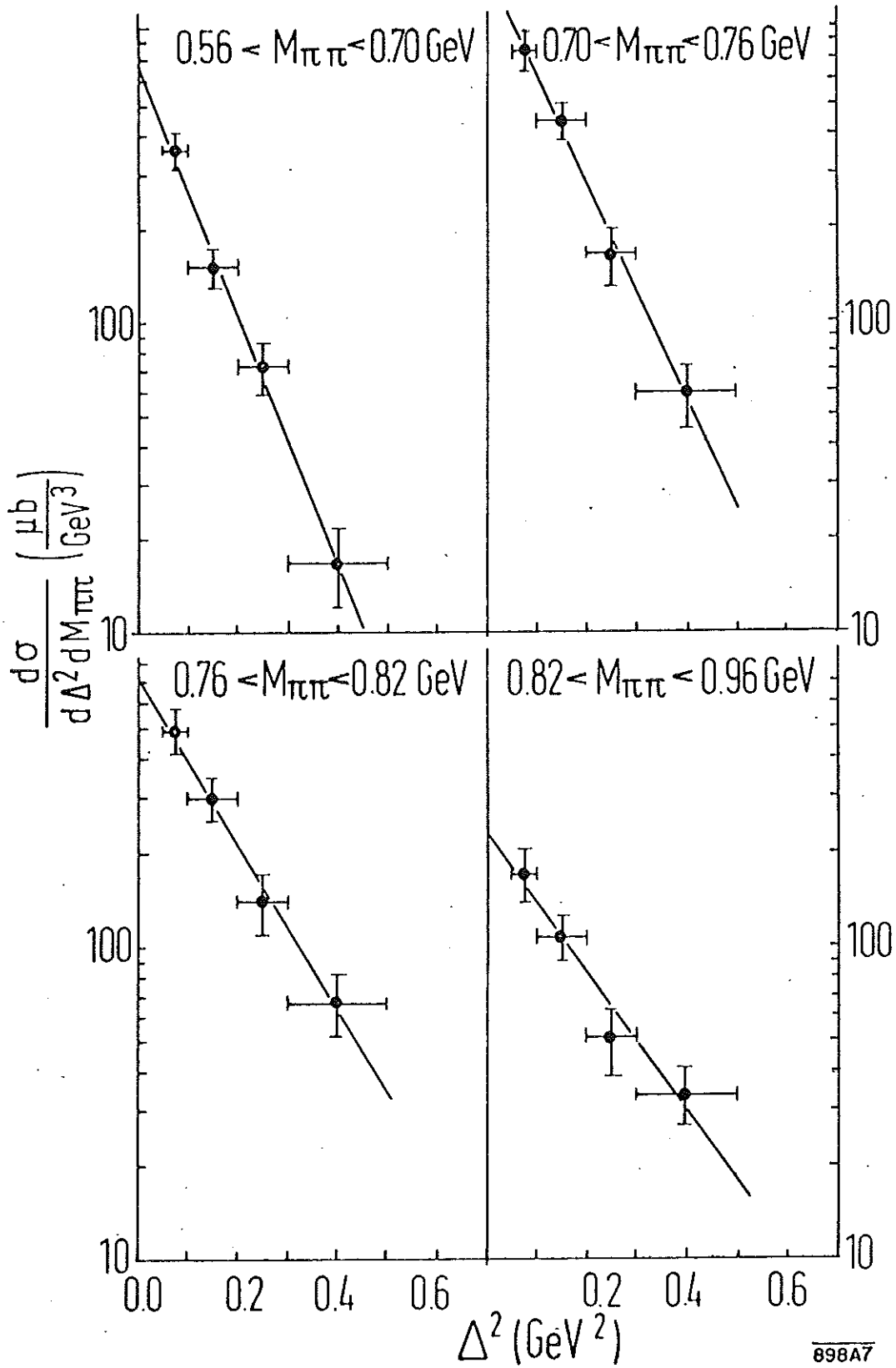


FIG. 6

$\gamma p \rightarrow p \pi^+ \pi^-$
 $3.5 \text{ GeV} < E_\gamma < 5.8 \text{ GeV}$

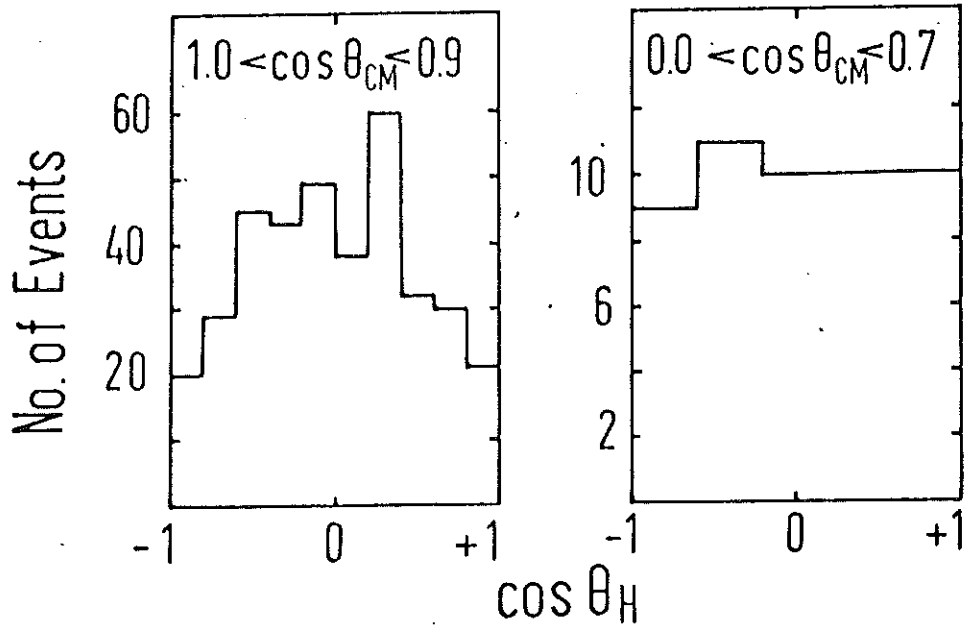


898A7

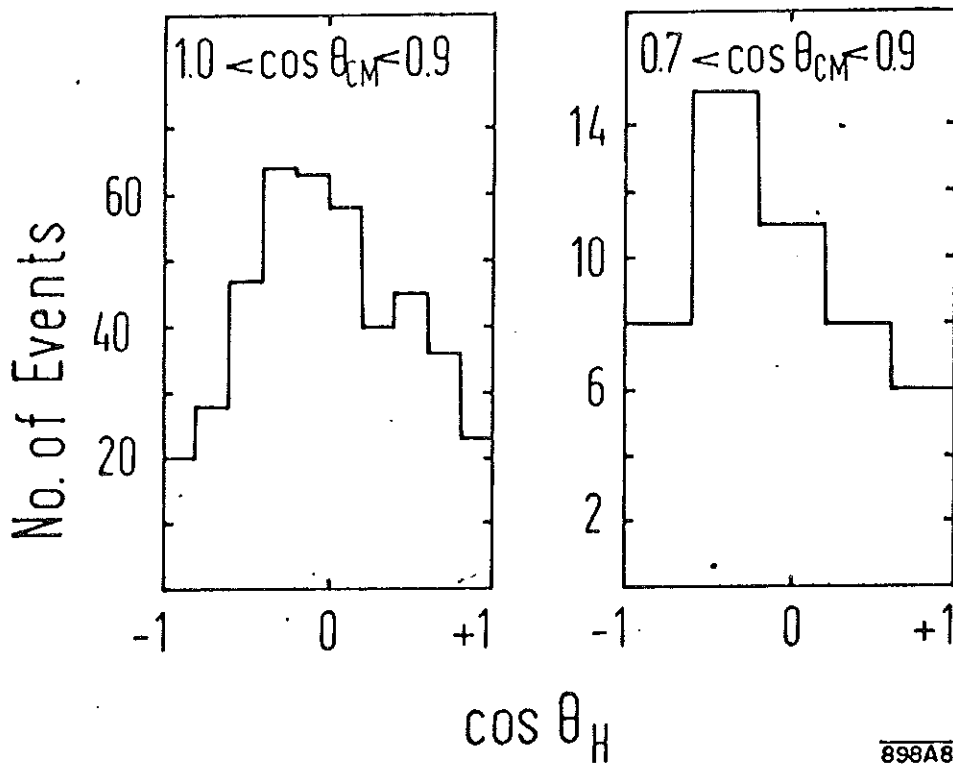
FIG. 7



$$2.5 < E_\gamma < 3.5 \text{ GeV}$$

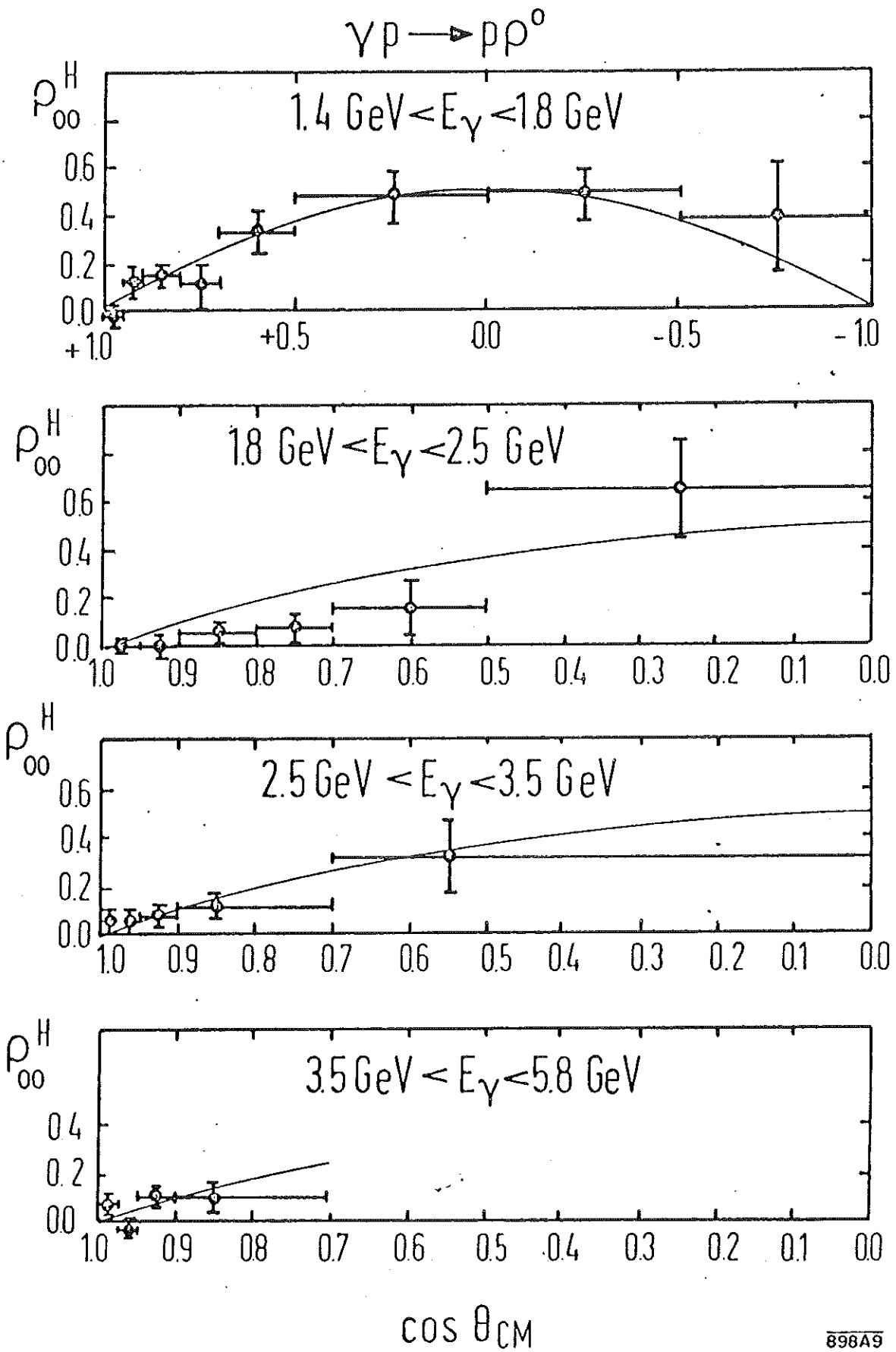


$$3.5 < E_\gamma < 5.8 \text{ GeV}$$



898A8

FIG. 8



898A9

FIG. 9

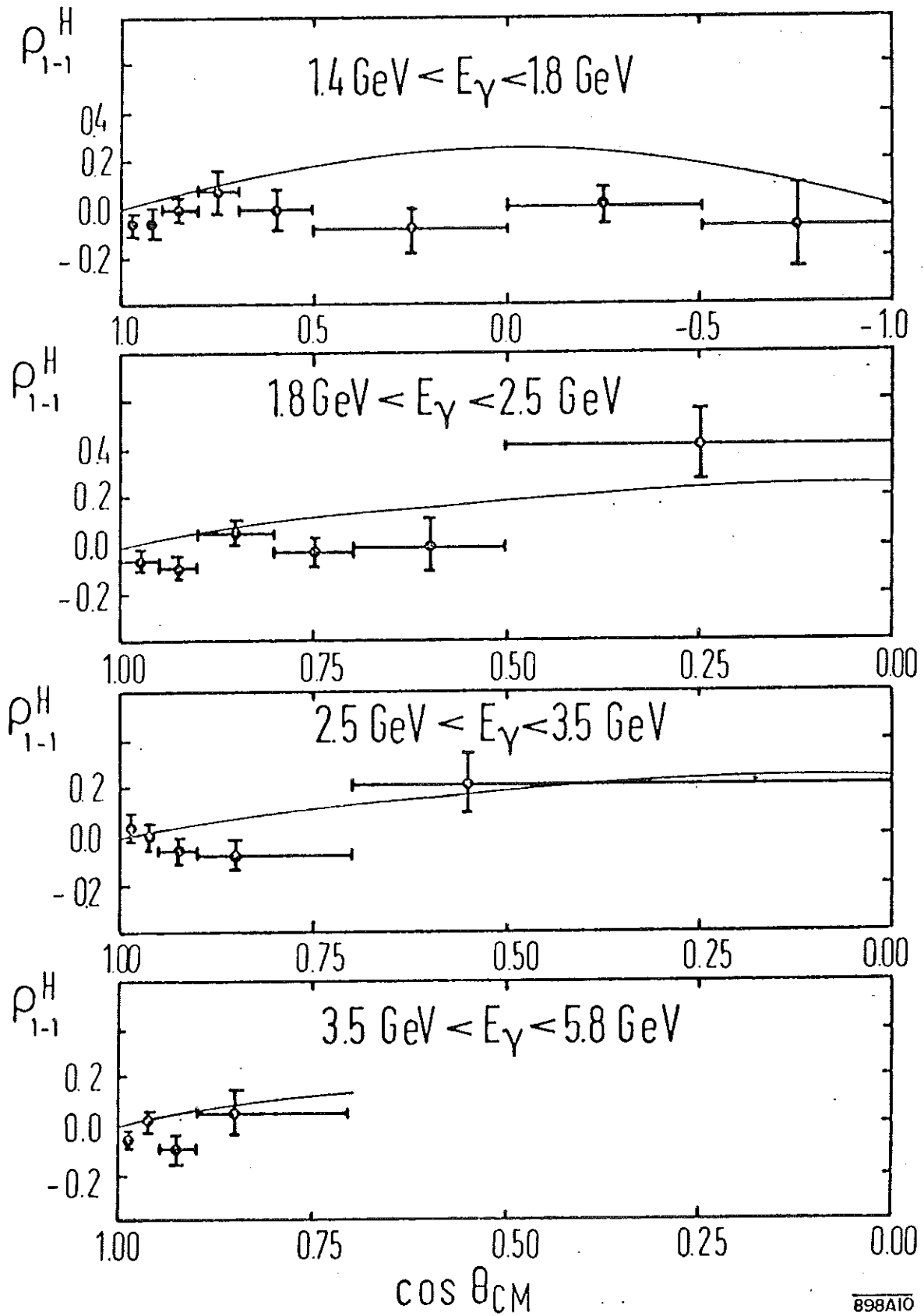


FIG. 10

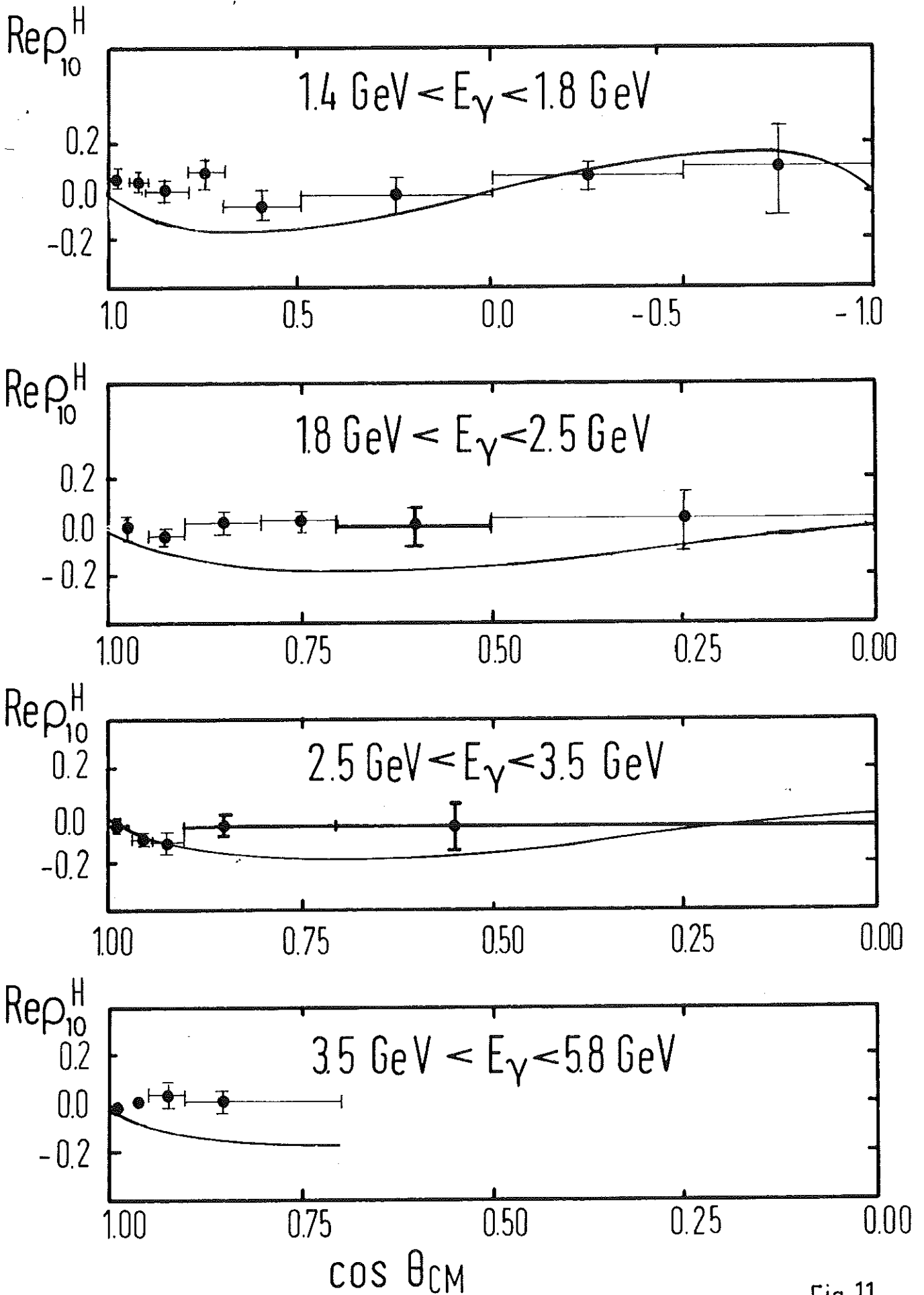


Fig.11

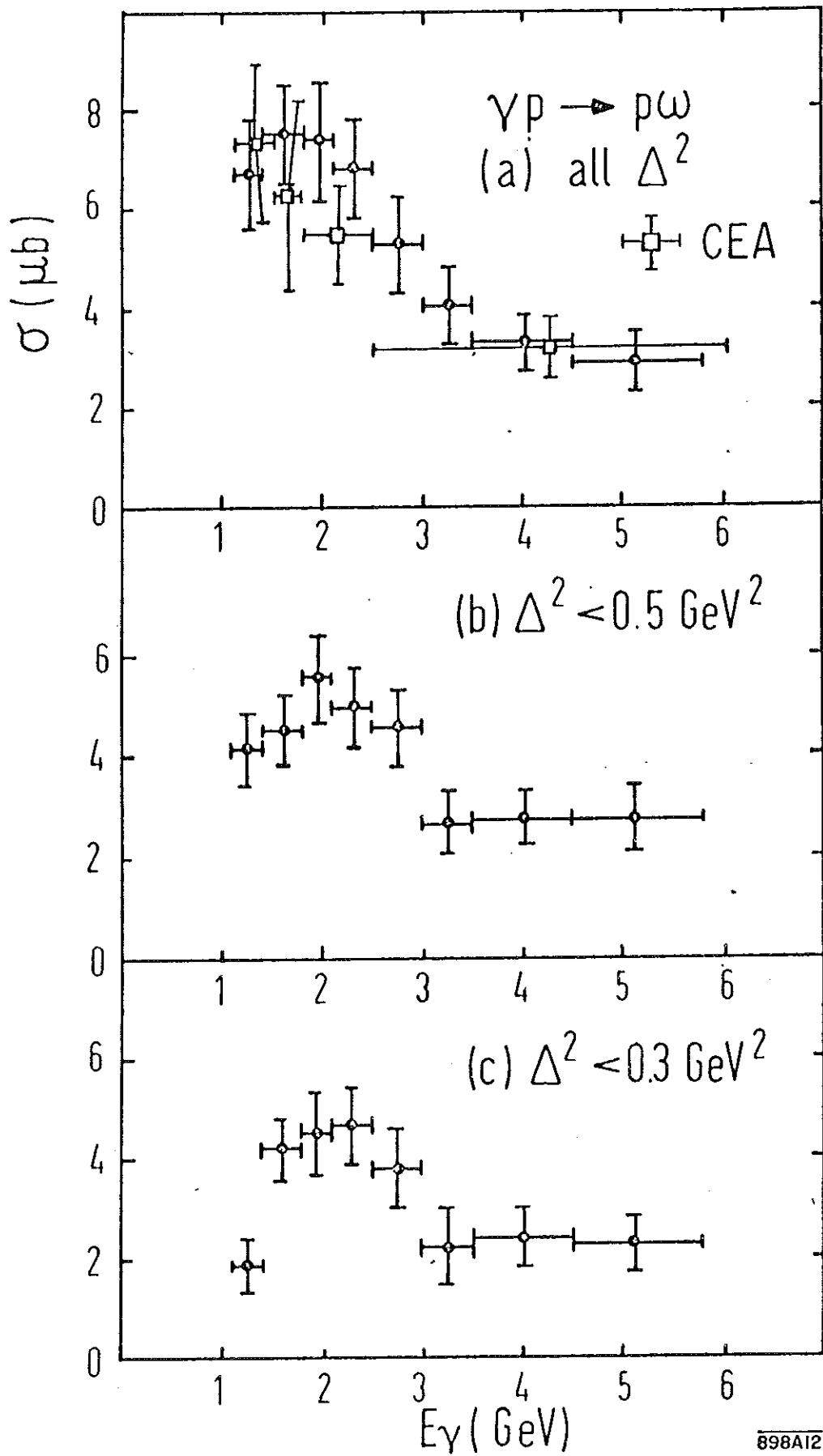


FIG. 12

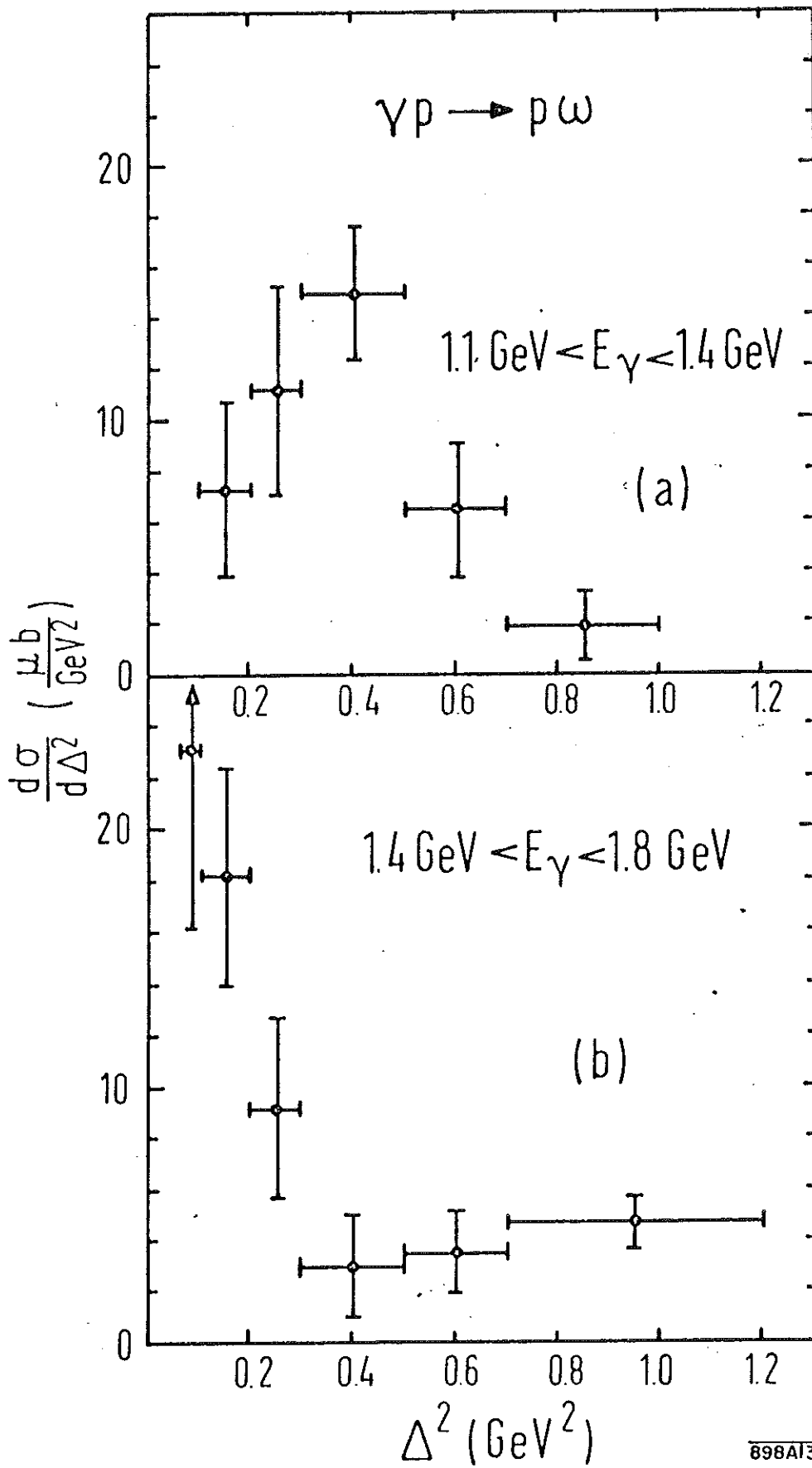


FIG. 13

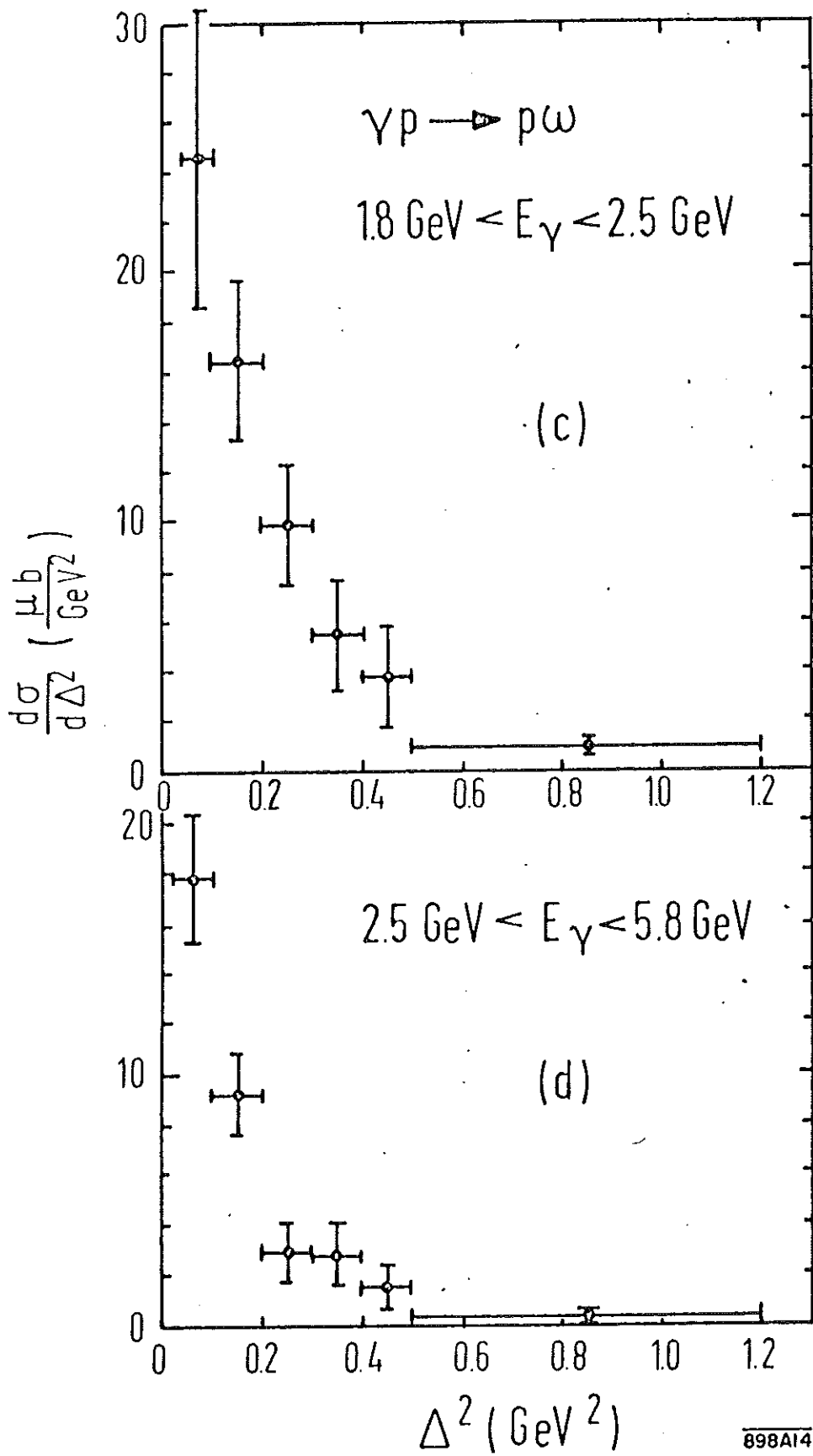


FIG. 14

898A14

$\gamma p \rightarrow p \omega$
 $1.4 \text{ GeV} < E_\gamma < 2.5 \text{ GeV}$

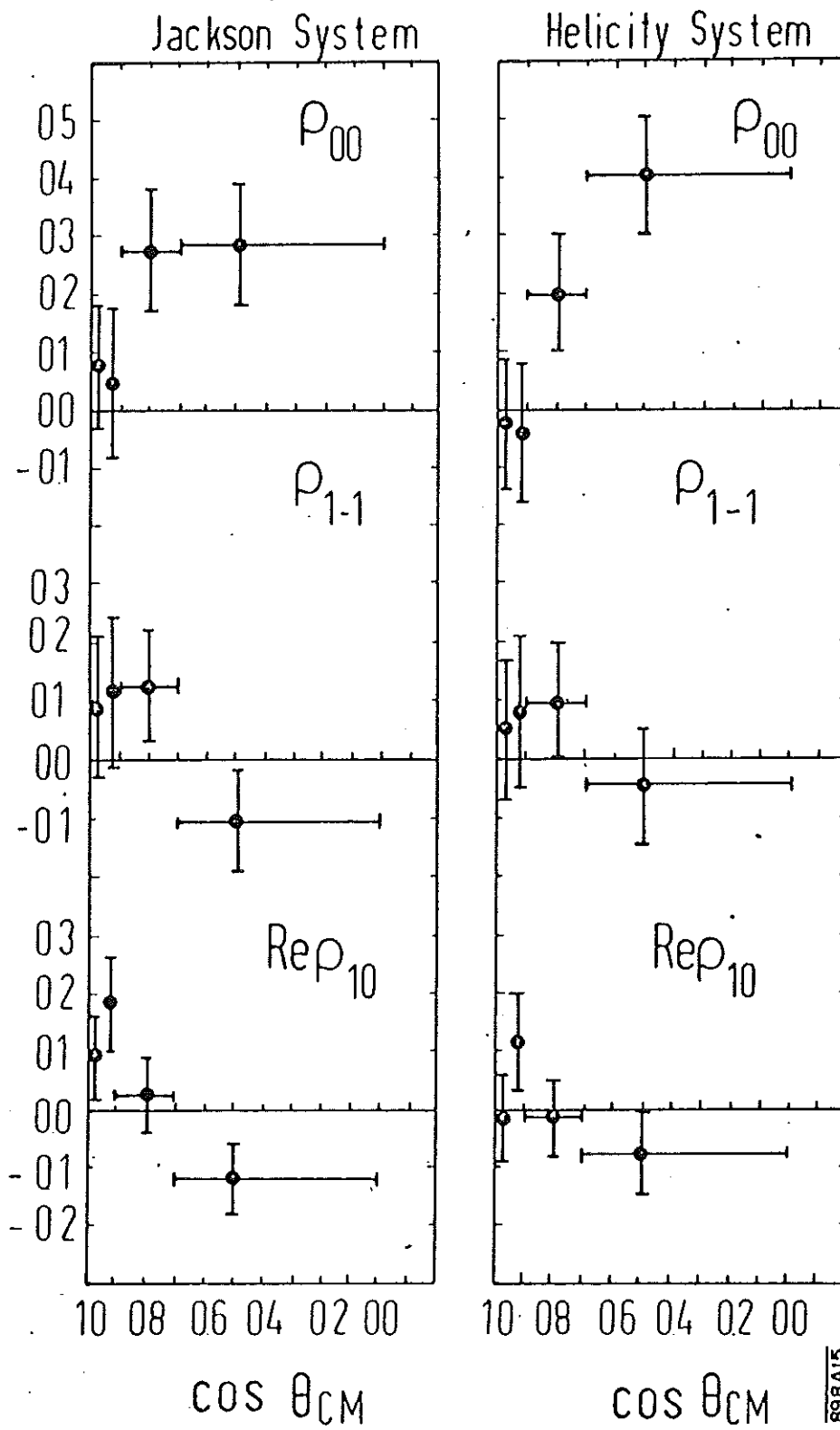


FIG. 15

898A15

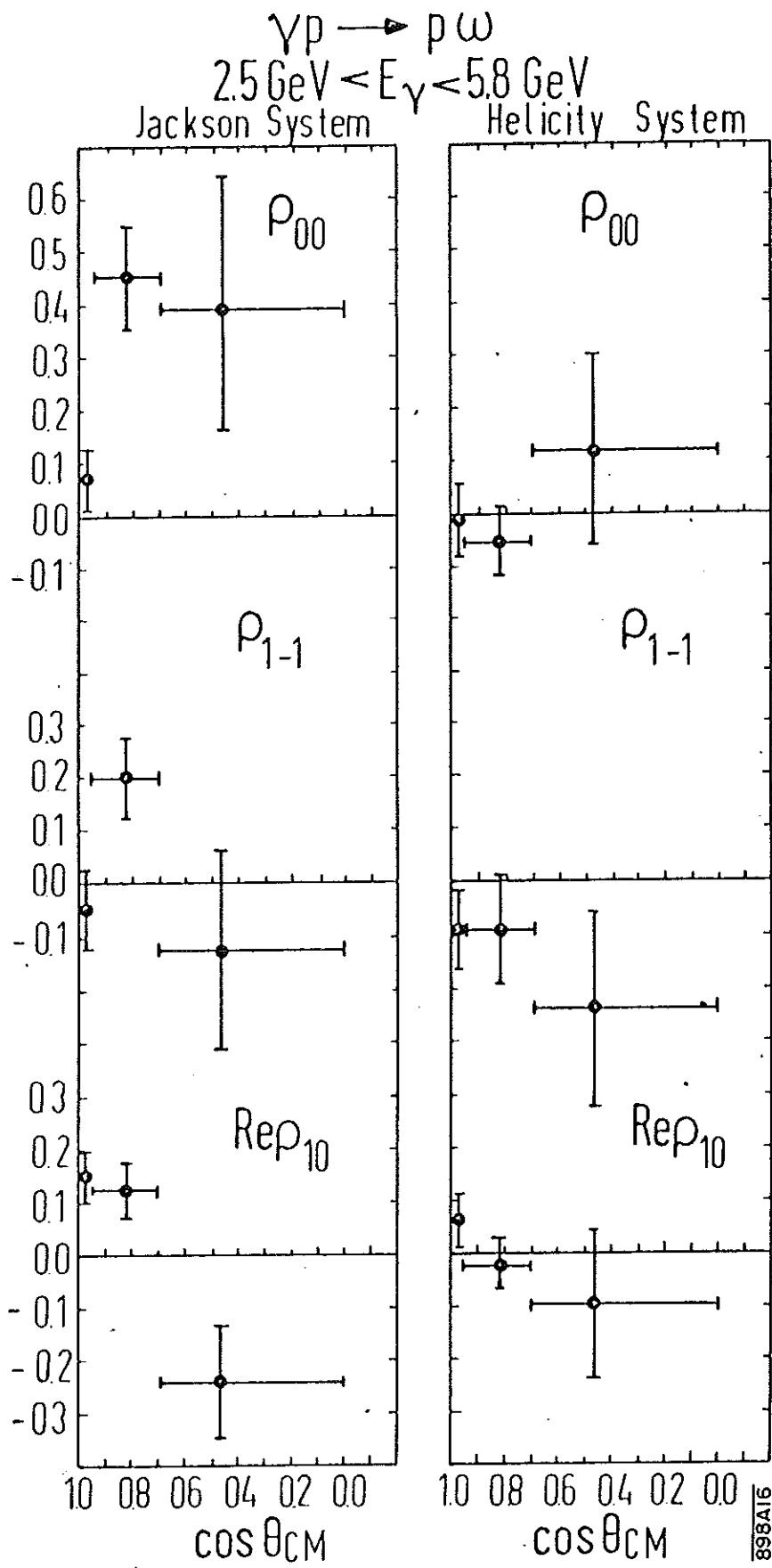


FIG. 16

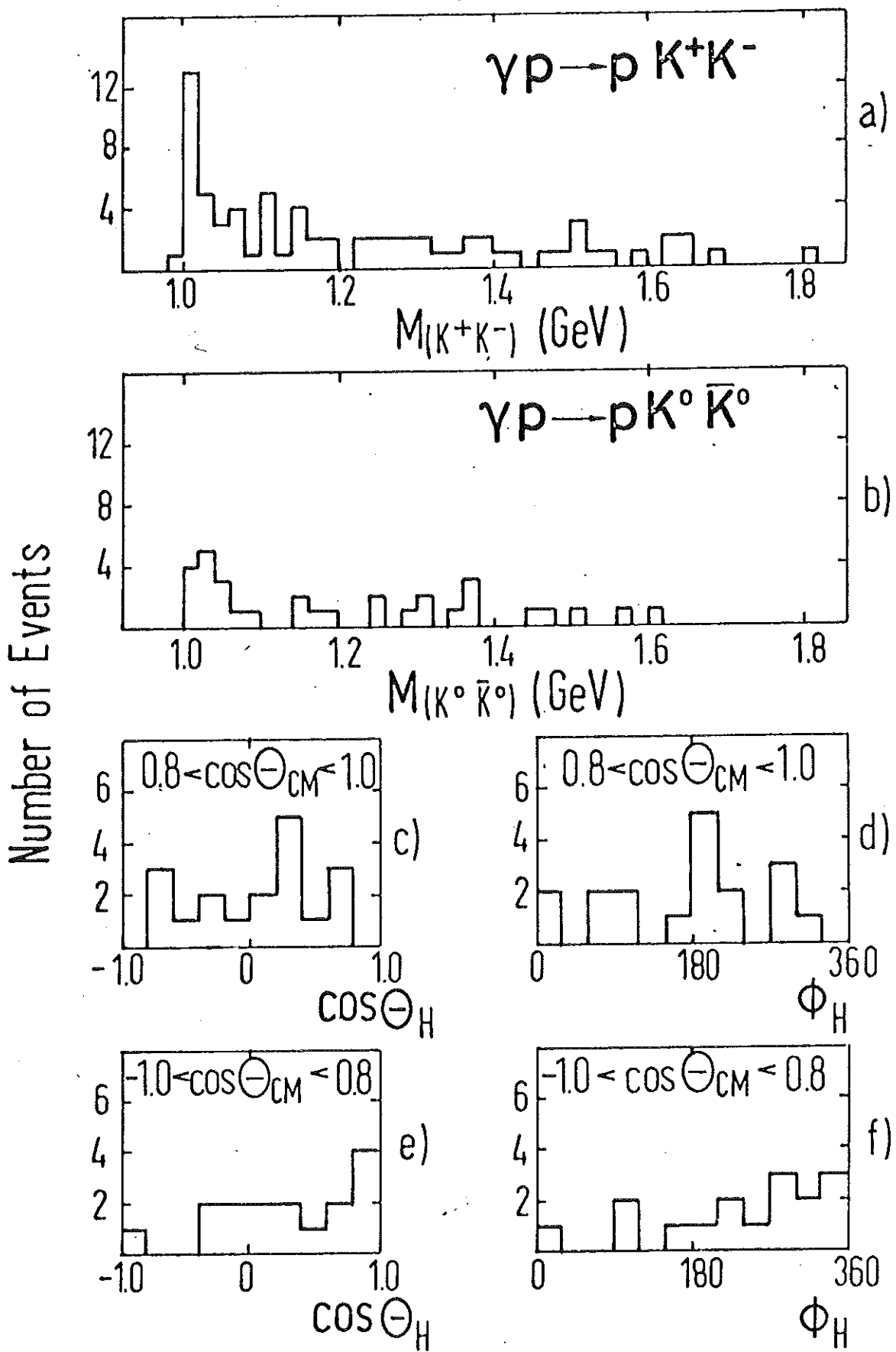


FIG. 17

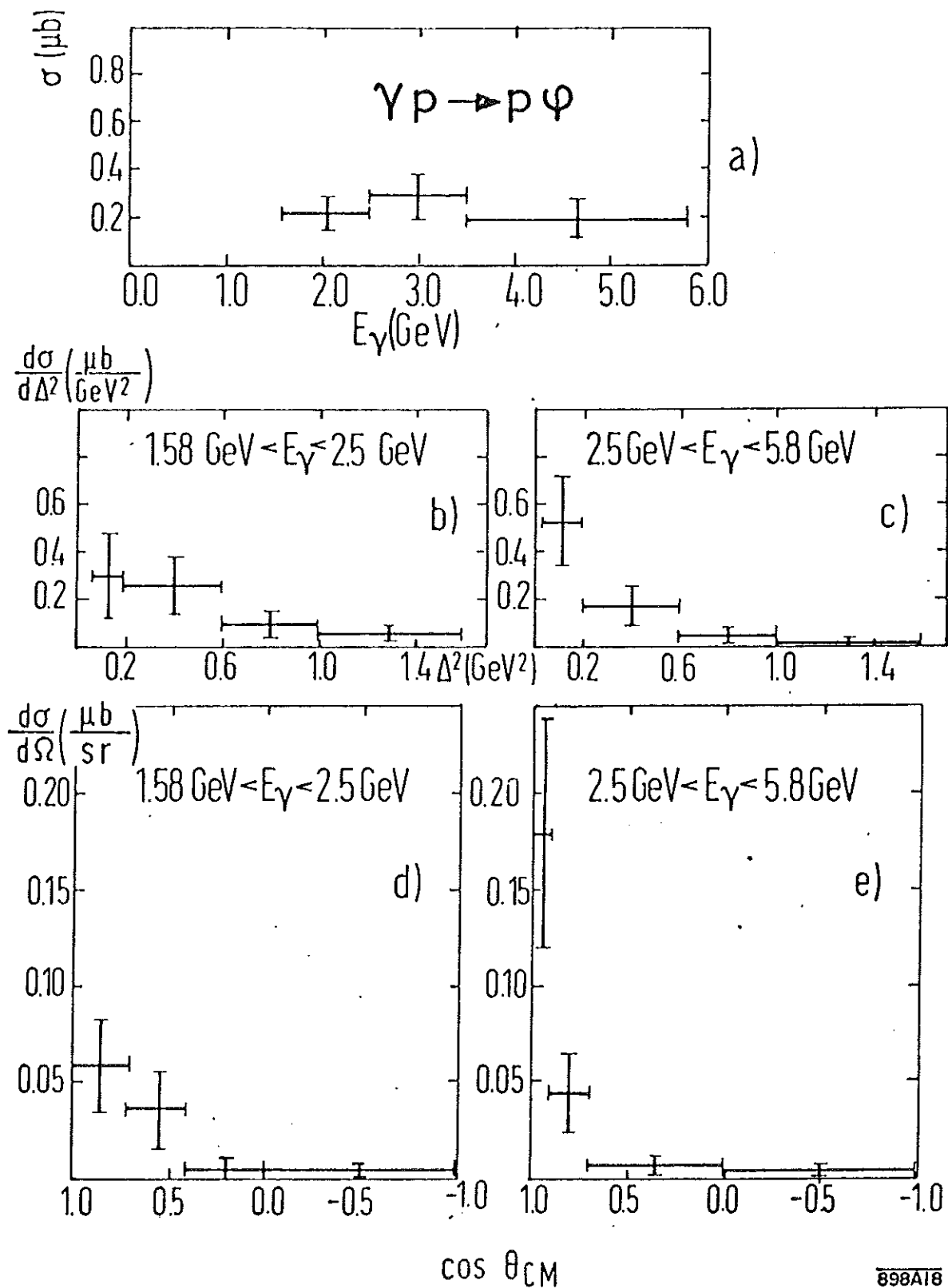
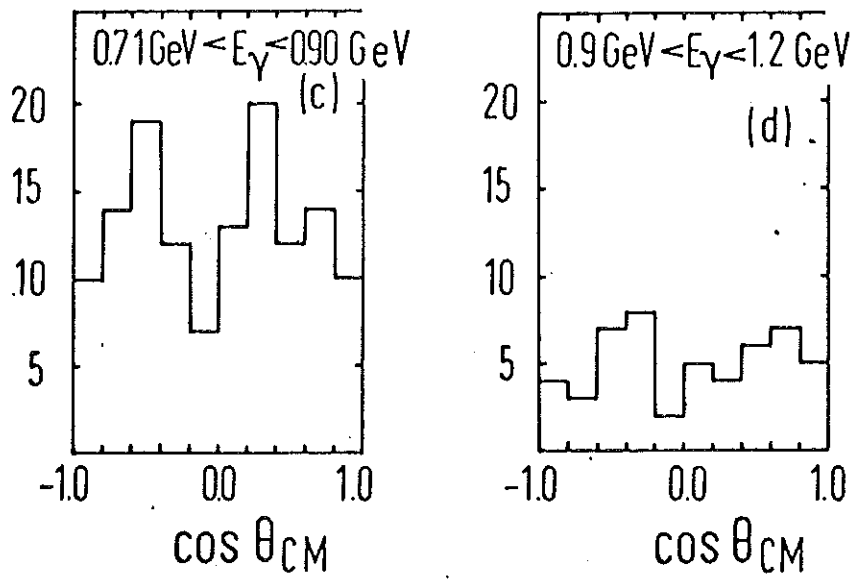
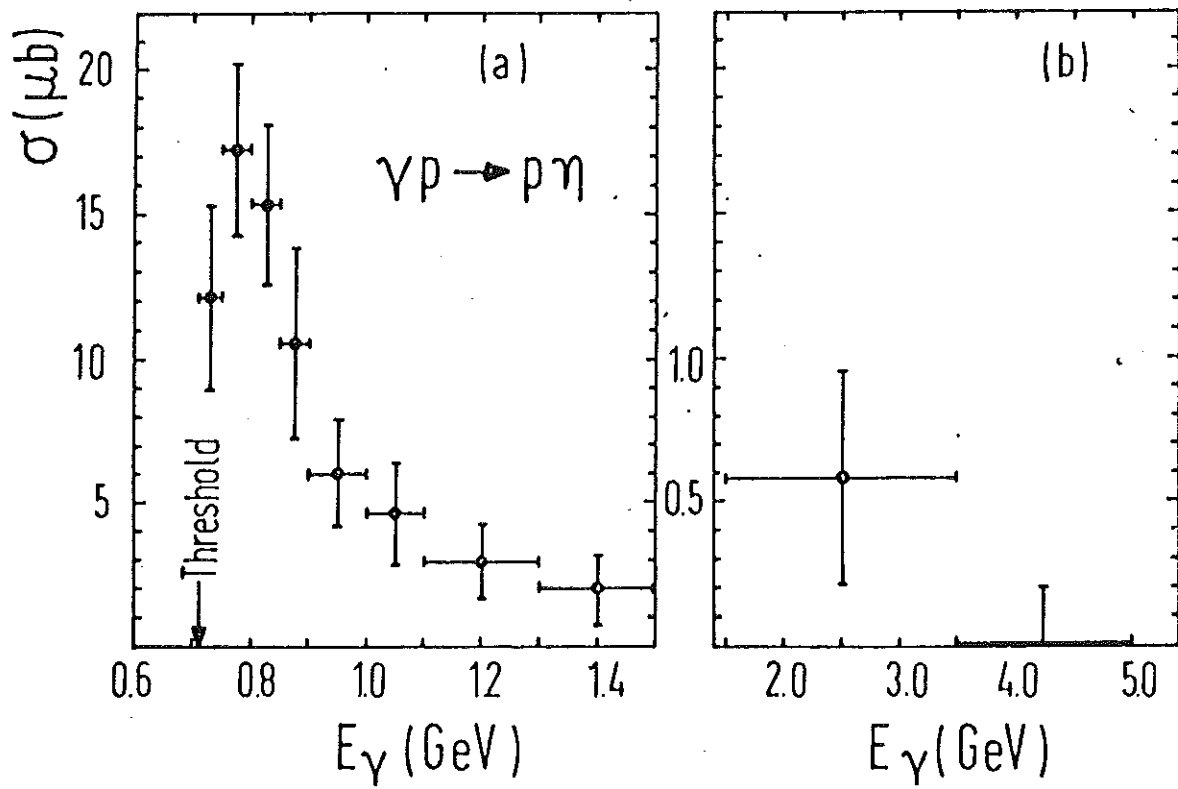
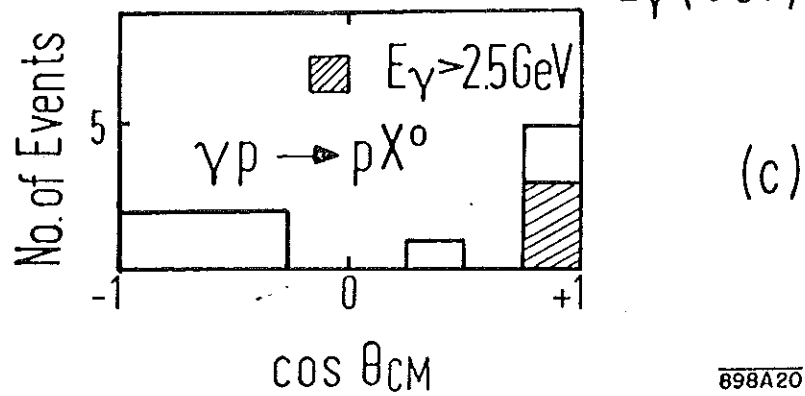
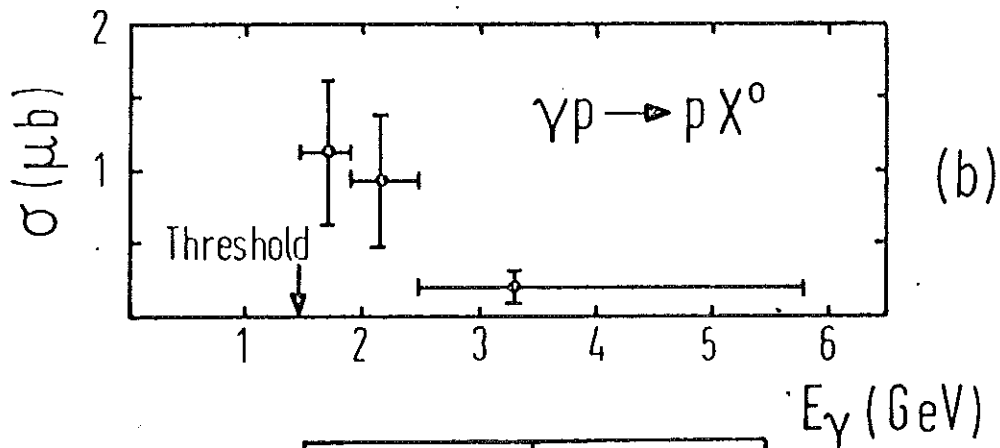
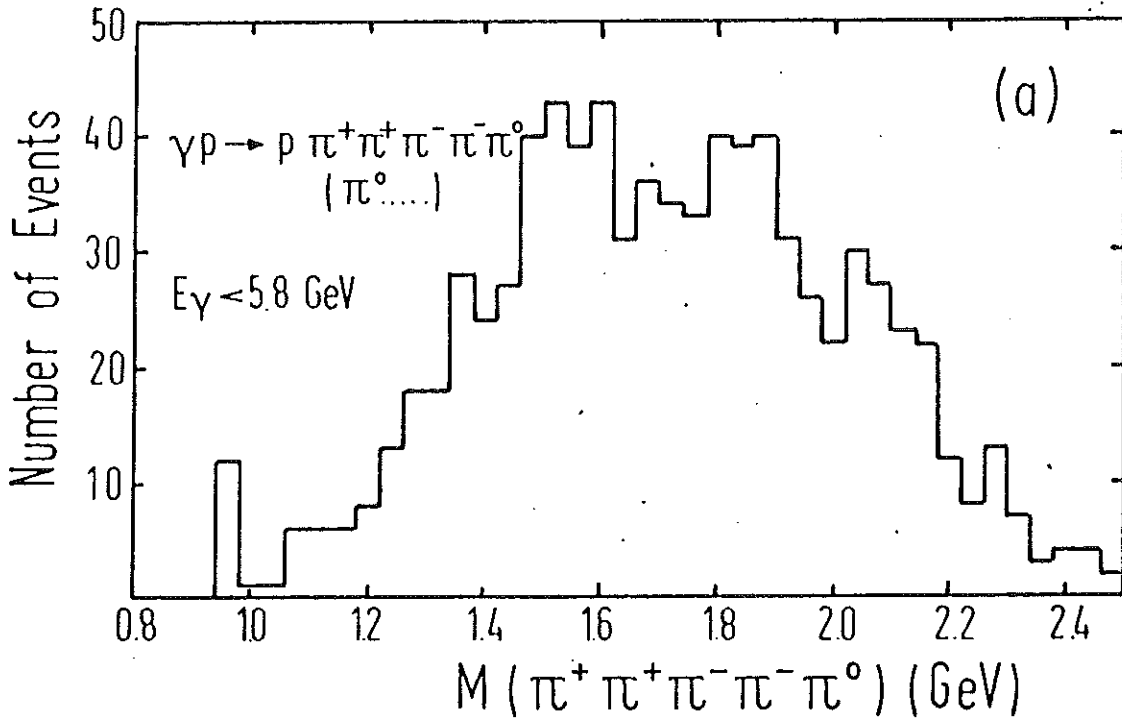


FIG. 18



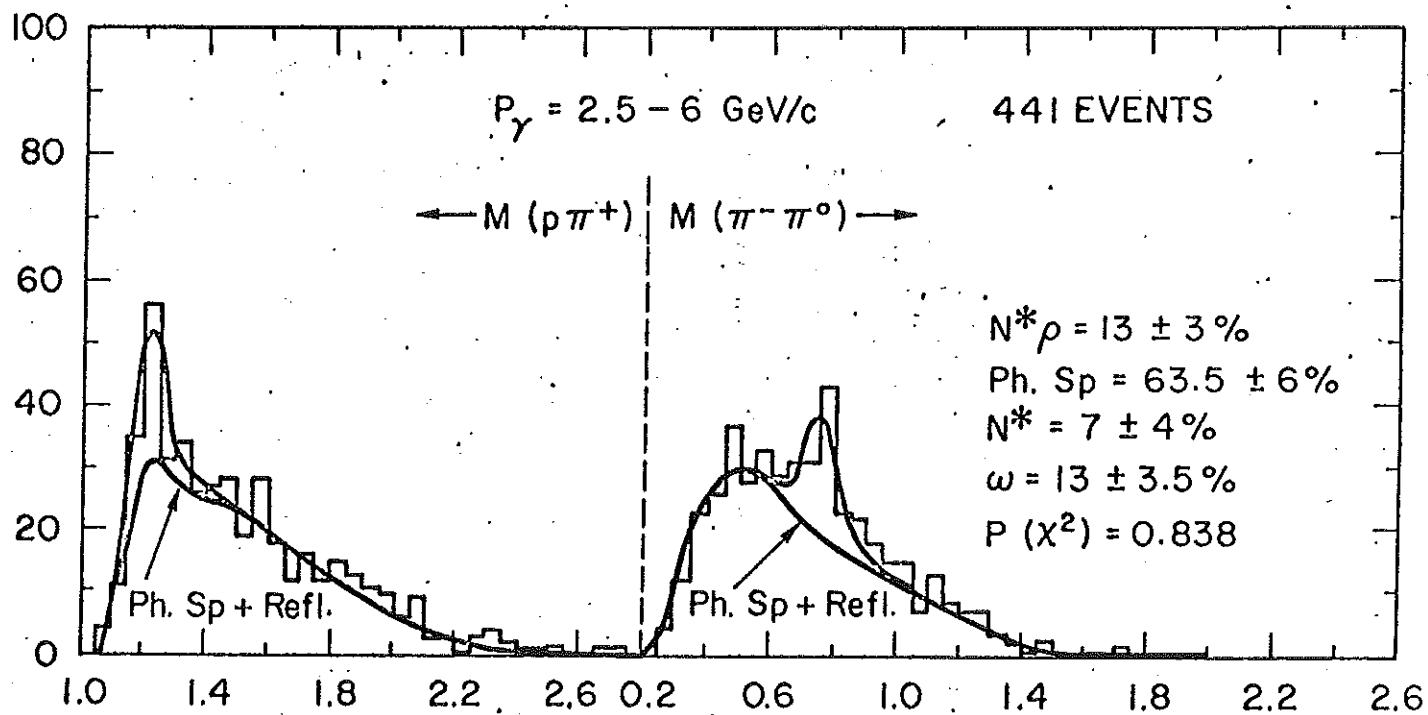
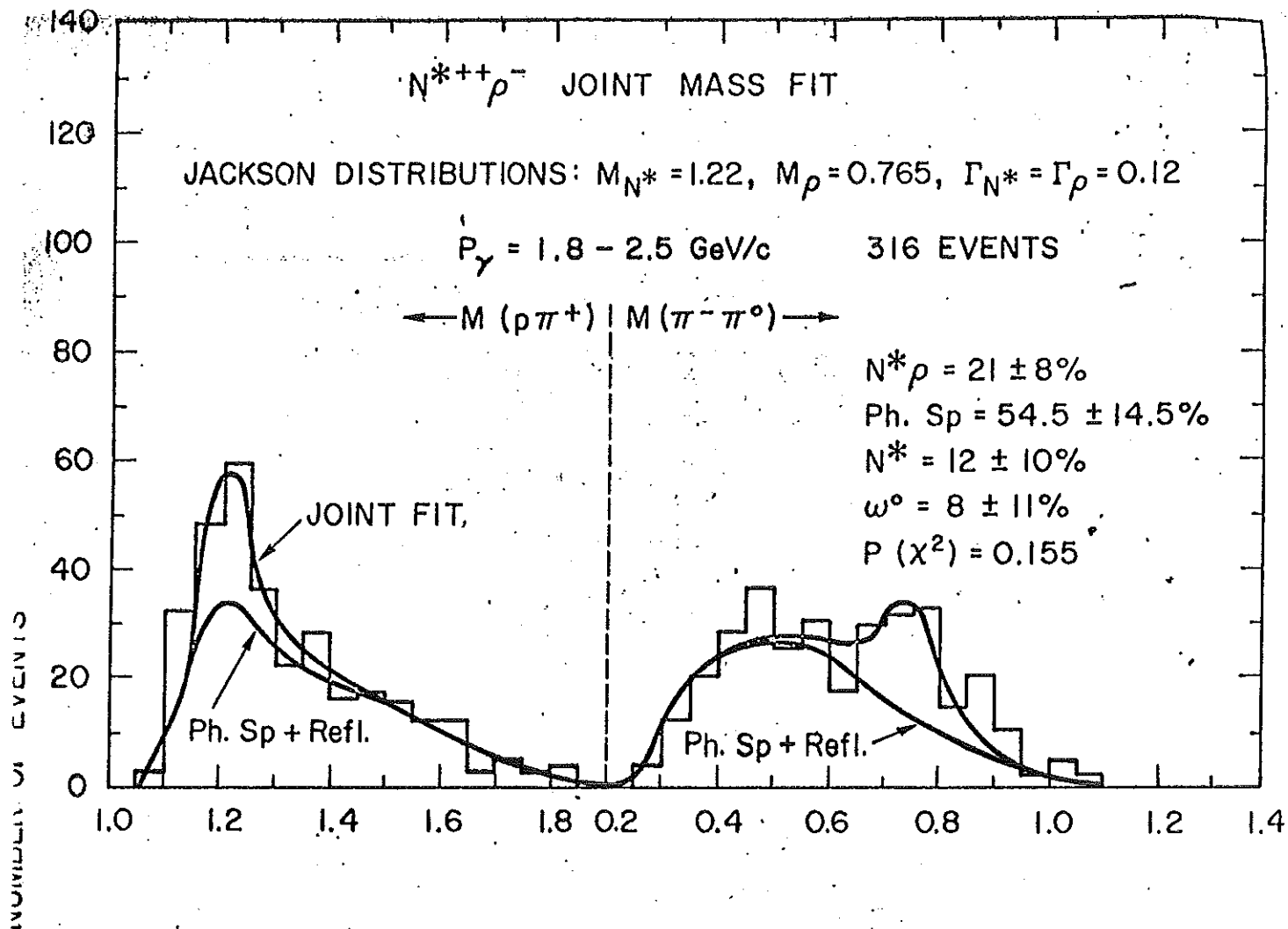
898A19

FIG. 19



898A20

FIG. 20



898A2I

FIG. 21

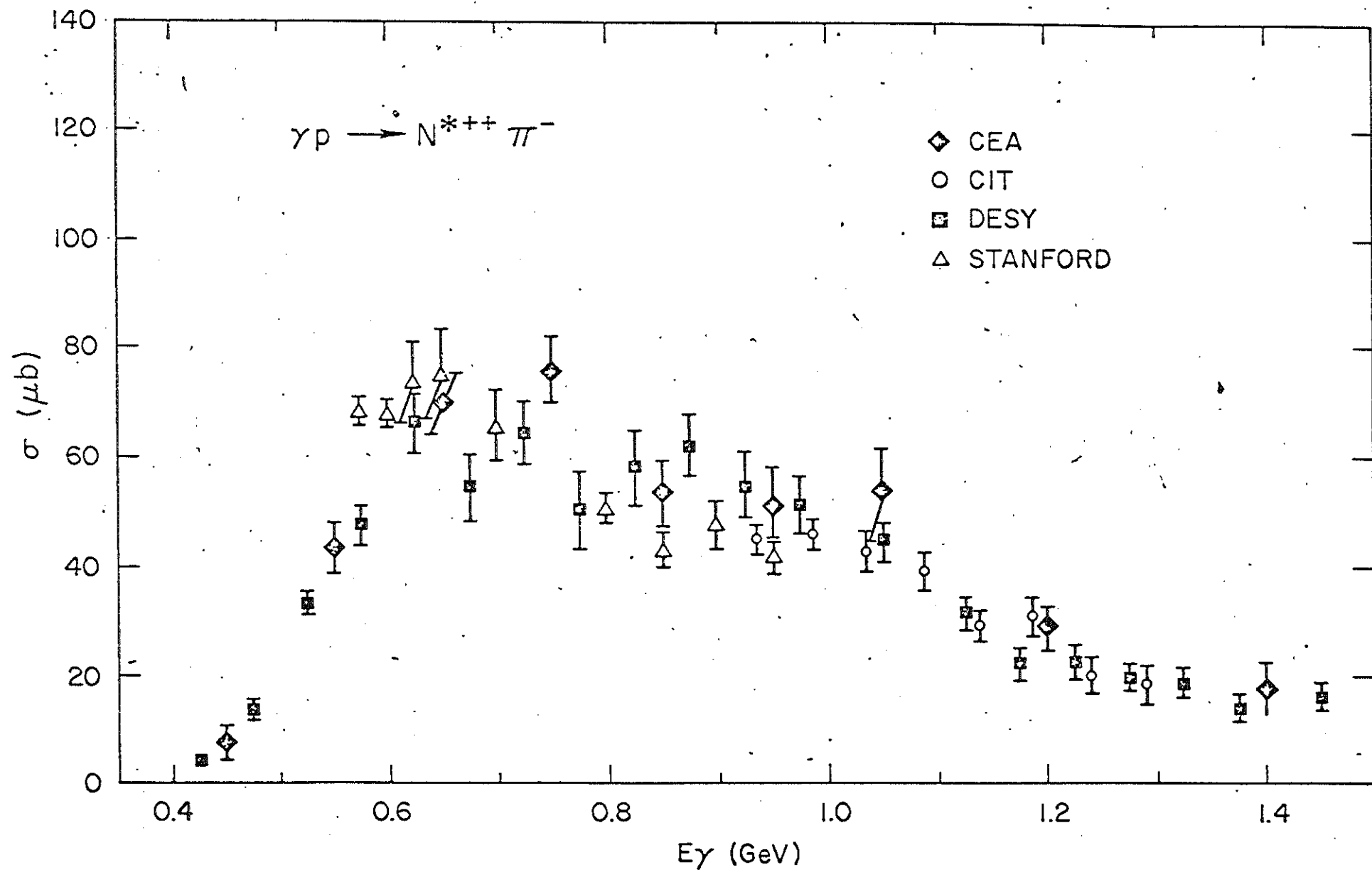


FIG. 22

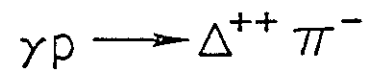
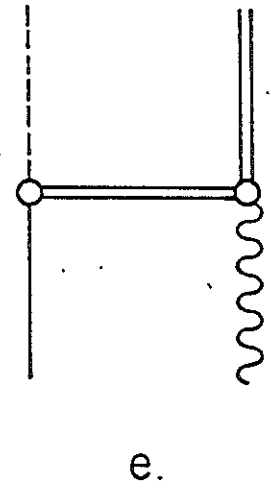
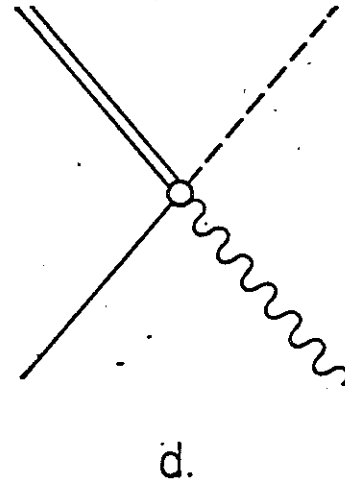
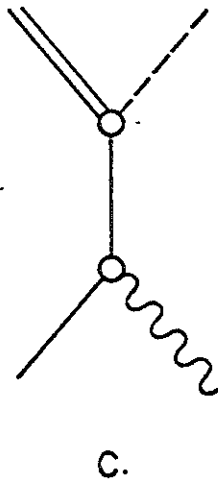
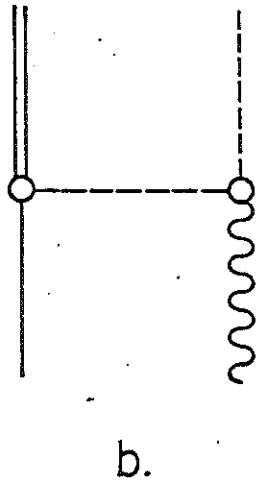
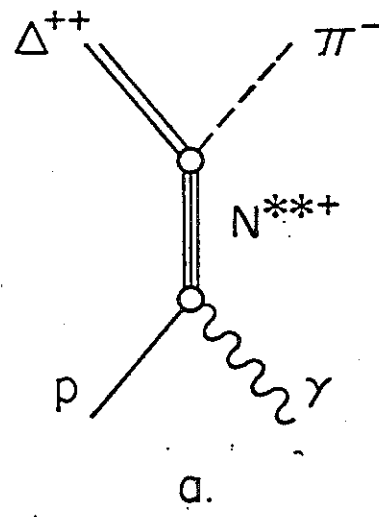


FIG. 23

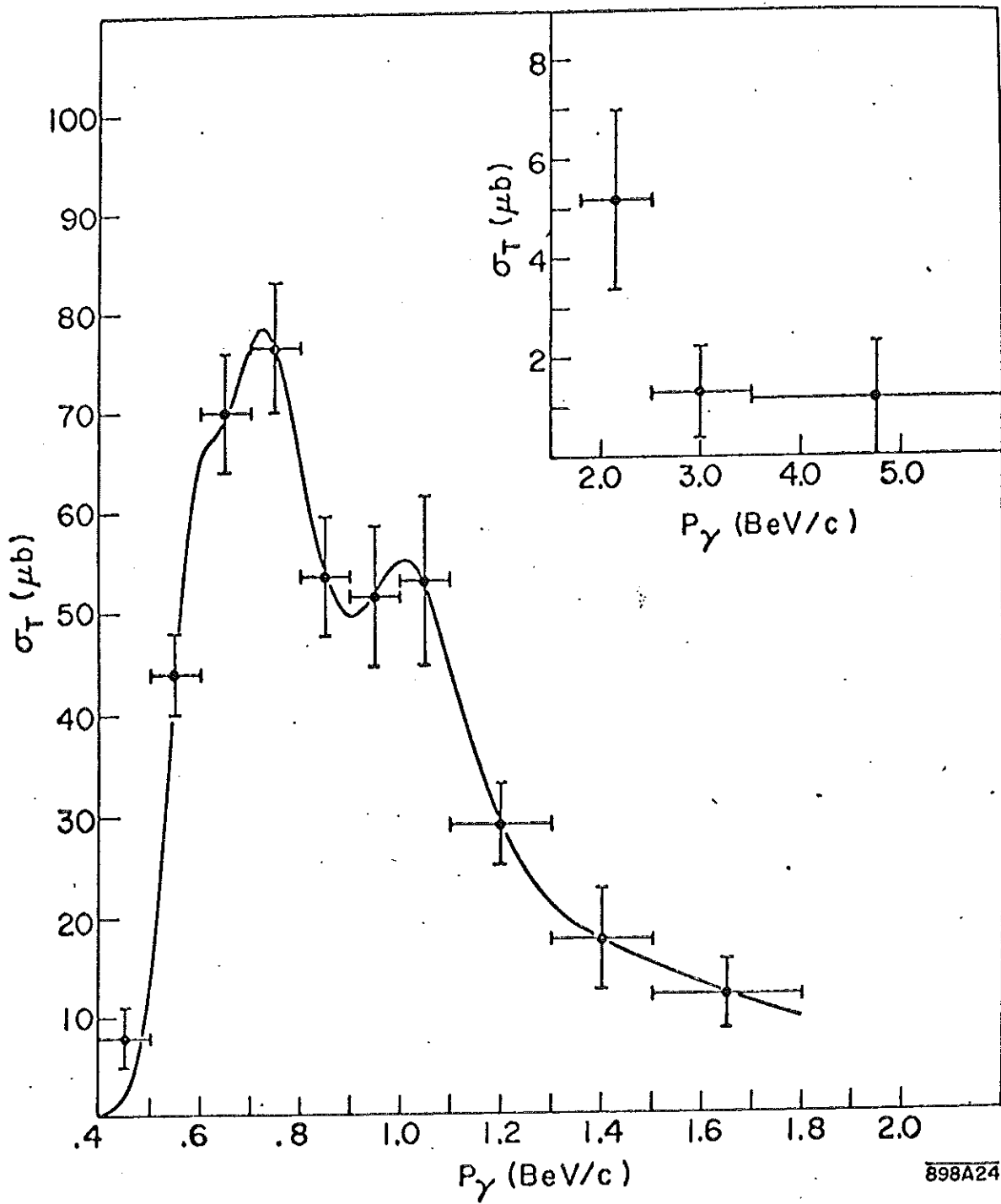


FIG. 24

898A24

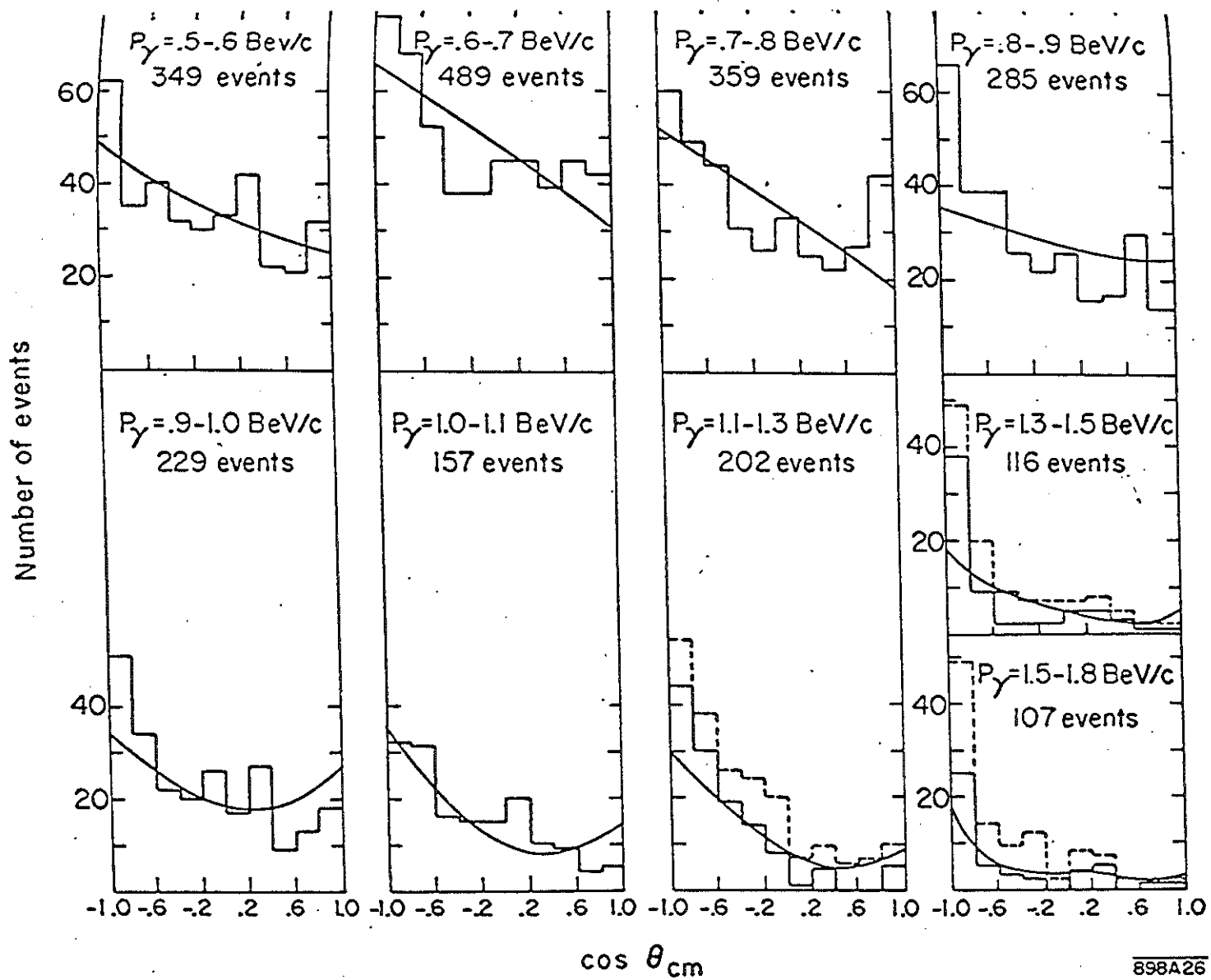
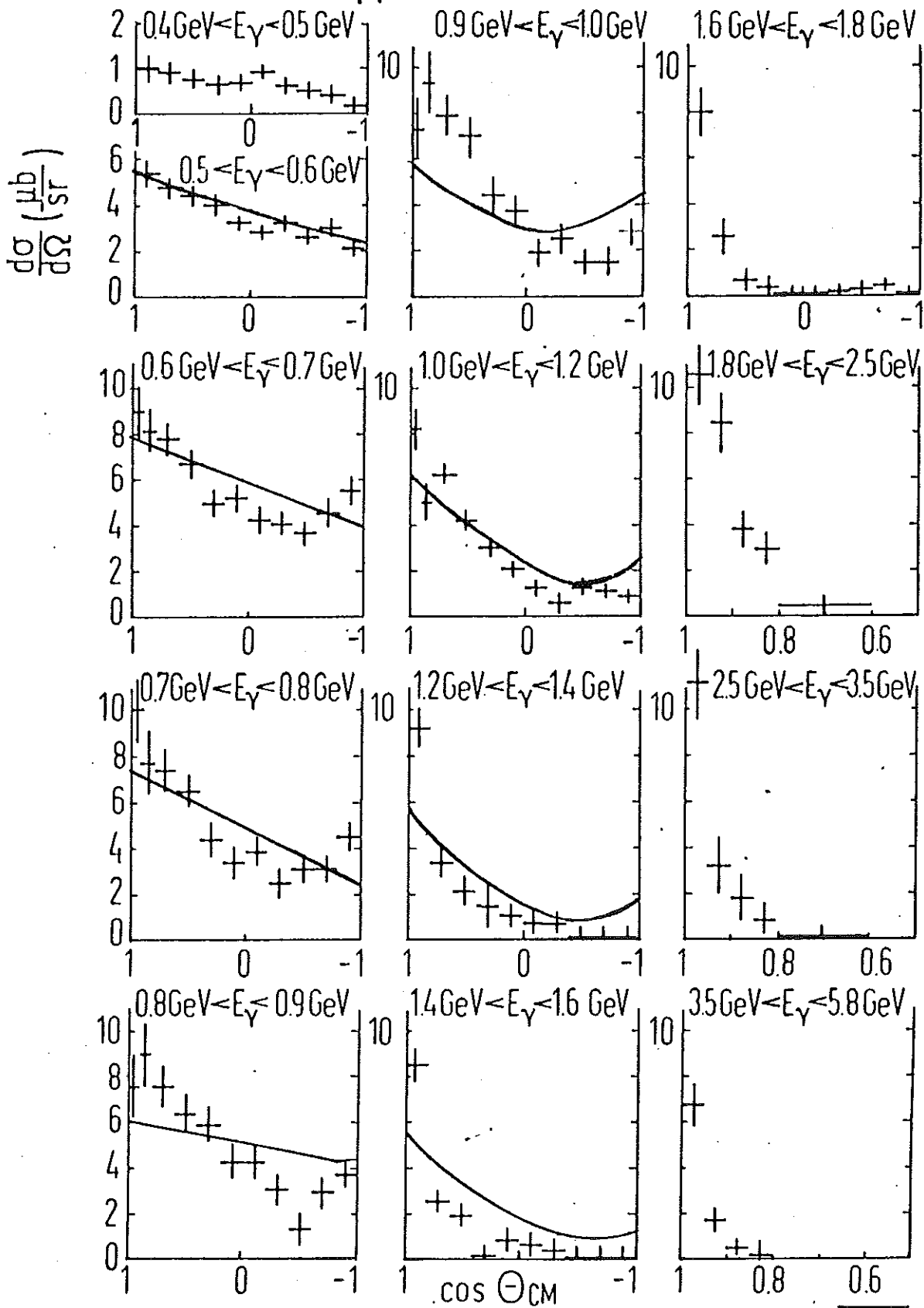
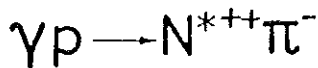


FIG. 25



898A25

FIG. 26

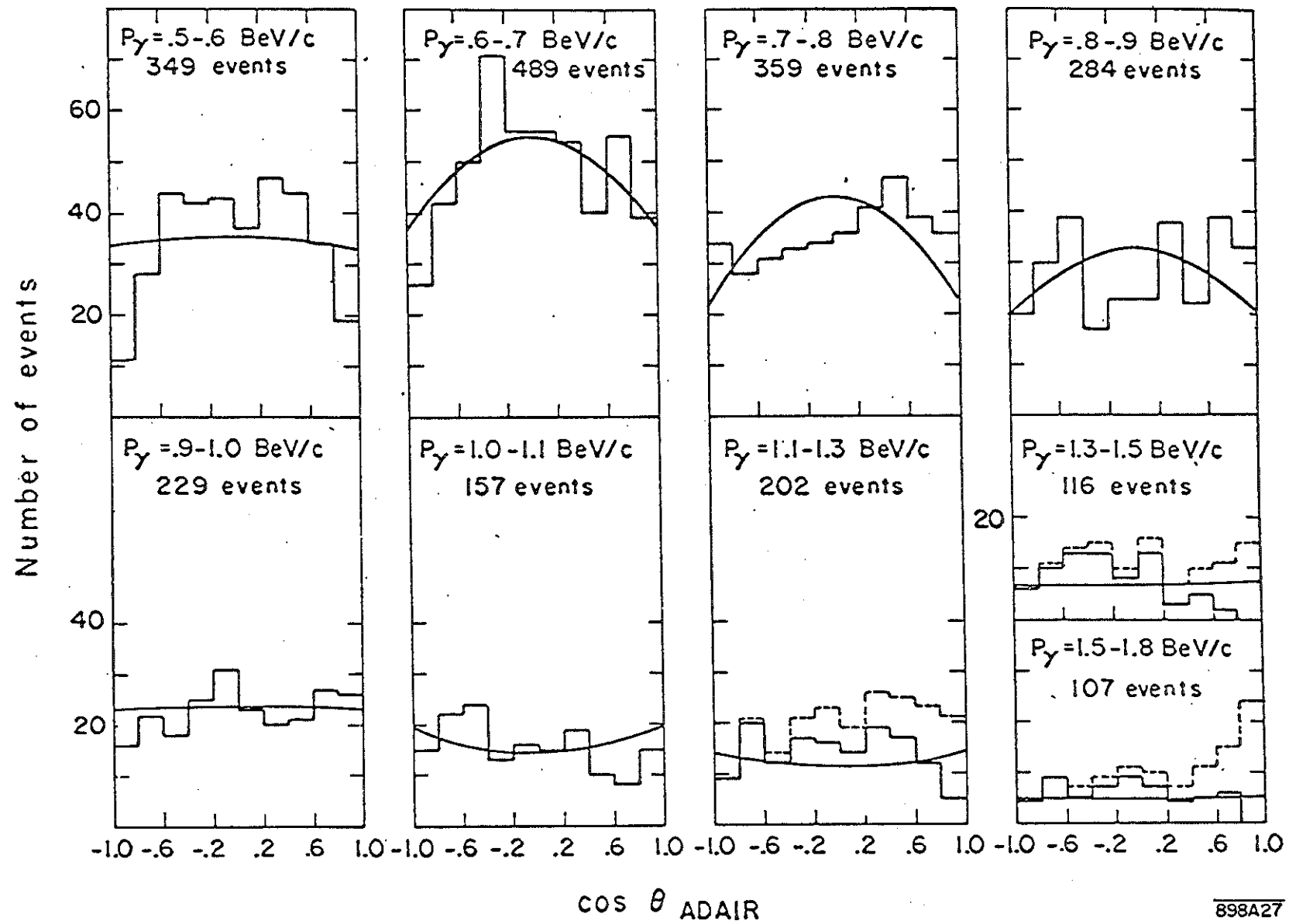


FIG. 27

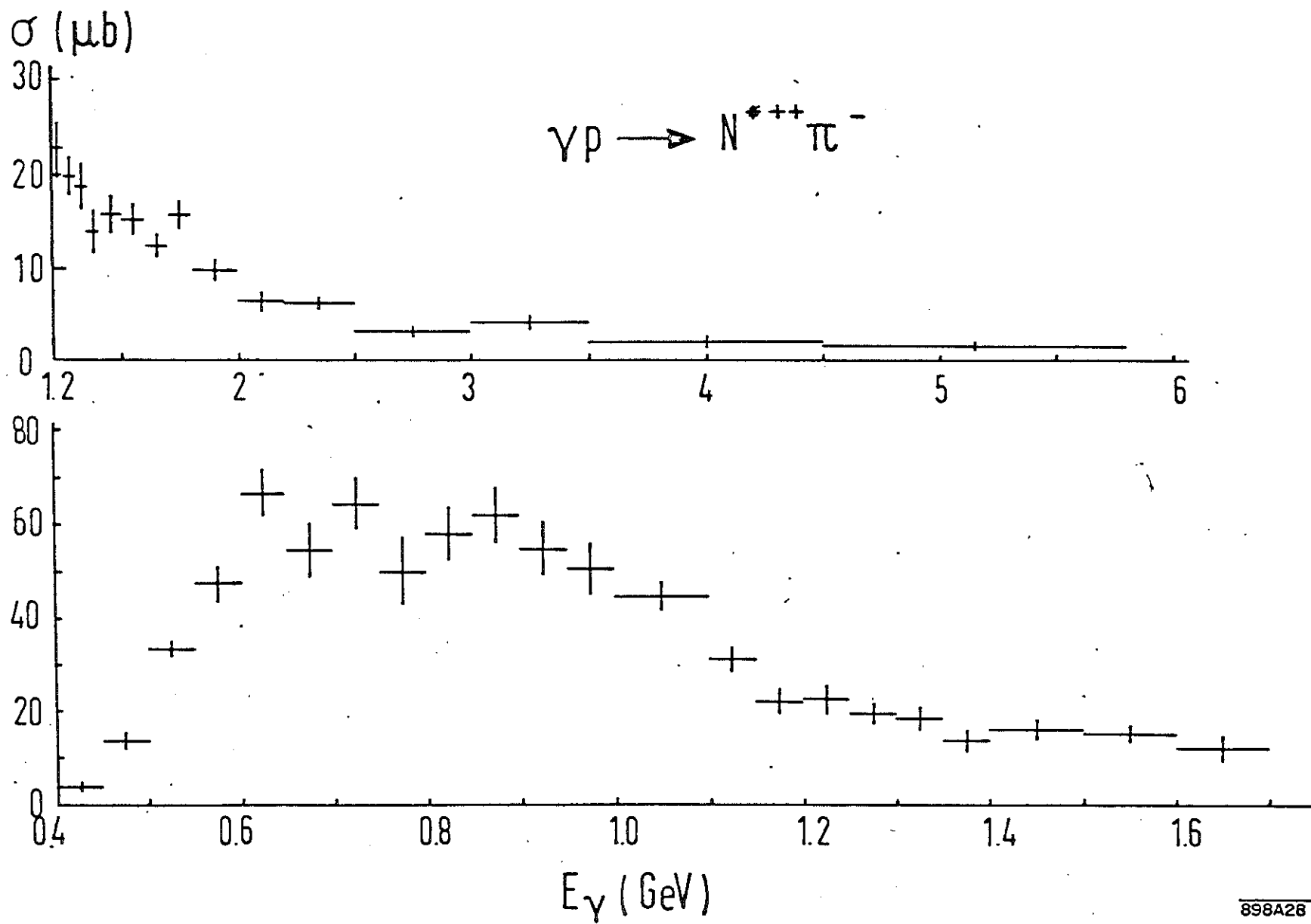


FIG. 28

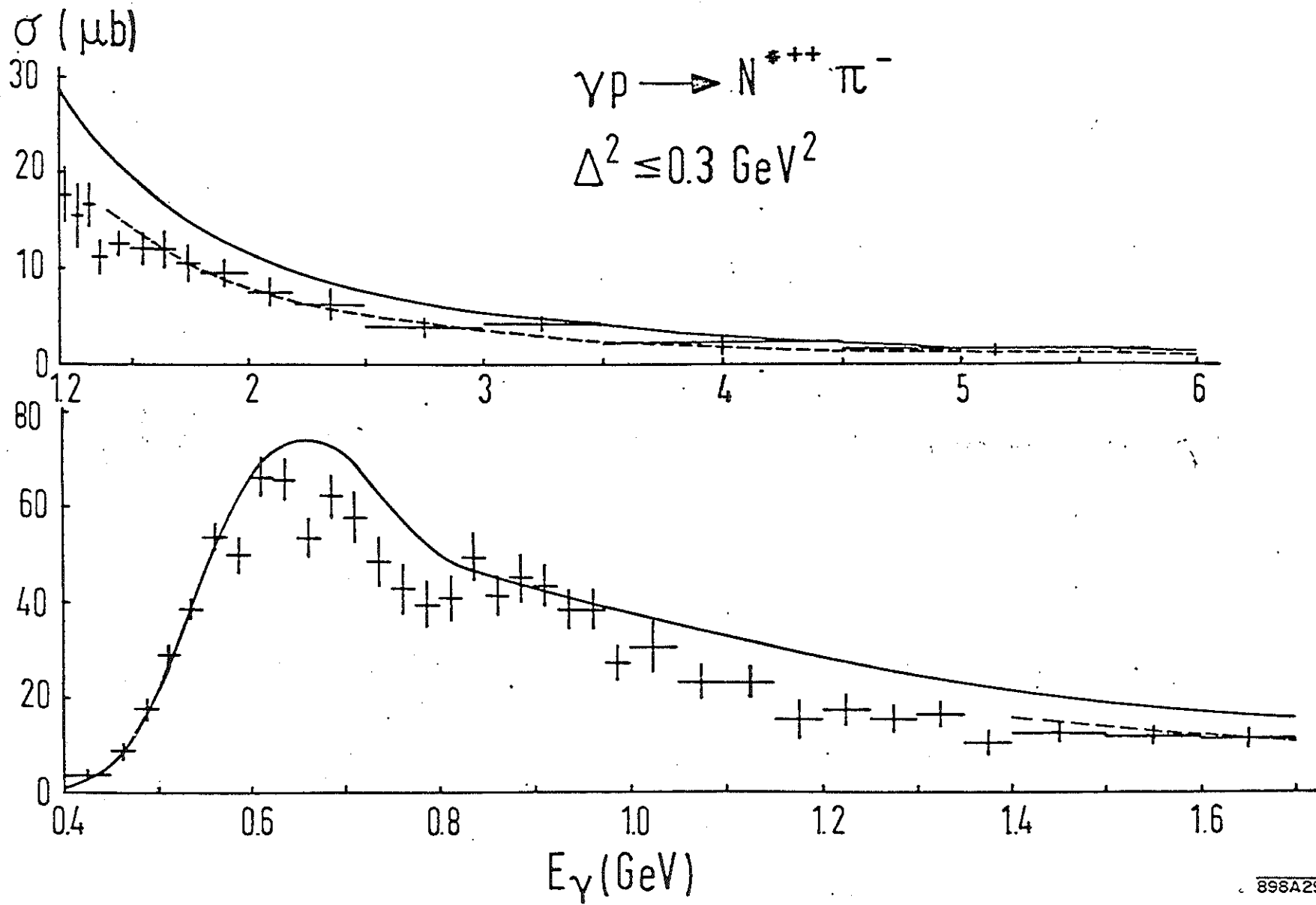


FIG. 29

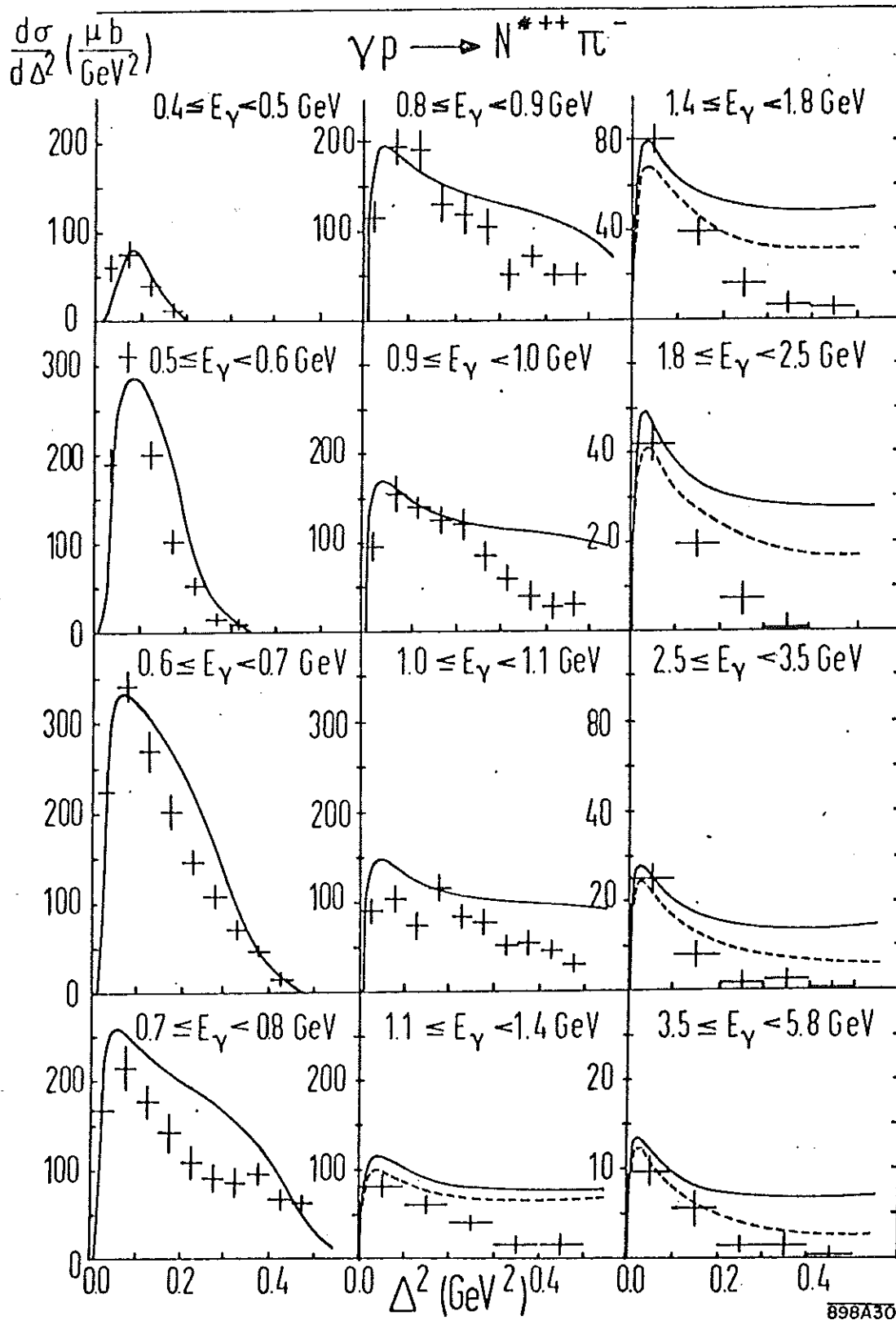
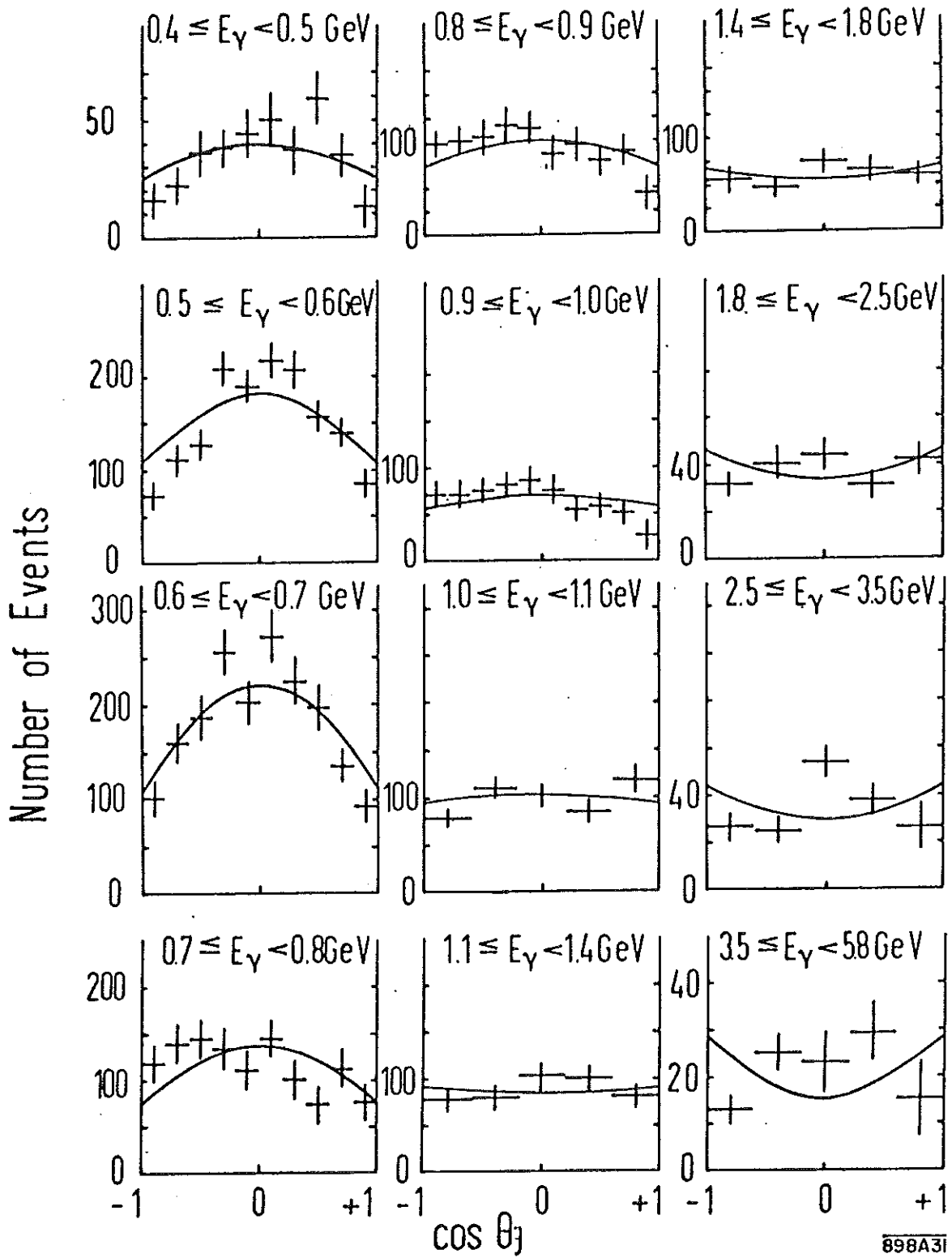
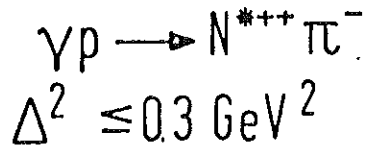


FIG. 30



898A31

FIG. 31

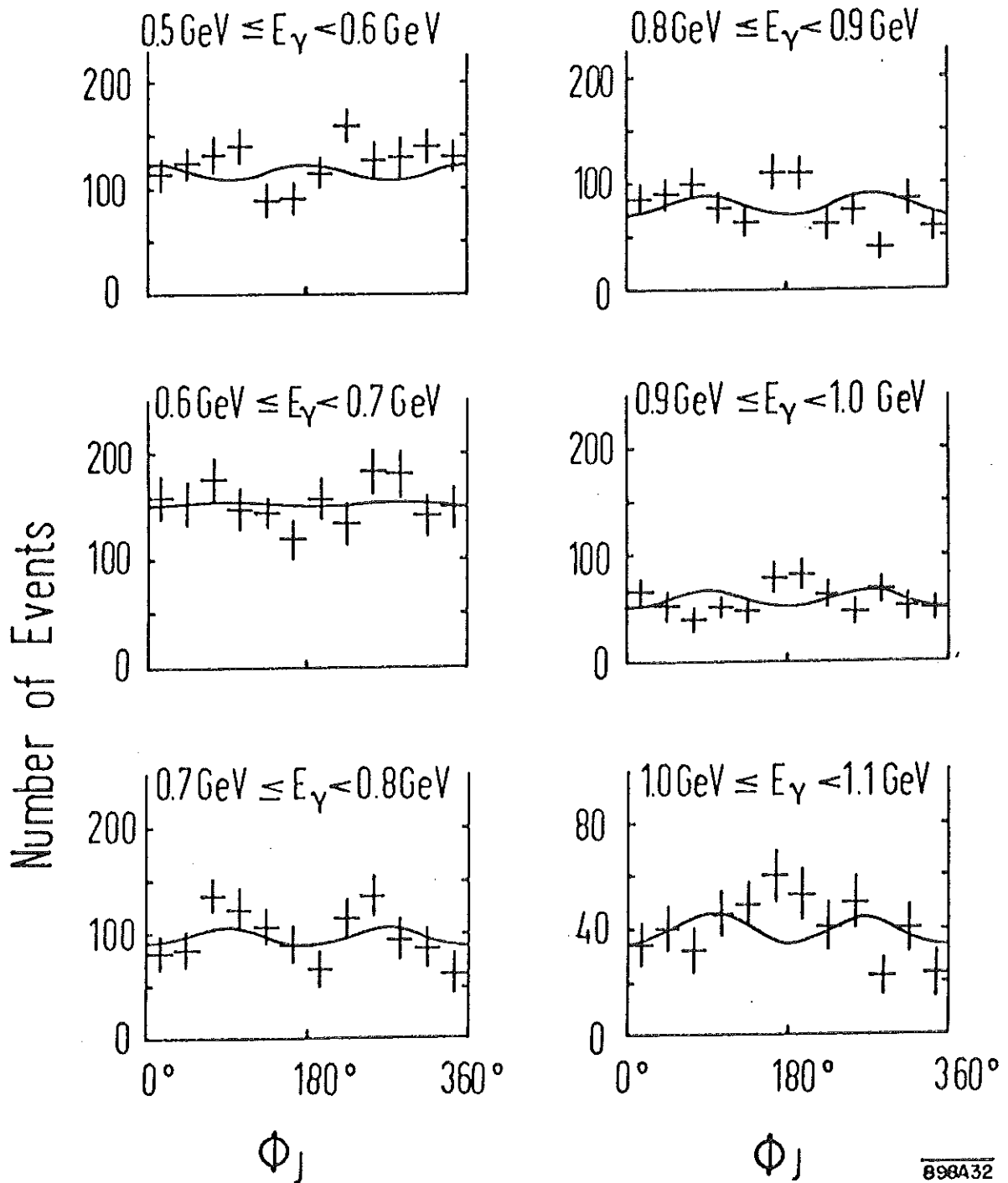
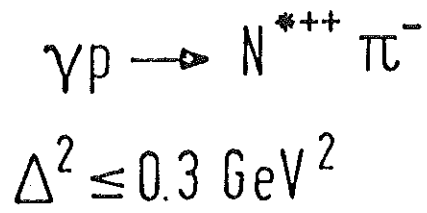
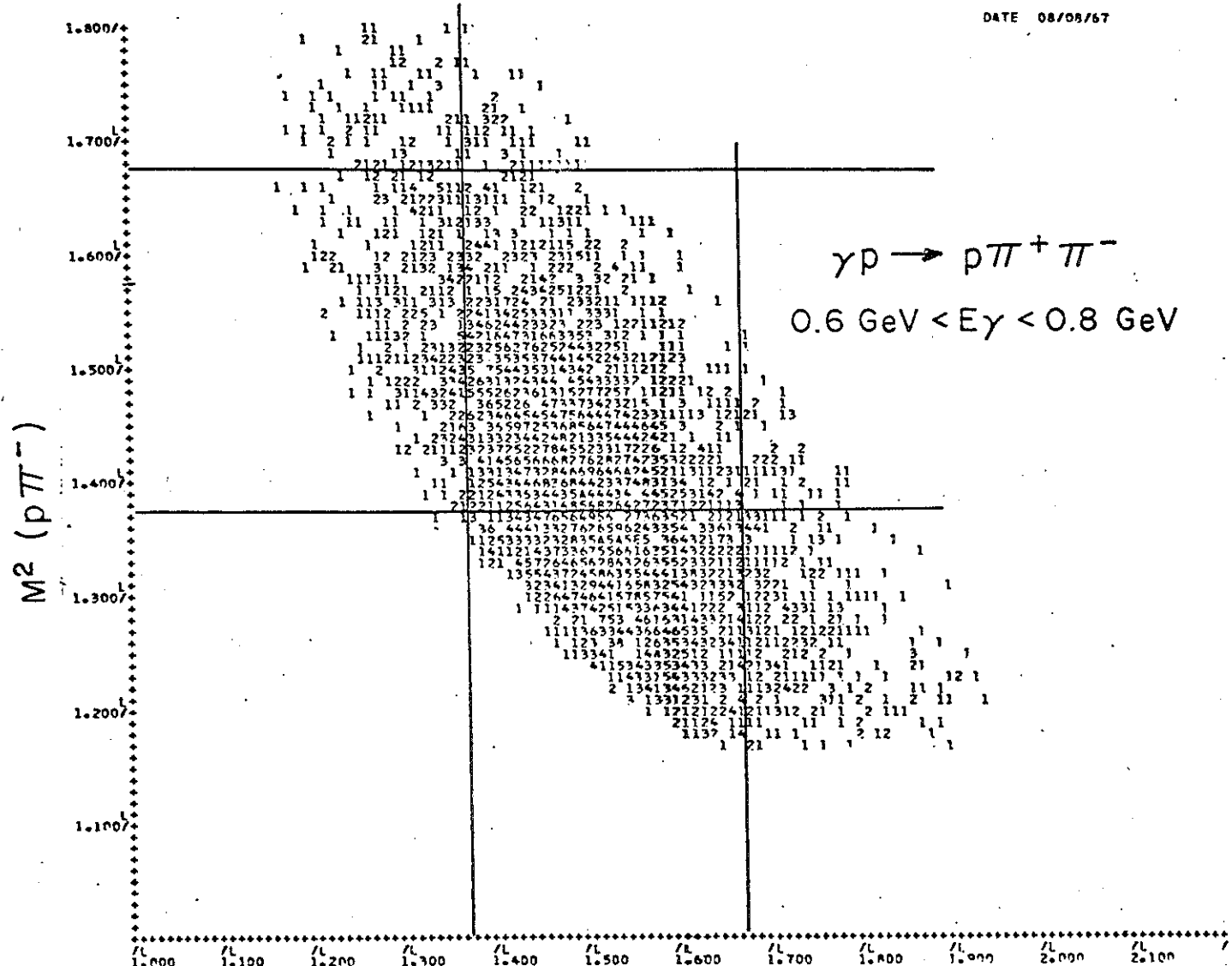


FIG. 32



THE PLOT CONTAINS 3952 EVENTS . 19 EVENTS OUTSIDE PLOT
 #1P-1002 / #1P+1002 E .6-.8 GEV

P-CODE OF 73

898A33

$M^2 (p\pi^+)$

FIG. 33

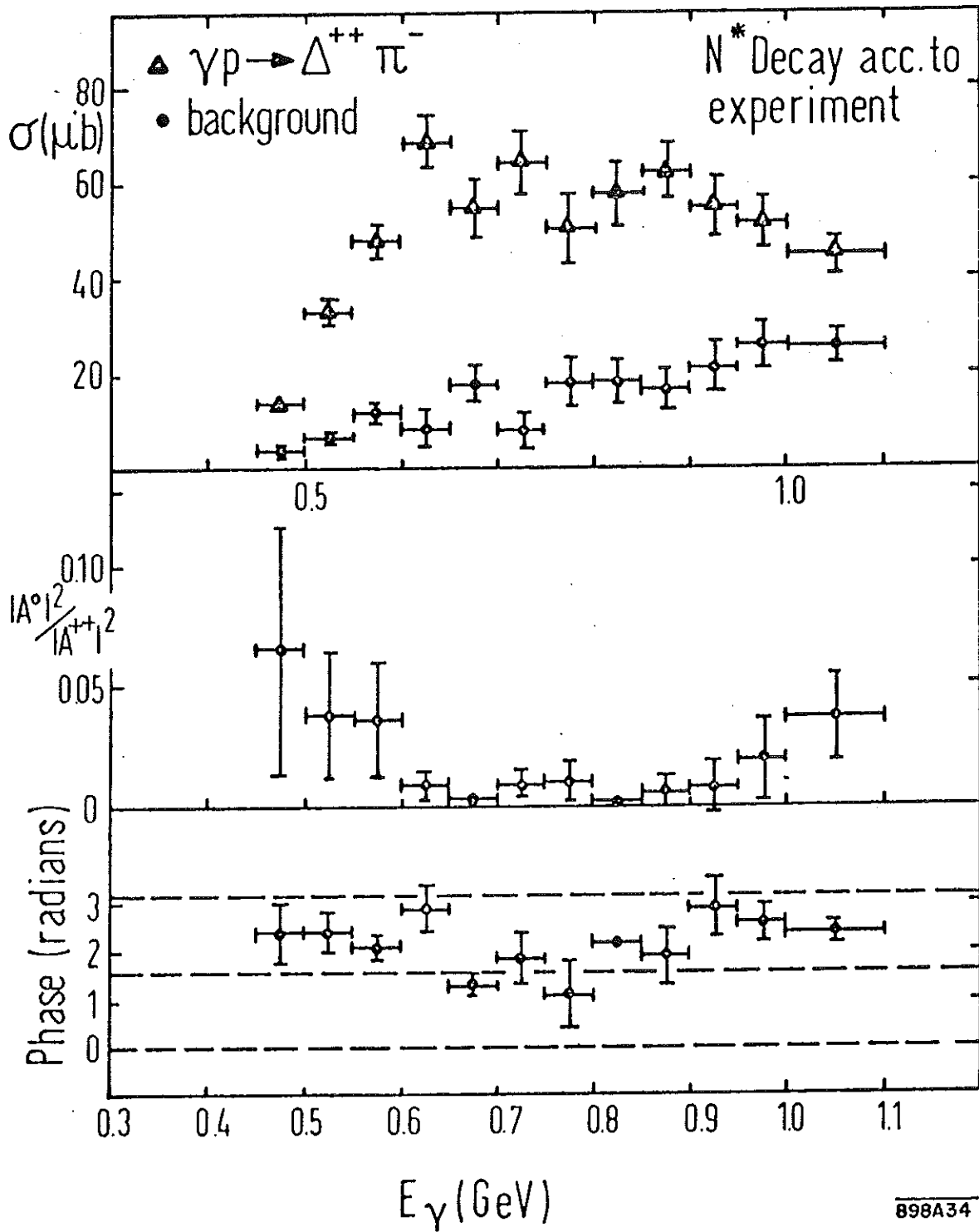


FIG. 34

898A34

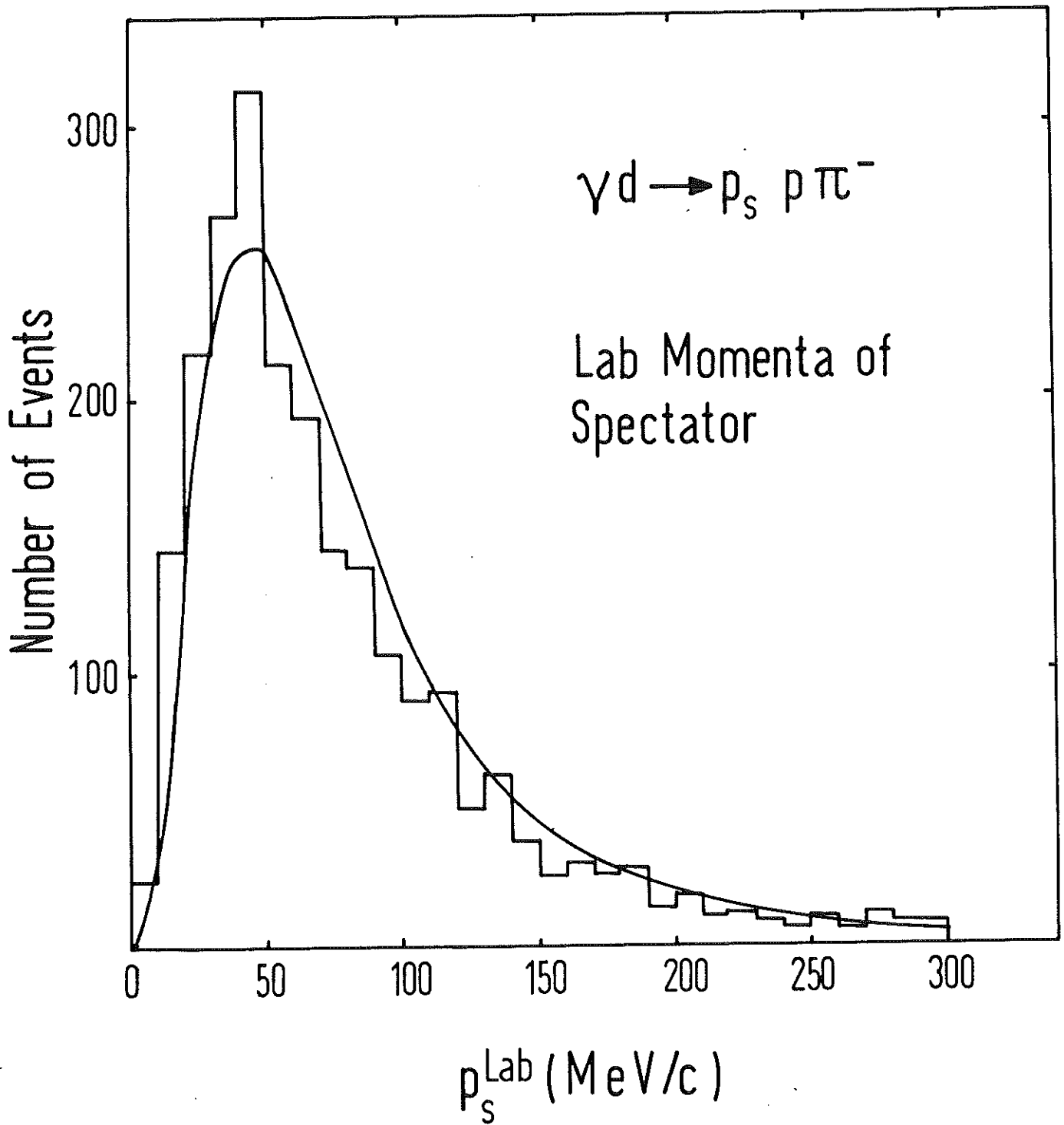
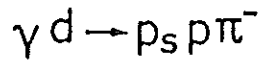


FIG.35



Angular Distribution of Spectator

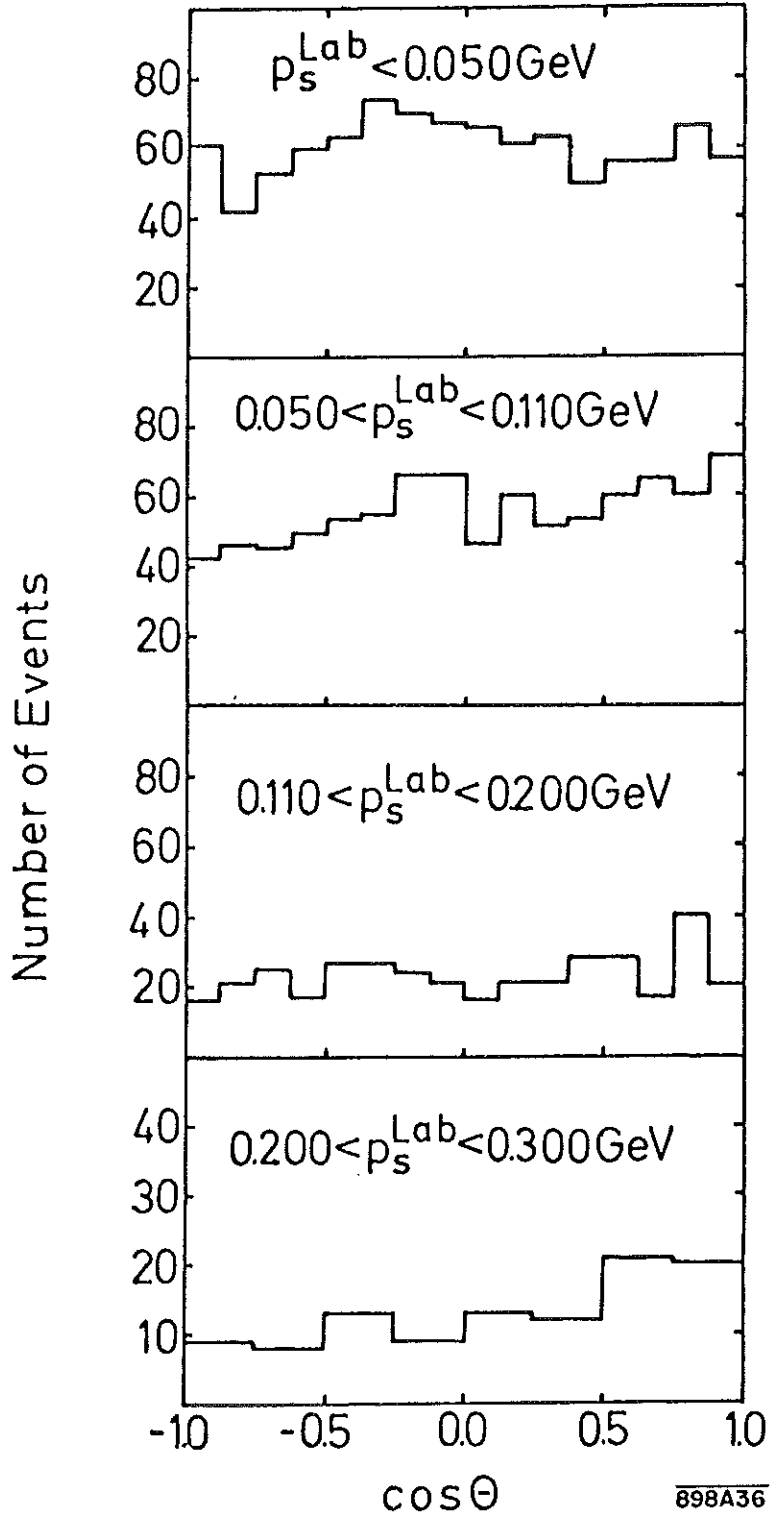


FIG. 36

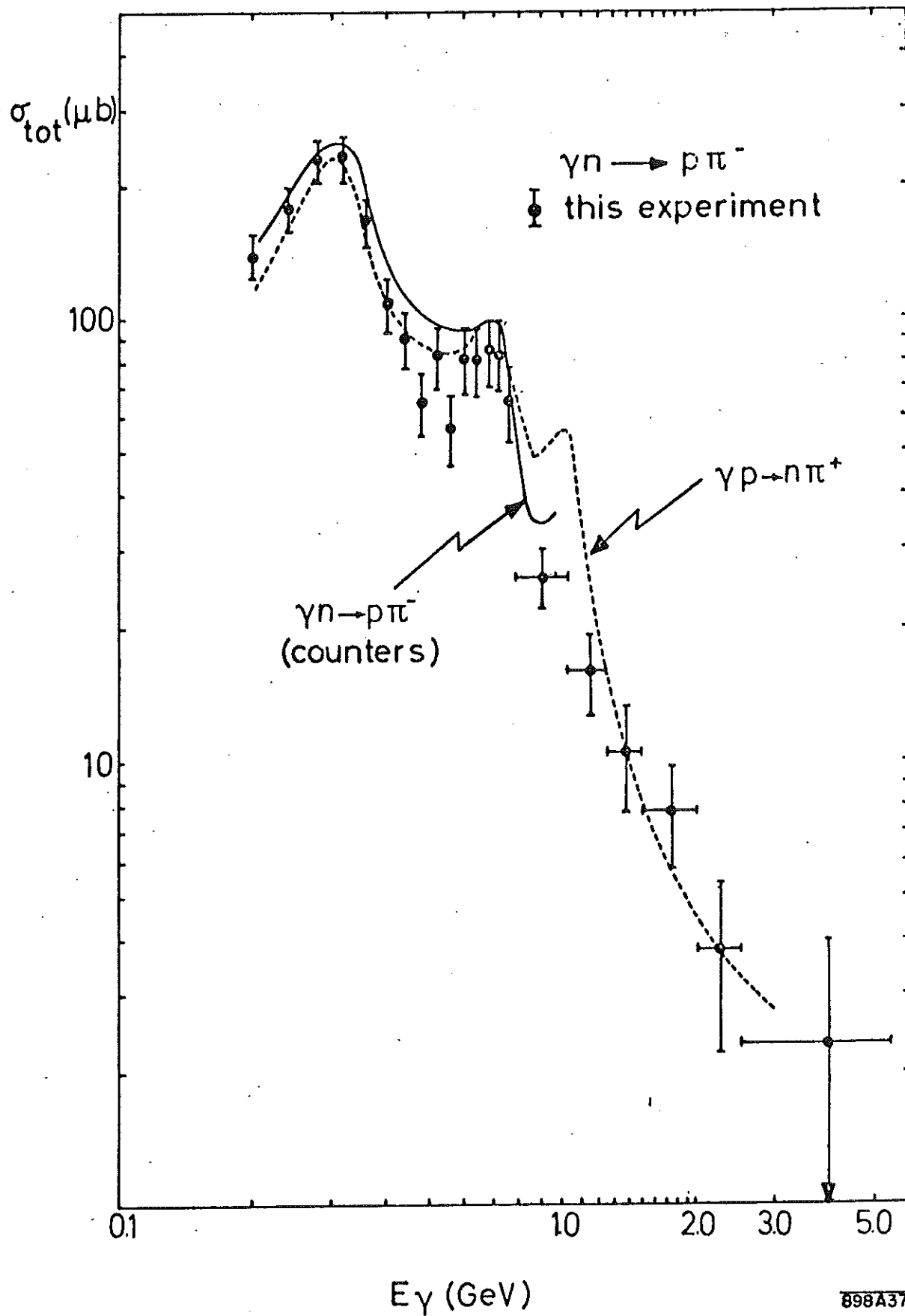
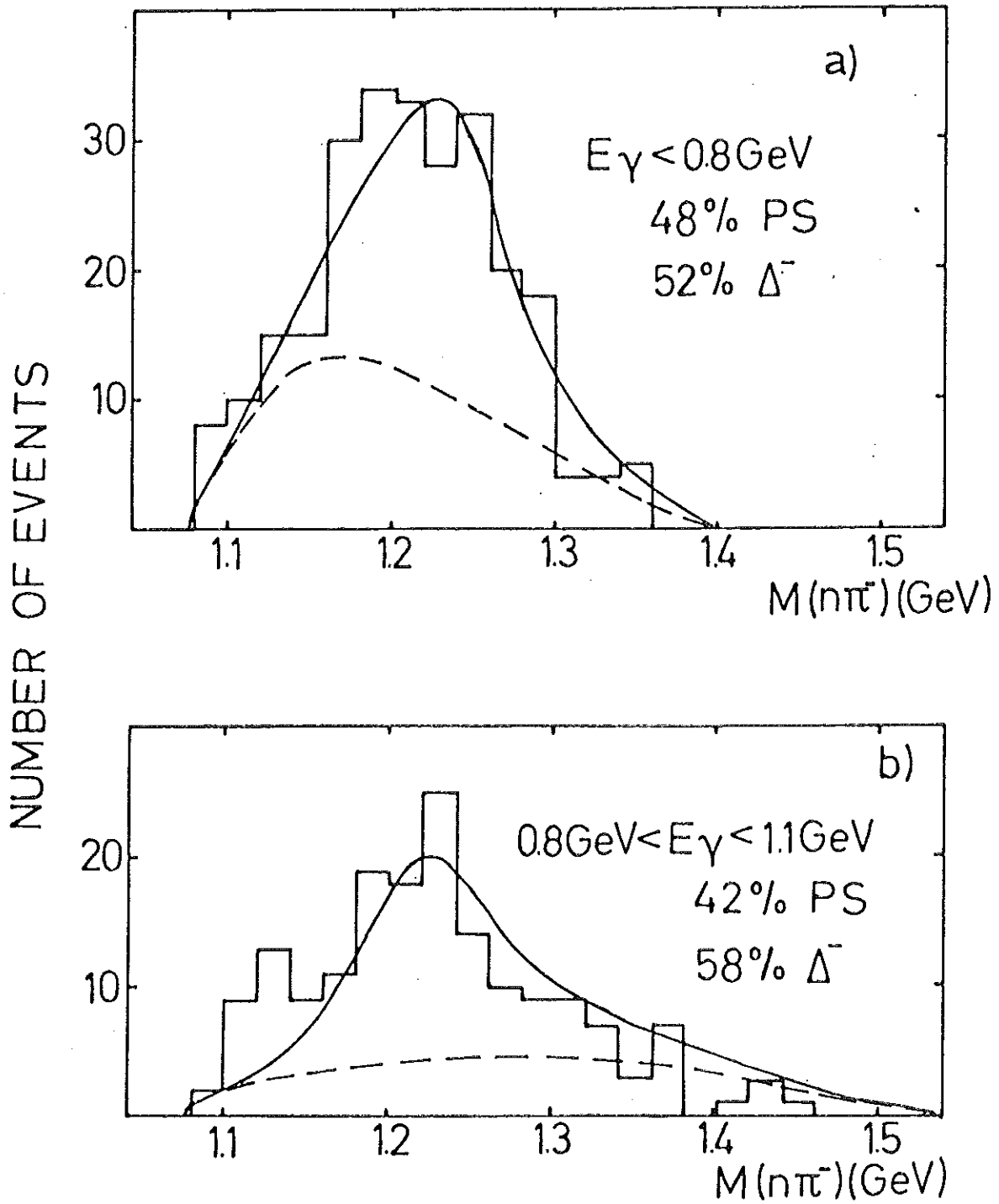
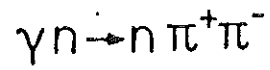


FIG. 37



898A38

FIG. 38

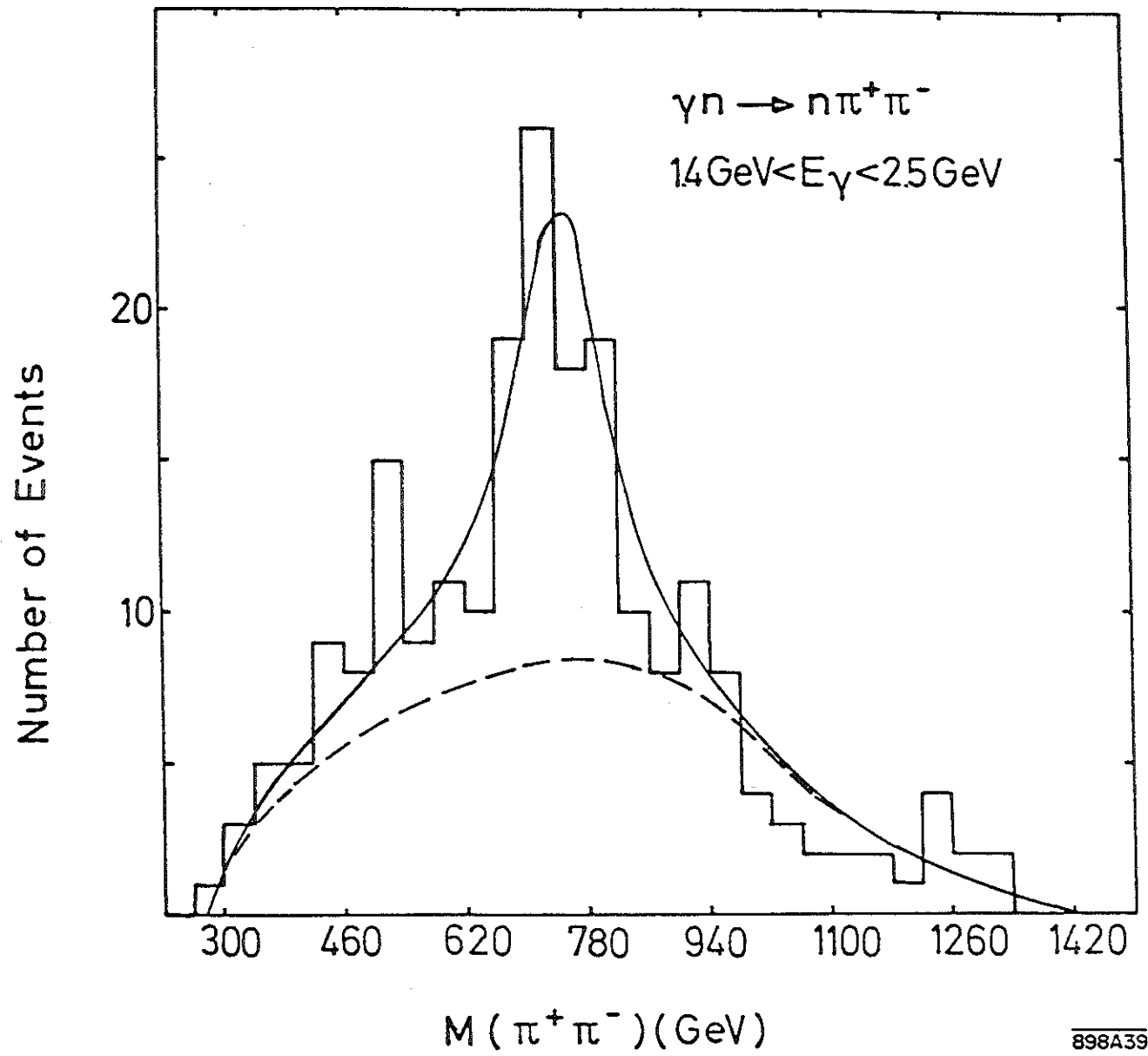


FIG. 39

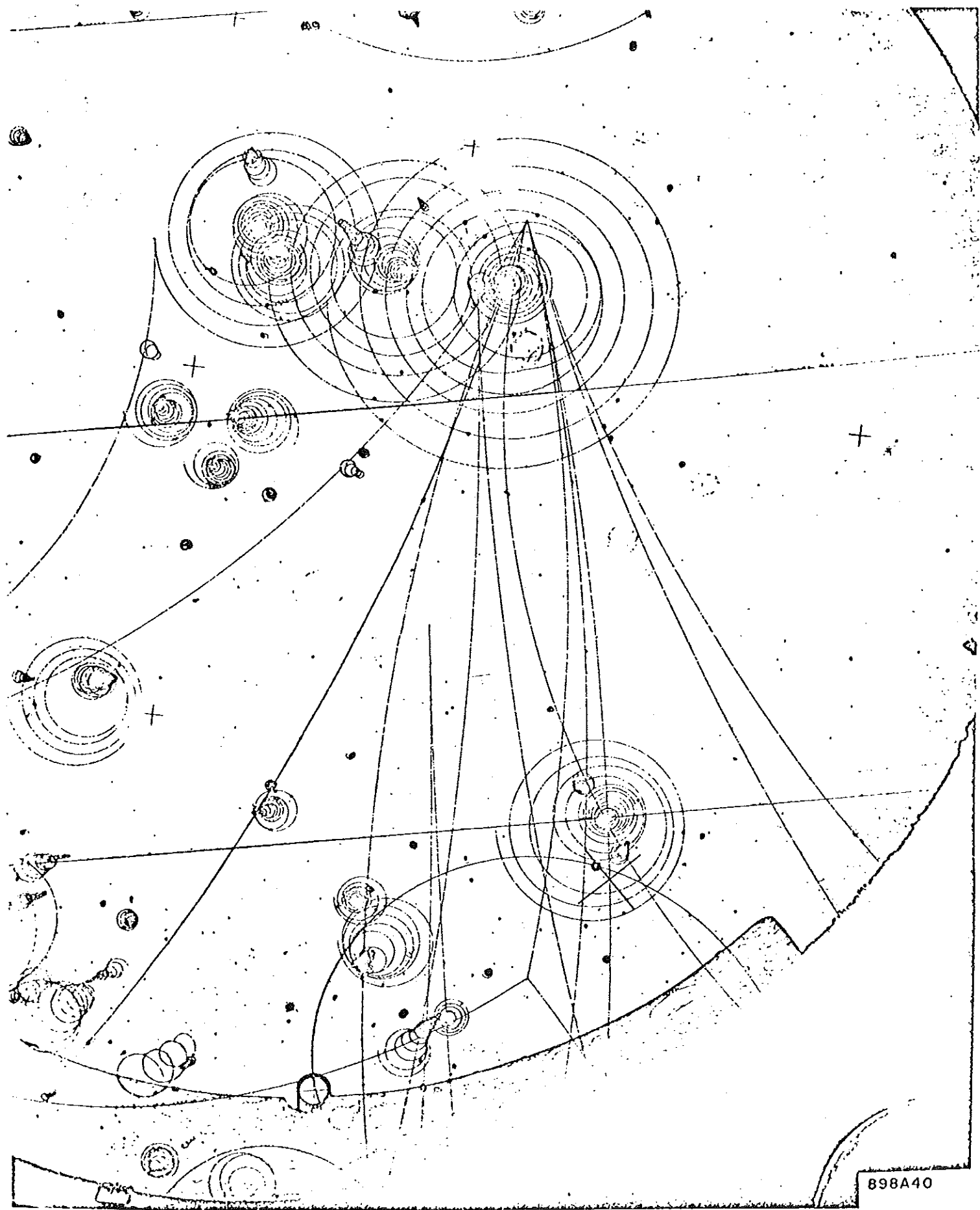


FIG. 40

B98A40

